# DEVELOPMENT OF A SURFACE ENHANCED RAMAN SPECTROSCOPY BASED BIOSENSOR TO DETECT CARDIAC BIOMARKERS

A Dissertation

by

JAVIER TRINIDAD GARZA

Submitted to the Office of Graduate and Professional Studies of
Texas A&M University
in partial fulfillment of the requirements for the degree of

DOCTOR OF PHILOSOPHY

| | |
|---|---|
| Chair of Committee, | Gerard L. Coté |
| Committee Members, | Michael McShane |
| | Kristen Maitland |
| | Jun Kameoka |
| Head of Department, | Anthony Guiseppi-Elie |

August 2017

Major Subject: Biomedical Engineering

ABSTRACT

Myocardial infarction (MI) is one of the most common causes of death in the world. The main symptom after the onset of MI is chest pain, which is one of the leading reasons for emergency department (ED) visits. When a patient arrives to the ED with chest pain, a rapid and accurate diagnosis is essential to immediately start the appropriate treatment. The measurement of cardiac biomarkers plays a key role in the diagnosis process, and improvements in this field could have a significant positive impact in the health of patients. Therefore, the development of fast, sensitive, and precise technologies to measure cardiac biomarkers is of great interest.

This work focuses in the development of a surface enhanced Raman spectroscopy (SERS)-based assay to detect cardiac biomarkers. SERS is an attractive technique because it exhibits multiplexing and high sensitivity capabilities. Several SERS active nanoparticles were synthesized and functionalized with antibodies to use them in assays. They were characterized and compared to select the nanoprobe that exhibited stability, intense SERS signal, and functionality. In addition, various techniques to collect nanoparticles were examined. A device and method to consistently collect nanoparticles for SERS measurements was developed, which allowed to detect nanoprobe samples (10 μL) across a range from nearly 27.4 fM to 1.7 pM with less than 10 % coefficient of variation (CV). Different assay formats were considered to implement the assay with the desired sensitivity and precision. After synthesizing the assay components, building the collection device, and selecting the sandwich assay format, an assay to detect cardiac troponin I (cTnI) was developed and tested. Various assay conditions were optimized to

improve the signal. Finally, a concentration curve that exhibited the expected response trend was obtained.

# DEDICATION

To God; my mom, Silvia Martínez de Garza; my dad, Javier Trinidad Garza; Alejandro Garza; Silvia Garza; and Andrea Ortega. Thank you for always being next to me in this journey.

ACKNOWLEDGEMENTS

First, I would like to thank God for everything.

I would like to thank my advisor Dr. Gerard Cote for guiding and supporting me throughout my time working in his lab. Thank you for your example, encouragement, and all the opportunities you facilitated.

I would also like to thank my committee members Dr. Mike McShane, Dr. Jun Kameoka, and Dr. Kristen Maitland for their support and counsel throughout the course of my research.

Specially, I want to thank all the past and current members of the OBSL lab. Thank you to each one of you for everything you taught me, for your help, motivation, guidance, and friendship.

Thanks to Texas A&M University for providing the best environment to learn and grow.

I would also like to thank to Dr. Duncan Graham for facilitating my summer research experience in Glasgow. Thank you for this amazing experience.

Finally, I want to thank my Mom, Dad, Alex, Kelly, and Andrea. Thank you for your patience and motivation.

## CONTRIBUTORS AND FUNDING SOURCES

### Contributors

This work was supervised by a dissertation committee consisting of Dr. Gerard Cote (chair), Dr. Michael McShane, and Dr. Kristen Maitland of the Department of Biomedical Engineering and Dr. Jun Kameoka of the Department of Electrical Engineering.

All work for the dissertation was completed by the student, under the advisement of Dr. Gerard Cote of the Department of Biomedical Engineering.

### Funding Sources

Graduate study was supported by the Texas A&M University Doctoral Diversity Fellowship and a by the Sloan Minority Ph.D. Program from the Alfred P. Sloan Foundation.

## NOMENCLATURE

| | |
|---|---|
| ACC | American Cardiology College |
| ACS | Acute coronary syndrome |
| AHA | American Heart Association |
| AMI | Acute myocardial infarction |
| BSA | Bovine serum albumin |
| CDC | Centers for Disease Control |
| CK-MB | Creatine Kinase-MB |
| cTnI | Cardiac Troponin I |
| CV | Coefficient of variation |
| CVD | Cardiovascular disease |
| DLS | Dynamic light scattering |
| DTNB | 5,5’-Dithiobis(2-nitrobenzoic acid) |
| ECG | Electrocardiogram |
| ED | Emergency department |
| ELISA | Enzyme linked immunoassay |
| LOD | Limit of detection |
| MBA | Mercaptobenzoic acid |
| MI | Myocardial infarction |
| MYO | Myoglobin |
| NACB | National Academy of Clinical Biochemistry |
| NHS | N-hydroxysuccinimide |

| | |
|---|---|
| NP | Nanoparticle |
| NSTEMI | non-ST-segment elevation myocardial infarction |
| NTA | Nanoparticle tracking analysis |
| PDMS | Polydimethylsiloxane |
| PEG | Polyethylene glycol |
| POC | Point of care |
| RRM | Raman reporter molecule |
| SEM | Scanning electron microscopy |
| SERS | Surface enhanced Raman spectroscopy |
| STEMI | ST-segment elevation myocardial infarction |
| TAT | Turnaround time |
| TEM | Transmission electron microscopy |
| TFMBA | 2,3,5,6-Tetrafluoro-4-mercaptobenzoic Acid |

TABLE OF CONTENTS

Page

LIST OF FIGURES

Page

LIST OF TABLES

Page

# CHAPTER I

# INTRODUCTION

## *I.1 Motivation and Significance*

According to the World Health Organization, cardiovascular disease (CVD) is the leading cause of death in the world. In 2012, an estimated 17.5 million people died from CVDs, representing 31% of all global deaths.[1] Cardiovascular diseases are pathological conditions affecting the heart and blood vessels, such as: coronary heart disease, cerebrovascular disease, peripheral arterial disease, rheumatic heart disease, congenital heart disease, and deep vein thrombosis and pulmonary embolism.[1] Among them, ischemic heart disease and stroke are the most prevalent. These diseases alone accounted for a combined 15 million deaths in 2015.[2]

Symptoms of cardiovascular disease vary depending on the type of disease. For many people, chest pain or discomfort is the first sign.[3] In a 2005 survey by the Centers for Disease Control and Prevention (CDC) 92% of the respondents recognized chest pain as a symptom of a heart attack.[4] However, not all chest pain indicates the occurrence of a heart attack. Angina, or angina pectoris, is a common type of chest pain or a recurring discomfort that usually lasts a few minutes. This occurs when the heart muscle does not get enough blood supply or oxygen, which can happen during exercise or emotional stress when heart rate and blood pressure increase. As opposed to a heart attack, an angina attack does not permanently damages the heart muscle.[5] In 2013, chest pain was the second leading reason for visiting the emergency department (ED).[6] When a patients arrive at the ED, clinicians have the challenge to identify those who need to be admitted for urgent

management and those who can be discharged. If a patient has chest pain or related symptoms, the American Cardiology College/American Heart Association (ACC/AHA) guidelines recommend that physicians must perform a 12-lead ECG within 10 minutes of arrival to diagnose and treat myocardial infarction (MI).[7-8] However, ECG is not a sensitive diagnosis and can be inconclusive even for a patient with MI.[9-10] Approximately one quarter of the patients with chest pain in the ED present atypical symptoms and about one third have non-diagnostic cardiogram (ECG) changes.[11] ECG is used to classify two different categories of acute coronary syndromes (ACS): ST-segment elevation myocardial infarction (STEMI) and 'non-ST-segment elevation ACS' (NSTEACS), which is further sub-divided into unstable angina and non-STEMI (NSTEMI).[11] The treatment and intervention associated for each category is different; therefore, it is important to diagnose them accurately. Figure 1 shows some of the recommended guidelines to diagnose a patient with MI symptoms.

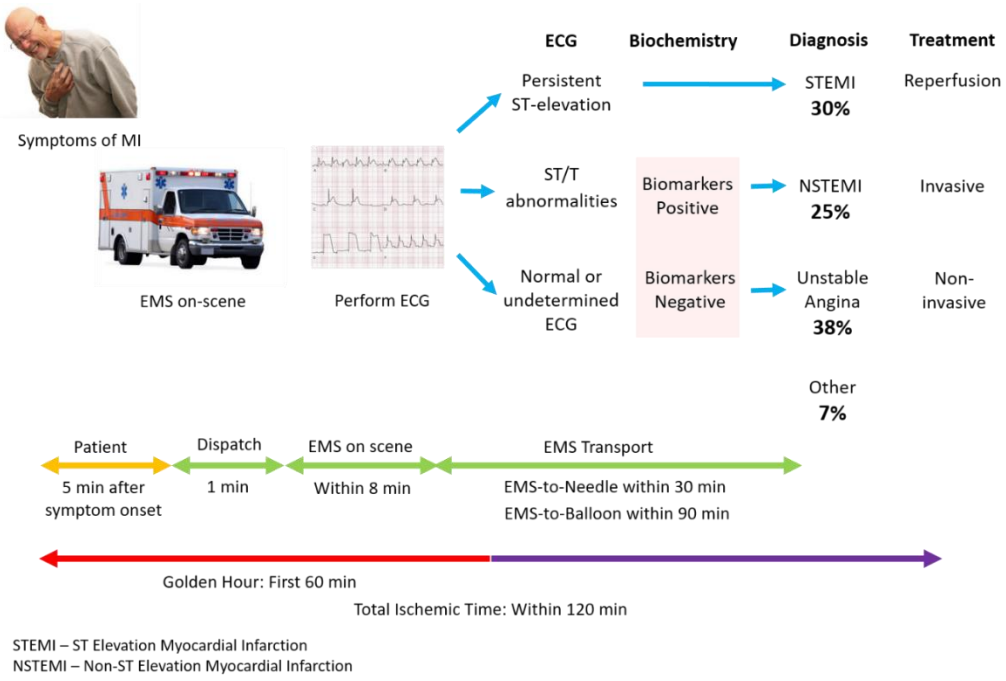


**Figure 1.** Guidelines to diagnose a patient with MI symptoms. Diagnosis should be completed in less than 2 h to start treatment as soon as possible. Cardiac biomarkers diagnosis plays an important role in determining treatment.

The lack of accurate diagnosis has negative consequences. About 5% of MI patients are incorrectly discharged from the emergency department.[11] It has been reported that those patients have a risk adjusted mortality rate almost two times greater than that of hospitalized patients for ACS.[12] In addition to adverse patient health outcomes, inadvertent discharge contributes to cases and payments of malpractice for ED physicians. Unintentional admissions and premature discharges also cause a significant financial burden.[11-12] Patients awaiting the ruling out of NSTEMI represent the most frequent and time-consuming source of overcrowding in the ED. For these patients, the availability of sensitive and accurate point-of-care (POC) technologies to measure cardiac biomarkers in

addition to the common ECG recordings would have a considerable impact on the time spent under diagnostic evaluation.[13]

No single diagnostic instrument can consistently detect and rule out the presence of an acute coronary syndrome at presentation to the ED.[13] Therefore, multiple diagnostic approaches are usually used to stratify risks and decide the appropriate treatment. Besides the common physical examination, assessment of medical history, and 12 lead ECG, additional methods for diagnosing MI include imaging and testing for cardiac biomarker levels. Imaging techniques such as X-ray, magnetic resonance imaging (MRI), or trans-thoracic echocardiogram can help in the diagnosis process but are usually insufficient, expensive, or unavailable.[14] As a result, the use of biomarkers such as troponin, myoglobin, and CK-MB has become a valuable tool to diagnose MI, apply the appropriate therapy strategy, and determine admissions and discharge decisions.[11] Although the presence of a biomarker can confirm a diagnosis and speed care, the absence of it can also indicate physicians that they can perform additional tests, such as exercise stress testing, that cannot be accomplished safely until the patient has ruled out of NSTEMI.[15]

Being able to diagnose patients with chest pain as early as possible is key because mortality caused by myocardial ischemia can be reduced significantly if definitive treatment is implemented rapidly[16]; however, this is not always possible in the ED due to uncertain ECG results and the time it takes to obtain blood test results.[13, 17] Blood samples are taken from the patient at the moment of arrival and sent to the central laboratory for testing. The AHA/ACC guidelines suggest that laboratory results should be available within 60 minutes, preferably 30 minutes according to the National Academy of Clinical

Biochemistry (NACB), but in a number of institutions the central laboratory is unable to meet this requirement taking up to 71 minutes to provide results.[7, 15, 17-18] Besides the approximate time required to perform some cardiac biomarkers assays (around 42 minutes), collection and transport methods to the central laboratory usually take at least 10 minutes, which contribute to the delay of the test results.[18]

## *I.2 Background*

### I.2.i Cardiac Biomarkers

Biochemical markers to diagnose acute myocardial infarctions (AMI) have been used for more than 50 years.[19] Cardiac biomarkers are defined as biological analytes that can be detected in the blood at elevated levels after myocardial damage or during any cardiovascular disease.[11] Currently, guidelines recommend the measurement of cardiac biomarkers in patients with suspected myocardial ischemia.[12] It is also recommended that several measurements should be obtained depending on the initial results and the time they were collected. Cardiac biomarkers should be specific for cardiac tissue and accessible to attain high sensitivity measurements and thus predict cardiac injury.[11] In addition, they need to be tested in clinical studies before they are accepted for clinical use. As technologies have advanced, different biomarkers have been discovered and monitored to diagnose AMI.[19]

In the last years, the most routinely used biomarkers have been creatine kinase MB (CK-MB), myoglobin (MYO), and cardiac Troponin I (cTnI).[10, 20] Cardiac troponin I is currently considered the gold standard or the biomarker of choice to diagnose AMI.[10, 18] However, one of the challenges of measuring only cTnI is its low concentration in the

blood at the first hours after an AMI onset, as can be observed in Figure 2. In contrast, higher levels of CK-MB and myoglobin can be detected moments after an AMI. The disadvantage of these biomarkers, especially myoglobin, is their low specificity to AMI, since their serum concentrations can increase in other clinical conditions other than AMI.[10, 21] As a result, measuring multiple biomarkers simultaneously has been recommended by international associations.[10]

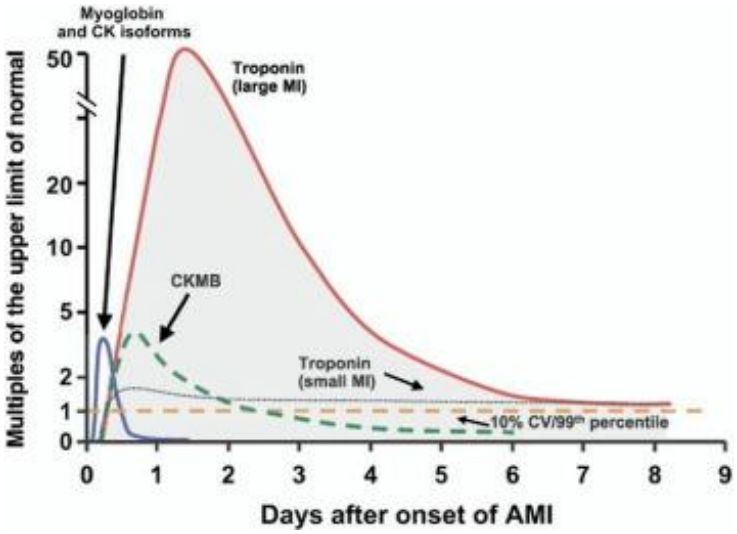


**Figure 2.** Release time of common cardiac biomarkers. Myoglobin is released faster than troponin or CK-MB. Each biomarker reaches its peak at different times. Reprinted with permission from Wright et al.[21] Copyright 2011 Wolters Kluwer Health, Inc.

Several assay technologies have been developed to simultaneously monitor cardiac troponin, CKMB, and myoglobin. A multimarker point-of-care (POC) test has been used in a 90 min protocol to diagnose AMI with good sensitivity and specificity (100% and 94% respectively). Of the 90% of patients discharged with negative cardiac biomarkers results, only one returned with a MI within one month.[22] Another study demonstrated that an assay technology that measures the three biomarkers allows rapid discharge of one-

third of patients admitted with chest pain and only 1% readmission.[23] Additional studies have also demonstrated benefit in using a multimarker approach to diagnose AMI.[24-25] However, studies have also shown that the measurement of myoglobin and CKMB, in addition to cTnI, does not add value to the diagnosis.[26]

*I.2.i.a Cardiac Troponin I*

Currently, troponin is the most sensitive and specific biomarker of irreversible myocardia injury available in clinical settings.[13] For this reason, cTnI is the most commonly used cardiac biomarker to detect AMI. This contractile protein is one of three sub-units (troponin C, troponin T, and troponin I) that compose the troponin complex of thin filaments of striated muscle.[27] The complex is involved in the calcium sensitive switch that regulates the interaction of actin and myosin in striated muscle to control muscle contraction. Specifically, Troponin I binds to actin and inhibits actomyosin ATPase activity in the absence of calcium.[28-29] It has a molecular mass of approximately 24 kDa and an isoelectric point (pI) of 9.9.

Troponin I has different isoforms expressed by different muscle tissues; however, cTnI is specific to the heart and is not expressed in normal skeletal muscle at any time.[30] The unique amino acid sequence of cTnI makes this protein an ideal biomarker for AMI and enables the development of monoclonal antibodies that do not cross react with skeletal troponins.[31] Cardiac troponins are released over time when necrosis of the myocardium occurs. It has been reported that between 15-48% of patients with unstable angina have elevated levels of the biomarker.[30] The concentration of cTnI in the blood increases about 4-8 h following myocardial injury and peaks at 12-24 hrs.[17, 32] The levels remain high for

at least 7 days.[30] In first generations of cardiac troponins assays elevated levels were linked with secondary conditions such as renal failure, cardiomyopathy, and congestive heart failure among others. However, the specificity and analytical performance of current assays has improved significantly.[11] The monitoring of cTnI levels has become an important information of the risk stratification process. It has been reported that patients who rule out for AMI, but who have high levels of troponins, have an outcome as poor as those who have had an AMI.[30]

*I.2.i.b Myoglobin*

Myoglobin is a protein that contains iron and has a molecular mass of 18 kDa.[33] It is very similar to hemoglobin, but only binds to one molecule of oxygen instead of four. Myoglobin takes up oxygen from hemoglobin and releases it for use into the mitochondria where oxidative reactions occur.[33]

Myoglobin is a sensitive early biomarker of AMI. It has been monitored because its plasma levels can be raised as early as 1 h from onset of infarction, which doesn't occur for other common cardiac biomarkers.[19] It peaks between 6 to 9 h and can return to baseline in less than 24 h.[34] The main disadvantage of using myoglobin as a cardiac biomarker is its low specificity. Myoglobin levels can be increased with several conditions, such as skeletal muscle disease or injury and renal impairment.[19, 35] In addition, since the physiological concentrations of myoglobin that reflect skeletal muscle turnover depend on different factors such as muscular mass and sex, there are difficulties in establishing a decision limit.[36] Furthermore, studies have demonstrated that high sensitivity troponin assays can have the same performance as myoglobin assays, making

the latter redundant.[36-37] Nonetheless, myoglobin is still used to aid the diagnosis and stratification of cardiac injury early after symptom onset.[35]

*I.2.i.c Creatine Kinase MB*

Creatine Kinase (CK) is a dimeric protein composed of two enzymatically active M (muscle-type) and B (brain-type) subunits with a molecular weight of 86 kDa.[33, 38] CK catalyzes the transfer of phosphate from creatine phosphate to adenosine diphosphate to produce ATP, which is the energy source of most tissues.[38] There are three dimeric isoenzymes of CK in human tissue: CK-MM, CK-MB, and CK-BB.[39] CK-MB is almost exclusively found in the myocardium. It produces approximately 15% to 30% of the total CK activity per gram of myocardium.[38] The other percentage (85% to 70%) is mostly produced by CK-MM.[40] Ninety-nine percent of skeletal muscle is composed of CK-MM.[40] A small amount of CK-MB is present in skeletal muscle (less than 1% of the total).[33] CK-BB is found in brain tissue and is essentially absent from skeletal or cardiac tissue.[38]

Total serum CK levels are not specific to cardiac muscle damage.[33] CK levels in serum can rise with increased muscle activity, stress, or trauma. It has been reported that CK serum levels of marathon runners were 21 times higher after the race and returned to baseline after 4 days.[38, 40] In patients with AMI, the levels of total CK and CK-MB in the blood increase within the first 4-6 after the onset of symptoms.[33] The levels peak at 18-24 h and return to baseline values after 72 h.[33] Since low levels of CK-MB are present in skeletal muscle, levels in the plasma can increase above the cutoff concentration indicative of AMI when skeletal muscle trauma occurs.[33, 38] The relative index of CK-MB, which is CK-MB (in ng/mL)/total CK (in U/L), can be used to determine if elevations are due to

skeletal muscle damage. However, the relative index is useful only if patients have myocardial injury or skeletal muscle injury, but not if they have both. A study compared the relative index and absolute CK-MB concentrations and found that when the relative index is used the specificity increases, but the sensitivity is reduced.[41] Therefore, it is not recommended to use the relative index or absolute CK-MB concentrations to diagnose myocardial damage when skeletal muscle disease is also present.[33]

The recognition of the lack of specificity of CK-MB to diagnose AMI reinforced the search of cardiac biomarkers with superior performance.[19] Reports found that cTnI tests exhibited similar detection limits than CK-MB but with substantially better specificity.[31] In 2000, new guidelines changed the definition of AMI and suggested cardiac troponin as the preferred biomarker.[42]

**I.2.ii Diagnostic Requirements**

Cutoff concentrations of some cardiac biomarkers, such as CKMB and myoglobin, are important to distinguish between AMI and non-AMI diseases, as some healthy subjects can have high concentrations of these markers due to skeletal muscle turnover. For cTnI, scientific international bodies (the European Society of Cardiology (ESC), the American College of Cardiology (ACC), the American Heart Association (AHA), and the National Academy of Clinical Biochemistry (NACB)) has recommended the use of a cutoff at the 99$^{th}$ percentile of the normal range with a coefficient of variance (CV) of 10% or less. However, since most commercial assays do not meet this criteria, the current recommendation is to use the lowest troponin concentration obtained with at least 10%

CV. In addition, it is recommended to measure the levels at different times after the first measurement (6 h and 12 h after measurement) to rule out AMI and 2-3 h to rule in AMI.[33]

The National Academy of Clinical Biochemistry (NACB) recommends less than 60 min (ideally 30 min) turnaround time (TAT) for troponin assays.[18, 43] Another limitation of current cTnI assays is their low sensitivity at the time when the patient presents in the ED due to the delayed increase of the troponin circulating levels for 3 to 4 h and the need for serial sampling.[44] The delay of plasma troponin levels is related to the time to develop cardiomyocyte necrosis and the time to develop irreversible injury of ischemic myocardium as a transmural wavefront.[9, 45] In general, assays usually take 15 min or less; however, the time also depends in the number of biomarkers being measured.[13]

In recent years, the improvement of available assays and the development of new assays have improved the precision at low concentrations of cardiac biomarkers such as cTnI.[46-47] These high sensitivity assays are up to 50-fold more sensitive that currently used assays, and they can even detect troponin levels of healthy subjects.[46] This enables for earlier and more sensitive detection of AMI.[47] Figure 3 shows the different detection ranges of different generations of troponin assays.

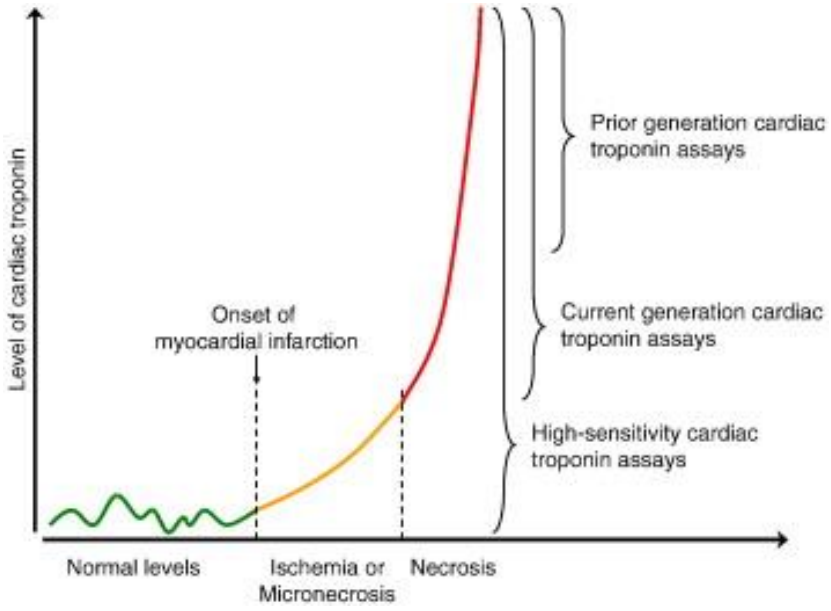


**Figure 3.** Detection range of different generations of troponin assays. Immediately after onset of MI, troponin levels increase slightly and can only be detected by high sensitivity troponin assays. After a couple hours, troponin levels increase and can be detected by less sensitive assays. Reprinted with permission from Hochholzer et al.[47] Copyright 2010 Elsevier.

Studies have demonstrated that using sensitive troponin assays can increase the diagnostic accuracy of AMI at initial presentation.[48] However, when the established cutoff ($99^{th}$ percentile) is used, sometimes the diagnosis is not sensitive enough to make immediate clinical decisions, and additional measurements are needed after the initial measurement to follow the current guidelines.[44, 49-50] Some studies suggest that serial testing after 3 h from presentation with AMI symptoms are not necessary if high sensitivity troponin assays are used.[15] It has also been reported that using the lower detection limit of the high sensitivity cTnI assays at presentation as an alternative criteria to rule out AMI allowed for a more sensitive diagnosis that could enable physicians immediately exclude AMI in up to 27.7% of patients.[49] Therefore, the use of high sensitivity troponin assays

can reduce the need of serial blood testing, which in turn can shorten the time for diagnosis and hospital discharge; in addition, it can also decrease the number of unnecessary hospitalization and the associated costs.[44]

Assays for CK-MB should be able to detect concentrations below 1 ng/mL with a dynamic range of at least 100 ng/mL A precision of less than 10% CV at the cutoff concentration is desirable.[33] A sensitivity of less than 5 ng/mL is desirable for myoglobin assays with a dynamic range of at least 500 ng/mL and a less than 10% CV at the cutoff concentration.[33] Based on the performance information of several high sensitivity cTnI assays, the detection range goal of a cTnI assay should be approximately from 0.01 ng/mL to 1 ng/mL with 10% CV or less.[51-52]

**I.2.iii Current Cardiac Biomarkers Diagnostic Technologies**

Currently, there are several manufacturers of cTnI assays with different formats, antibodies, epitopes specificity, and detection techniques, such as fluorescent, chemiluminescent, electrochemical, or spectrophotometric. Each of them is vulnerable to interference from different variables such as haemolysis, icterus, lipaemia, anticoagulant, ascorbic acid, biotin, autoantibodies that can cause false positives and false negatives.[19] This also leads to differences in sensitivity, limits of detection (LOD), and values at which there is less than 10% coefficient of variation (CV).[19] Since there is no standardization of cTnI measurements, each assay technology has its cutoff levels. Additionally, there is variation in the amount and type (blood, plasma, or serum) of measured sample used in the assays.[13]

There are currently few commercial high sensitivity cTnI assays (hs-cTnI) that meet the cutoff criteria of the 99th percentile of the normal range with less than 10% CV.[9, 52] However, assays with less than 20% CV at the 99th percentile can be used to make diagnosis and risk assessments.[13, 33] Cardiac troponin I assays are available from many manufacturers; as opposed to the cardiac troponin T assays which is sold by only one manufacturer due to patent restrictions.[33] Examples of current cTnI assay technologies with their corresponding CV% at the 99th percentile are shown in Table 1 and Table 2. As can be noted, most of the assays that have a CV of less than 10% at the 99th percentile are not FDA approved. The sensitivity and precision of POC assays is lower than the other technologies.

**Table 1.** Overview of troponin assays. Reprinted by permission from Macmillan Publishers Ltd: Nature Reviews Cardiology [53], copyright 2017

| Company and platform or assay | LoD (ng/L) | 99th percentile (ng/L) | CV at the 99th percentile (%) | FDA clearance |
|---|---|---|---|---|
| Ortho Clinical Diagnostics hs-cT | 1 | 16-23 | 10 | No |
| Abbott Architect STAT hs-cTnI | 1.1-1.9 | 16-34 | <6 | No |
| Roche E 2010 / cobas e 411 / E 170 / cobas e 601 / 602 hs-TnT (fifth-generation | 5 | 14-22 | <8 | Yes |
| Ortho-Clinical Diagnostics VITROS Troponin I ES | 12 | 34 | 10 | Yes |
| Abbott Architect 12000 STAT cTNI | 9 | 28 | 14 | Yes |
| Beckman Coulter AccuTNI+3 | 10 | 20 | 14 | Yes |
| Abbott AxSYM ADV | 20 | 34 | 14 | Yes |
| Siemens Dimension RXL TNI | 40 | 70 | 20 | Yes |

**Table 2.** POC troponin assays. Reprinted by permission from Macmillan Publishers Ltd: Nature Reviews Cardiology [53], copyright 2017

| Company and platform or assay | LoD (ng/L) | 99th percentile (ng/L) | CV at the 99th percentile (%) | FDA clearance |
|---|---|---|---|---|
| LSI Medience PATHFAST cTnI | 1-8 | 20 | 5-28 | Yes |
| bioMerieux Vidas | 10 | 10 | 27.7 | Yes |
| Alere Triage Cardio 3 | 10 | 12 | NA | No |
| Philips MiniCare | 18 | 43 | 18.6 | No |
| Abbott i-STAT | 20 | 39 | 16.5 | Yes |

### I.2.iv Point of Care Assays

Point-of-care (POC) testing is defined as laboratory testing in or near the patient location.[15] Advances in technology have permitted the development of POC assays that can be used in the ED. Since the average length of stay in the ED has been increasing particularly for patients from ethnic minorities, there is a clinical interest to reduce it.[54] The implementation of POC tests in medical centers has proven to be very advantageous. It has been demonstrated that POC tests can reduce the length of stay in the ED.[19, 55] EDs that have employed POC testing identify it as necessary to achieve the recommended turnaround time (TAT) requirements.[18, 56] When the worst TAT of the POC device (25 in) is compared to the worst TAT of the laboratory (92 min) an estimated annual bed-minutes savings of $1,209,600 can be calculated.[18] In addition, it has been reported that the introduction of POC devices has reduced the charges to patients by 25%.[57] POC devices, such as the i-Stat cTnI assay, have demonstrated good correlation compared to the core laboratory tests.[9]

The use POC devices has also increased the capacity of both the laboratory and ED without adding staff or equipment.[18] Many POC devices are platforms utilized to perform multiple diagnostic tests by just changing the cartridge. This reduces the training requirements for the nursing staff because they only need to be trained to use the platform where several analytes are measured.

Although POC tests have many potential advantages, such as rapid diagnosis and increased flexibility, there are concerns about their accuracy.[15] Currently, POC tests for cTnI are less sensitive than central laboratories tests, which could limit their use to rule out AMI.[13] Studies that compared the results from POC devices and central laboratories using the same decision limits found that laboratory assays identified about 88% of all patients who died of CV disease during 35 months of follow-up compared with 54% for the POC assays.[13] In addition, the lack of standardization has led to poor correlation and agreement between assays.[19] The ideal POC test for diagnosis of AMI is not available yet;[58] however, as new assays and technologies are developed, they will be able to meet the desired requirements.

### I.2.v Raman Spectroscopy

Raman spectroscopy is a spectroscopic technique used to measure vibrational, rotational, and other low-frequency energy in a system [59]. When light interacts with a molecule it can be absorbed or scattered. The scattered light can be classified as Rayleigh or Raman scattering.[60] They are also known as elastic or inelastic scattering respectively. Rayleigh scattered light has the same frequency of the incident light. In contrast, in Raman scattering the photon exchanges energy with the analyte, which changes the energy of the

scattered photon. This energy interaction can be measured to obtain information about the vibrational modes of the molecule of interest.[61] Raman scattering can also be categorized as Stokes scattering and anti-Stokes scatting (see Figure 4). In stokes scattering, the molecule is in its ground state when the photon interacts with it. At the interaction, energy is transferred to the molecule thus resulting in a higher vibrational energy level.[62] Alternatively, in anti-Stokes scattering, the molecule is already in an excited vibration level when the photon interacts with it. Therefore, energy is transferred from the molecule to the photon at the interaction, causing the molecule to lose energy and return to its ground state.[62] The energy loss or gain during Raman scattering is related to the energies of the vibrational and rotational modes of a molecule.[63]

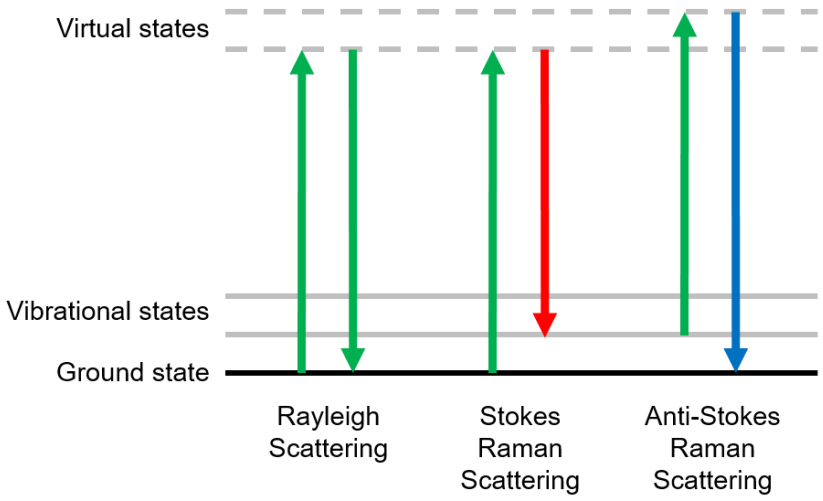


**Figure 4.** Elastic and inelastic scattering. In Rayleigh scattering or elastic scattering no energy is transferred. Stokes scattering and anti-Stokes scattering are inelastic scattering. In inelastic scattering energy is exchanged.

Raman spectral bands can be translated to the vibrational mode they represent.[60] To produce Raman scattering events, polarized monochromatic light is used to excite the molecule. This light distorts the electron cloud surrounding the molecule to an extent

dependent on the electrons ability to polarize. Polarizability is what causes the Raman scattering events.[63] Therefore, vibration modes of molecules are Raman active if they cause a change in polarizability. The number of vibrational modes of a molecule is 3N-6 for non-linear molecules and 3N-5 for linear molecules, where N is the number of atoms.[64] Examples of vibration modes are symmetric stretch, bending mode, and asymmetric stretch. Usually, symmetric vibrational modes cause the largest polarizability and produce the greatest scattering.[63]

Raman scattering is expressed as the change in energy from the exciting radiation and its units are $cm^{-1}$.[63] The intensity of Raman scattering can be defined by using Equation 1, where K is the speed of light, l is the laser power, ω is the frequency of the incident radiation, and α is the polarizability of the electrons in the molecule.

**Equation 1**

$$I = Kl\alpha^2\omega^4$$

Raman spectroscopy is not efficient to detect analytes at trace levels due to the relatively low number of Raman scattered photons compared to the Rayleigh scattered ones. Approximately one in $10^6$ - $10^8$ photons is Raman scattered.[63] Raman scattering is enhanced when small wavelength light is used. However, this light can also cause fluorescence, and broad fluorescent signals of higher intensity can overshadow the Raman signal.[65]

### I.2.vi Surface Enhanced Raman Spectroscopy (SERS)

The Raman scattering signal can be greatly enhanced in the vicinity of metal structures such as gratings, island films or colloids [66]. This enhancement scattering process

is referred as surface enhanced Raman spectroscopy (SERS). The enhancement can be explained by the electromagnetic and chemical mechanisms.

The electromagnetic mechanism explanation to SERS is based on the effect that surface plasmons of a metal have on the incident field intensity.[67] Plasmons can be defined as a collection of free electron gas oscillating at the surface of a dielectric material, such as nanoparticles. Enhancements of less than $10^6$ have been calculated for single nanoparticles.[63] However, when metallic nanoparticles are collected or aggregated, they produce SERS hotspots which can cause greater enhancements, up to $10^{14}$.[68] In this case, the increased electric field occurs at the interface between the nanoparticles. A simple description of the electromagnetic field can be explained with a model of a metallic sphere. When an electromagnetic field is applied to a nanoparticle with a laser, the field at the surface can be approximated with Equation 2.

**Equation 2**

$$\mathrm{Er} = \mathrm{E0}\cos\theta + \mathrm{g}\left(\frac{\mathrm{a}^3}{\mathrm{r}^3}\right)\mathrm{E0}\cos\theta$$

In the expression, Er is the total electric field at a distance r from the sphere surface, a is the radius of the sphere, θ is the angle relative to the direction of the electric field, and g is a constant related to the dielectric constants (see Equation 3).

**Equation 3**

$$\mathrm{g} = \left(\frac{\varepsilon_1(\mathrm{v_L}) - \varepsilon_0}{\varepsilon_1(\mathrm{v_L}) + 2\varepsilon_0}\right)$$

In this equation, $\varepsilon_0$ and $\varepsilon_1$ are the dielectric constants of the medium surrounding the sphere and of the metal sphere respectively. The value $\mathrm{v_L}$ is the frequency of the incident radiation.[63] The value of g will be at a maximum when the denominator is at a minimum.

At the frequency when this occurs, the plasmon resonance frequency, the excitation of the surface plasmon increases the local field on the metal surface. The molecule adsorbed on the metal surface is then immersed in a freely moving electron cloud that intensifies the polarization of its surface electrons, which cause intense Raman scattering. As can be observed in Equation 2, the electric field is inversely proportional to $r^3$. This means that the molecule has to be close to the metallic surface to experience the greatest electric field.[63] The theoretical SERS enhancement factor is the fourth power of the electromagnetic field enhancement at the nanoparticle surface or $E^4$.[69]

Another theory that explains the SERS enhancement is the chemical mechanism. Chemical enhancement occurs when a bond between a molecule and a nanoparticle exists.[63] This bond allows the transfer of charge from the metal surface to the molecule. In this mechanism, electrons or holes can travel to the metal-molecule bond, interact with the molecule causing an increase in the polarizability, and return back to the metal surface.[63] For chemical enhancement to occur, the molecule has to be attached to the nanoparticle surface. Although, evidence suggests that both the electromagnetic and chemical enhancement occur, it is believed that electromagnetic enhancement has a greater effect.[63]

# CHAPTER II

# FUNCTIONALIZATION OF SERS ACTIVE NANOPARTICLES*

## *II.1 Introduction to Nanoparticle Functionalization*

Nanoparticles are particles with a diameter from 1 to 100 nm.[70] There are many types of nanoparticles composed of different materials. Among them, gold and silver are the most common and investigated.[70] Nanoparticles have unique properties, such as biocompatibility, optical, and electronic properties, that make them useful for many applications, including biosensing applications.[71] Specifically, nanoparticles have high surface-to-volume ratio and high surface energy that can help to immobilize biomolecules on them. Some nanoparticles, such as gold NPs, can allow fast and direct electron transfer between electroactive species and electrode materials. Moreover, they have light-scattering properties and a local electromagnetic field that allows them to be used as signal amplification labels in different sensors, such as SERS based sensors.[72] Some nanoparticles can also exhibit magnetic behaviors that can be used to separate or concentrate them in a solution.[71]

Nanoparticles synthesis techniques have been continuously evolving, leading to improvements that have allowed to control their size, shape, and morphology.[70] The ability to manipulate these parameters permits to optimize them in order to meet their application requirements. In addition, the surface and core of the nanoparticles can be modified for

---

* Part of this chapter is reprinted with permission from Garza, J. T.; Cote, G. L. In *Design of Raman active nanoparticles for SERS-based detection*, Proc. of SPIE Vol, 2016; pp 97221B-1. Copyright 2016 Society of Photo Optical Instrumentation Engineers

specific purposes such as bio-recognition, chemical sensing, drug delivery, therapeutics, and imaging.[70-71] Interest in this field has made the development of new protocols to control nanoparticles and make them functional an active research area.[70]

Nanoparticles have been used in numerous assays. They can be conjugated with antibodies, proteins, aptamers, DNA, or many other compounds to be utilized in colorimetric, fluorescent, SPR, ELISA, SERS, and electrochemical based sensors. Several reviews discuss the use of nanoparticles in biosensors.[70-71, 73-74]

**II.1.i SERS Active Nanoparticles**

In order to obtain a SERS signal, a substrate that enhances the spectrum of a Raman active molecule is needed. Numerous SERS substrates have been synthesized to produce high signal enhancement and thus create more sensitive assays. Examples of substrates are silver or gold nanoparticles[75-76], nanocubes[77], nanostars[78], nanorods[79], and other structures.[80] The morphology of these metallic structures can affect the degree of enhancement. Therefore, when the appropriate excitation laser wavelength is used, some substrates are affected more than others. Another way to increase the SERS enhancement is by aggregating the metallic substrates to create hot spots between them. Hot spots are confined regions of intense local field enhancement produced by surface plasmon resonances that usually occur between junctions of metallic structures.[81] Clusters of nanoparticles have been used as SERS substrates, and in order to protect and stabilize the aggregated nanoparticles functionalized with Raman reporter molecules (RRM), they have been encapsulated in silica.[82-83] These silica encapsulated aggregates can also be functionalized with biomolecules to create nanoprobes that can be used in assays.[84]

### *II.2 Nanoparticles and Bioconjugation Approaches Tested*

Different nanoparticles were synthesized to functionalize them and analyze their potential use as assay components. Also, several conjugation approaches were explored to determine the one with best performance according to the selected factors of interest. The stability of the functionalized nanoparticles, the SERS intensity, and the successful conjugation of proteins on the nanoparticles were defined as the factors to be analyzed for each approach. The nanostructures that were synthesized included gold (Au) and silver (Ag) nanoparticles. A Raman reporter molecule was conjugated to make them SERS active, and various PEG linkers were used to conjugate cardiac Troponin I.

## II.2.i Materials and Methods

### *II.2.i.a Materials*

Cardiac Troponin I (cTnI) was purchased from GenScript (NJ, USA). Hetero bifunctional silane-PEG-NHS (5 kDa) and thiol-PEG-NHS (3 kDa) linkers were bought from NanoCS (NY, USA). EDC-HCl and sulfo-NHS were acquired from CovaChem (IL, USA). CA-PEG (441.5 Da) and NHS-PEG-NHS (532.5 Da) linkers were purchased from Thermo Fisher Scientific (MA, USA). Gold chloride trihydrate ($HAuCl_4$), sodium citrate tribasic dihydrate, hydroxylamine hydrochloride, sodium hydroxide, silver nitrate, tetraethyl orthosilicate (TEOS), (3-Aminopropyl)trimethoxysilane (APTMS), ammonium hydroxide (28%), TRIS base, HEPES, 5,5'-Dithiobis(2-nitrobenzoic acid) (DTNB), sodium chloride (NaCl), ethanol, and isopropanol (IPA) were obtained from Sigma Aldrich (MO, USA).

*II.2.i.b Measurements Methods*

Absorbance measurements were acquired on a Tecan microplate reader. TEM images were collected on a FEI Morgagni TEM. A Thermo Scientific DXR Raman confocal microscope with a 780 nm or 532 nm laser was used to measure the SERS signal. The laser power used was varied in different experiments.

*II.2.i.c Gold Colloid Synthesis*

Gold nanoparticles were synthesized based on the method described by Bastus[85] and modified by You[86]. In summary, 335 µL of 25 mM $HAuCl_4$ was added to a 200 mL round bottom three neck flask with 50 mL of boiling 2.2 mM sodium citrate solution. The mixture was stirred and boiled under reflux for 10 min. As the Au NP seeds were formed the color of the solution turned red. The seed solution was cooled to 90° C. Then, 335 µL of 60 mM sodium citrate was added. After 2 min, 335 µL of 25 mM aqueous $HAuCl_4$ was also added. The mixture was left stirring at 90° C for 30 min under reflux.

*II.2.i.d Silver Colloid Synthesis*

Silver nanoparticles were synthesized based on the method described by Leopold and Lendl.[75] Briefly, 1 mL of hydroxylamine hydrochloride ($1.50 \times 10^{-1}$ M) was mixed with 89 mL of sodium hydroxide ($3.33 \times 10^{-3}$ M) under vigorous stirring. Silver nitrate solution (10 mL, $1 \times 10^{-2}$ M) was added drop-wise to the stirring solution. The solution was left stirring for 15 min at room temperature. This nanoparticle solution was then used for the functionalization procedures moving forward as described below.

### II.2.ii Au-RRM-Antigen

The RRM used to make the nanoparticles SERS active is DTNB. DTNB is a molecule that contains a thiol group that binds to gold or silver to form a self-assembled monolayer (SAM) on the surface of the nanoparticles. This molecule also contains a nitro and a carboxyl group. In this conjugation strategy, EDC/NHS chemistry was used to conjugate Troponin I by forming a bond between the carboxyl group of the DTNB and an amine group present in the protein.

*II.2.ii.a Protocol*

To conjugate the proteins 100 µL of 10 mM of DTNB in ethanol was added to 6 mL of Au nanoparticles and incubated overnight. The nanoparticles solution was centrifuged (2000 g, 15 min), redispersed in 2 mL of HEPES (pH 6), and sonicated. Then, 10 µL of EDC (0.019 mM) and 10 µL of Sulfo-NHS (0.047 mM) were mixed and incubated at room temperature for 15 min. The solution was centrifuged, redispersed in 2 mL of HEPES (pH 7.2), and sonicated. After that, 67 µL of the protein solution (672.6 ng/mL) was mixed and incubated for 2 hrs. Finally, the reaction was quenched with 50 mM TRIS, and the nanoparticles solution was washed and redispersed in 2 mL of HEPES (pH 7.2). Figure 5 shows the conjugation schematic.

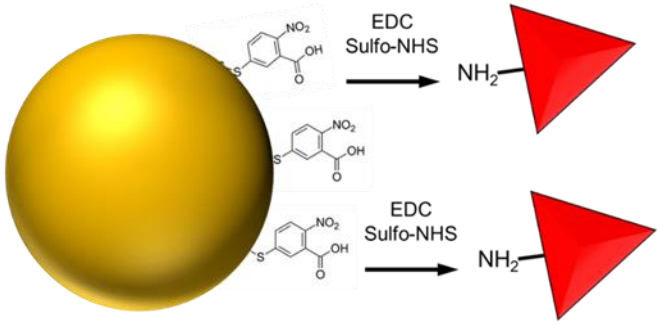


**Figure 5.** Au-RRM-Antigen conjugation strategy. EDC and sulfo-NHS are used to conjugate cTnI to DTNB, which is attached to the Au nanoparticle.

*II.2.ii.b Characterization*

The extinction spectrum of the nanoparticles at each stage of the functionalization process (Au nanoparticles, Au nanoparticles functionalized with DTNB, and Au nanoparticles functionalized with DTNB and troponin I) was measured to examine the degree of aggregation. As can be observed in Figure 6, the Au nanoparticles functionalized with protein exhibit increasing values at high wavelengths. This indicates uncontrolled aggregation as red shifts or increasing extinction values at high wavelengths occur when nanoparticles aggregate. In addition, aggregation was observed by visual inspection.

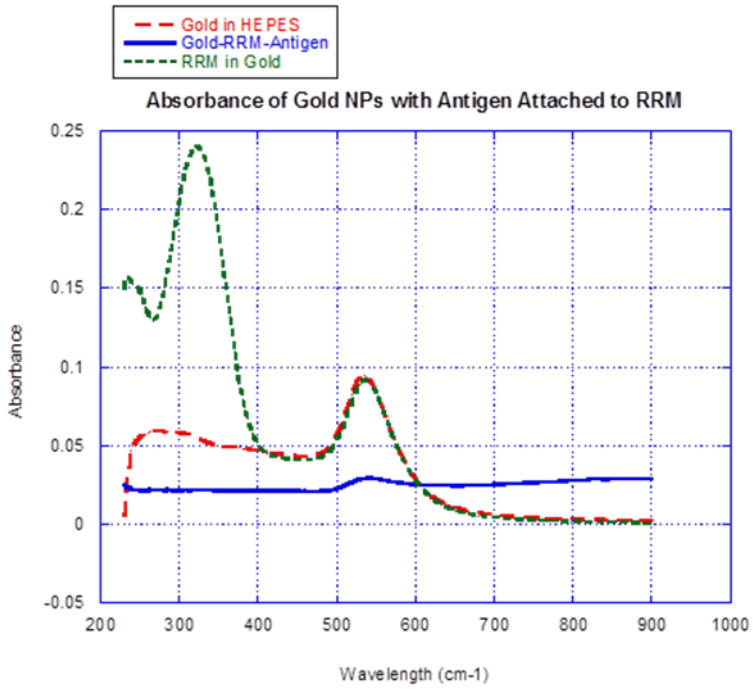


**Figure 6.** Extinction spectrum at different steps of the functionalization process of Au-RRM-Antigen.

A higher amount of troponin I could have been conjugated to prevent instability. In addition, a hydrophilic linker or other stabilizing proteins, such as BSA, could have been introduced to improve stability and prevent aggregation.

### II.2.iii Au-RRM-CAPEG-Antigen

In this conjugation strategy, a hydrophilic PEG linker was used to attach cTnI to the Au nanoparticles functionalized with the reporter molecule DTNB. The 441.5 Da PEG linker (CA-PEG) consisted of an amine functional group in one side and a carboxyl group on the other side. In this case, EDC/Sulfo-NHS chemistry was used to conjugate the carboxyl group of the DTNB molecule with the amine group of the PEG linker. Then, the

cTnI protein was attached to the carboxyl end group of the PEG linker with the same conjugation chemistry.

*II.2.iii.a Protocol*

For the conjugation, 100 µL of 10 mM of DTNB in ethanol was added to 6 mL of Au nanoparticles and incubated overnight. The nanoparticles were washed by centrifugation and redispersion in 2 mL of HEPES (pH 6). Then, 10 µL of EDC (2 mM) and 30 µL of Sulfo-NHS (1.7 mM) were added and incubated at room temperature for 15 min. After washing them and redispersing them in HEPES (pH 7.2), 10 µL of the CA-PEG solution (0.45 mM) was added and incubated for 2 hrs. The free NHS groups were quenched with TRIS, and the nanoparticles were washed three times and redispersed in HEPES (pH 6). EDC (10 µL, 0.019 mM) and Sulfo-NHS (10 µL, 0.047 mM) were added again for the conjugation of the carboxyl groups of the linker with the amine groups of the proteins. Following the EDC and Sulfo-NHS mixing with the nanoparticles, the solution was incubated for 15 min, washed, and 67 µL of protein solution (672.6 ng/mL) was added. After 2 hrs of incubation, the nanoparticles were washed and redispersed in HEPES (pH 7.2). Figure 7 shows the schematic of the conjugation strategy.

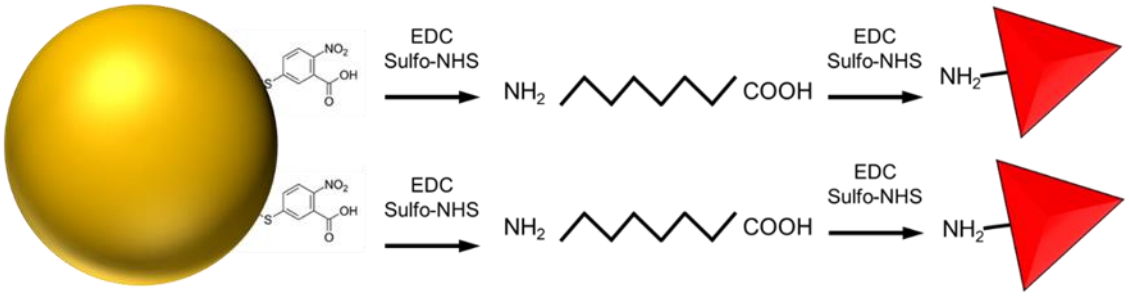


**Figure 7.** Au-RRM-CAPEG-Antigen conjugation strategy. EDC and sulfo-NHS are used to attach DTNB to a PEG linker and the linker to cTnI.

*II.2.iii.b Characterization*

The extinction spectrum was also measured at different stages of the functionalization process to analyze how the original plasmon peak of the gold nanoparticles changes as the protein is conjugated. Figure 8 shows the recorded extinction spectra. As can be observed, this conjugation approach also causes an increase in extinction values at higher wavelengths when protein is attached, which indicates aggregation of the nanoparticles.

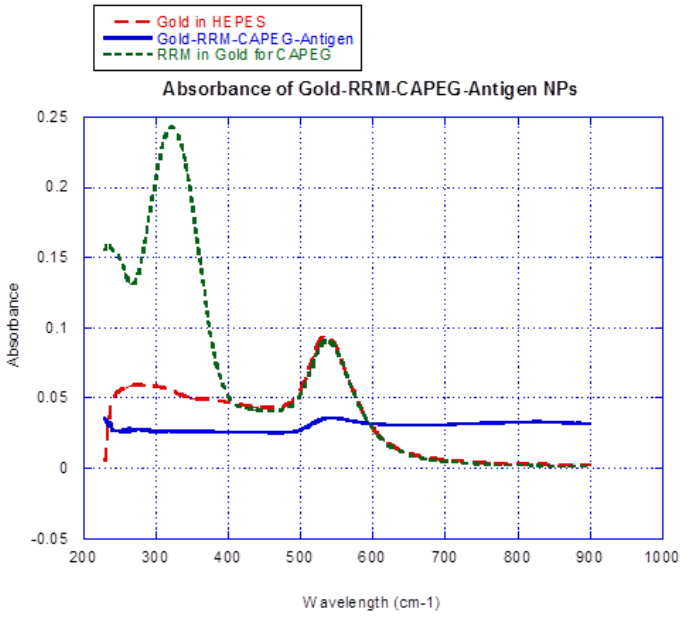


**Figure 8.** Extinction spectrum at different steps of the functionalization process of Au-RRM-CAPEG-Antigen.

For the described protocol, the addition of the hydrophilic PEG linker did not improve the stability of the nanoparticles to prevent aggregation. However, the optimization of different factors, such as the amount and ratios of RRM, PEG linker, and cTnI protein used could improve the stability of the nanoparticles to prevent aggregation.

### II.2.iv Au-RRM-PEG-Antigen

Another functionalization approach was tested in which the RRM and a PEG linker were also used. However, in this case the PEG linker was not attached to the DTNB molecule. In this functionalization strategy, a thiol-PEG-NHS linker was used to conjugate it with the Au nanoparticles directly through the thiol-Au reaction. Then, the cTnI protein was conjugated through the reaction of the amines present in the protein with the NHS of the linker.

*II.2.iv.a Protocol*

To functionalize the Au nanoparticles 21.4 µL of the thiol-PEG-NHS linker (0.6 mM) and 40 µL of DTNB in ethanol (10 mM) were mixed with 1 mL of nanoparticles. The solution was vortexed, and citrate buffer (60 µL, 250 mM) was also added to improve the conjugation efficiency. After 30 minutes, the nanoparticles solution was centrifuged and redispersed in 100 µL of HEPES (pH 7.5). Subsequently, 100 µL of cTnI (10 µg/mL) and 10 µL of CAPEG linker (0.12 mM) were added to react with all the free NHS groups. The solution was incubated for 30 min, washed two times and redispersed in HEPES buffer. Figure 9 demonstrates the conjugation strategy.

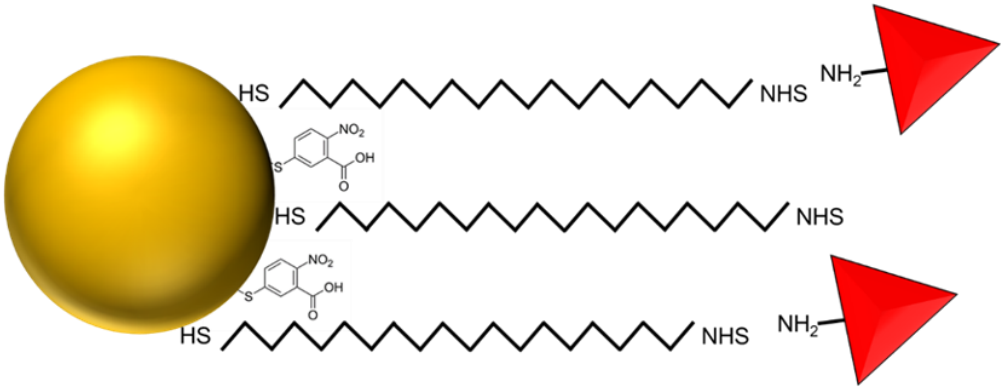


**Figure 9.** Au-RRM-PEG-Antigen conjugation strategy. DTNB and a PEG linker attach to the Au nanoparticle through their thiol group. Then, cTnI is attached to the linker.

*II.2.iv.b Characterization*

The extinction spectrum of the nanoparticles was measured before and after the conjugation of the PEG linker and protein, as can be observed in Figure 10. In this case, both spectra had the same shape, and the spectrum of the functionalized nanoparticles did not exhibit an increase in extinction values at higher wavelengths. This suggests that the nanoparticles did not aggregate after conjugating cTnI. Nevertheless, after functionalization, the nanoparticles were sticking to the walls of the microtube (inset of Figure 10). The loss of nanoparticles due to washing steps and sticking to the wall caused a decrease in nanoparticle concentration, which subsequently resulted in a spectrum of lower extinction values than the spectrum of the Au nanoparticles stock solution.

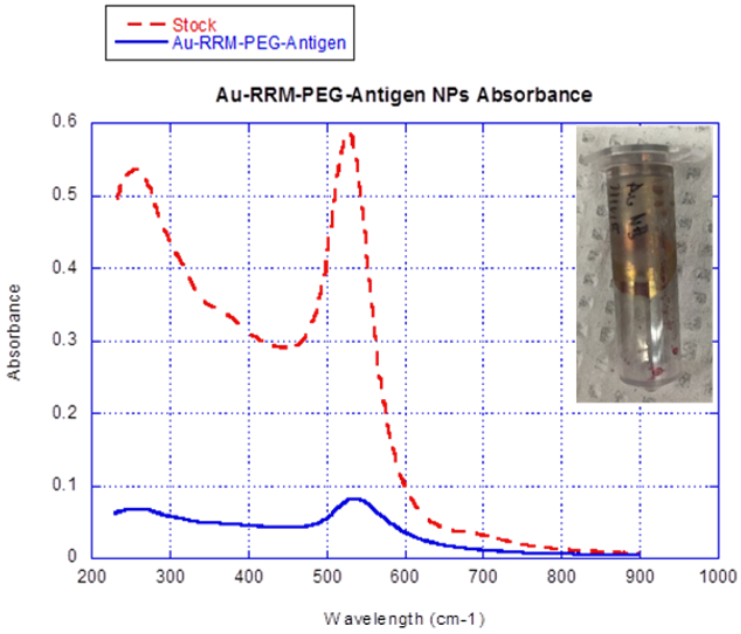


**Figure 10.** Extinction spectrum at different steps of the functionalization process of Au-RRM-PEG-Antigen. Inset: Nanoparticles sticking to the walls of the microtube.

The nanoparticles sticking to the wall of the microtube could have been caused by the hydrophobic nature of the cTnI protein attached.[87] The addition of BSA or Tween 20 could have been used to reduce nonspecific binding and improve the stability of the nanoparticles.

### II.2.v Au-RRM-Silica-PEG-Antigen

An alternative functionalization approach was tested to make the nanoparticles SERS active and attach the protein of interest. In this case, the RRM formed a SAM around the nanoparticles to cover them completely. Then, the nanoparticles functionalized with DTNB were aggregated and encapsulated in silica. An NHS-PEG-NHS linker was used to conjugate the cTnI protein to the silica nanoparticles.

*II.2.v.a Protocol*

Specifically, 50 µL of DTNB in ethanol (10 mM) was mixed with 1 mL of Au nanoparticles and incubated overnight. Then, the nanoparticles were washed two times and redispersed in 2 mL of ethanol. APTMS (10 µL, 0.001% in ethanol) was added and incubated for 10 min to form a thin layer of silica around the nanoparticles. The nanoparticles were washed and redispersed in 1000 µL IPA, 360 µL DI water, and 24 µL ammonium hydroxide (28%). After sonication, 10 µL of TEOS (1% in IPA) was added three times in an interval of one hour under stirring. The nanoparticles solution was incubated overnight under stirring, washed the next day, and redispersed in 2 mL of ethanol. Subsequently, 5 µL of APTMS (0.001% in ethanol) was added and incubated for 30 min to introduce amine groups on the surface of the silica nanoparticles. The nanoparticles were washed two times, and redispersed in 2 mL of ethanol. Then, 5 µL of the NHS-PEG-NHS linker (90 mM) was added and incubated for 30 min. The solution was washed two times and redispersed in HEPES buffer. The protein cTnI (45 µL, 30 nM) was introduced for conjugation, incubated for 30 min, quenched with TRIS buffer (1 M) and washed to redisperse it in 2 mL of HEPES. Figure 11 shows the conjugation schematic.

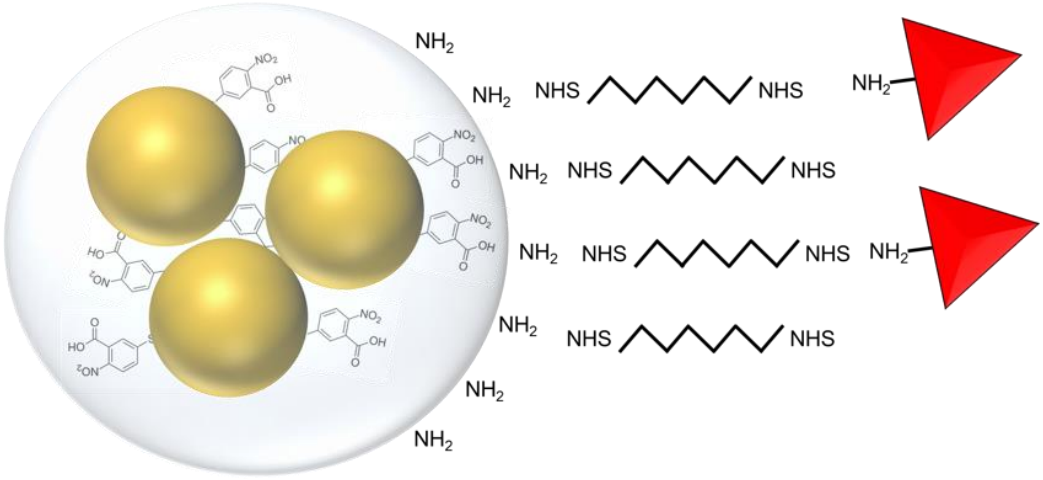


**Figure 11.** Au-RRM-Silica-PEG-Antigen conjugation strategy. Au nanoparticles are functionalized with DTNB, aggregated, and encapsulated in silica. An NHS-PEG-NHS linker is then used to conjugate cTnI to the silica surface through their amine groups.

*II.2.v.b Characterization*

The extinction spectrum at different stages of the functionalization process was measured to analyze the aggregation and stability of the nanoparticles. In this case, as can be observed in Figure 12, the aggregation of the nanoparticles encapsulated in silica resulted in an extinction spectrum with two localized surface plasmon resonance (LSPR) peaks. This occurred because the LSPR peaks are related to the interparticle gap distance, which changes as the nanoparticles aggregate. A main advantage of this conjugation method is the protection that the silica shell provides to the functionalized nanoparticles. In addition of preventing the binding of molecules other than the RRMs, the silica shell immobilizes the controlled aggregates. The silica surface also provides flexibility for further conjugation methods since it can be treated to add the desired functional groups.

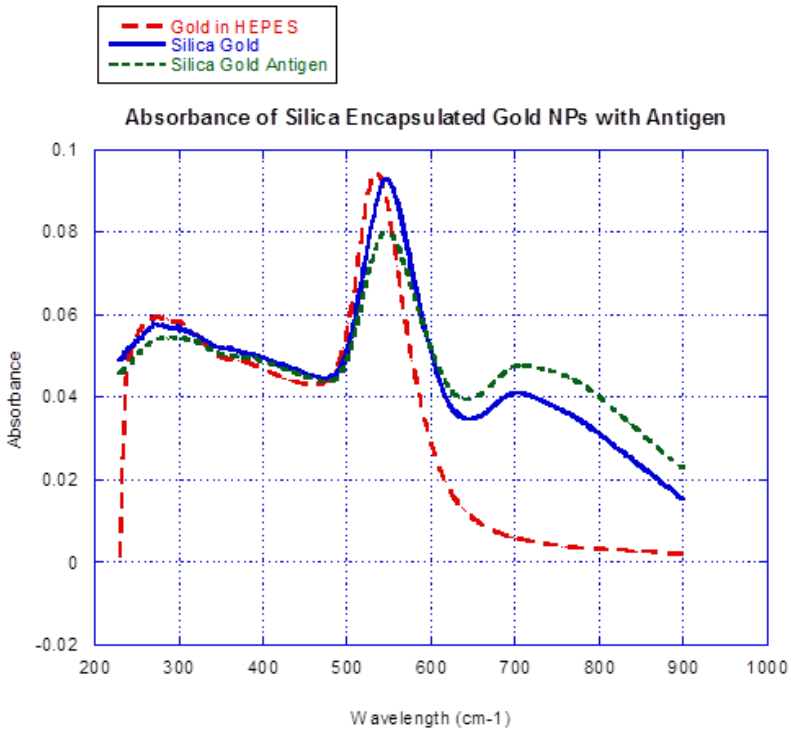


**Figure 12.** Extinction spectrum at different steps of the functionalization process of Au-RRM-Silica-PEG-Antigen. The second peak indicates controlled aggregation.

Even though the nanoparticles were aggregated in a relatively controlled manner inside the silica shell, the silica encapsulated nanoparticles functionalized with cTnI were not very stable. A couple hours after functionalization, they tended to agglomerate and it was difficult to redisperse them. The addition of BSA or Tween 20 could have improved the stability of the nanoparticles by blocking free spaces and preventing non-specific binding.

### II.2.vi Nanoparticles SERS Intensity Comparison

The SERS spectra of the stock solutions of the Au nanoparticles functionalized with different methods were measured and compared. Factors that can affect the SERS intensity of SERS active substrate solution include: type of substrate, concentration,

degree of aggregation, and amount of RRM on the substrate. In Figure 13 the intensities of the spectra can be compared. As can be observed, the spectrum of the silica encapsulated nanoparticles exhibited the highest intensity. This occurred because the nanoparticles were aggregated inside the silica, and hotspots or regions of intense local field enhancement were created between the junctions of the metallic nanoparticles. The SERS signal increases with increasing number of hotspots. The nanoparticles functionalized with methods that indicated aggregation in their extinction spectra (two approaches in which the antigen was attached to the RRM) had lower SERS intensity than the silica encapsulated nanoparticles but higher intensity than the method which did not indicate aggregation in its extinction spectrum (approach in which thiol-PEG-NHS linker was used). The lack of aggregation and the lower amount of RRM on each nanoparticle prevented the method with the lowest intensity (Au-RRM-PEG-Antigen) to have high SERS intensity.

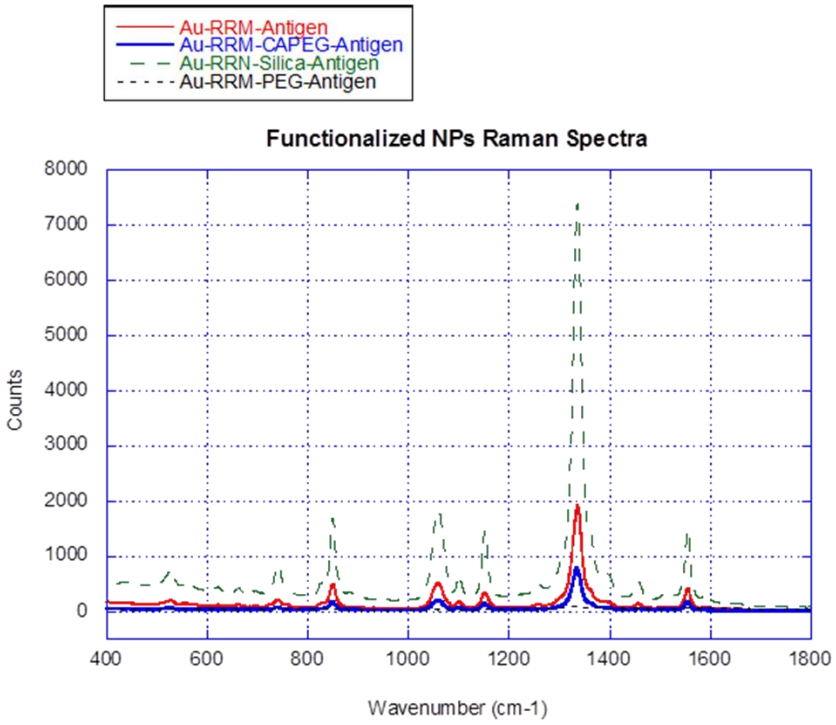


**Figure 13.** SERS signal of Au nanoparticles functionalized with cTnI by using different strategies. Au-RRM-Silica-PEG-Antigen exhibited the greatest SERS signal.

The volume used to measure the SERS spectra was 30 µL. However, it is important to note that the concentrations of the stock solutions were different. The stability of the functionalized nanoparticles caused some particles to stick to the wall; as a result, nanoparticles were lost and the concentrations decreased for some approaches. Even though the concentrations were not the same for the functionalization approaches, the analysis provided useful information. The comparison of the extinction spectra, the visible inspection of aggregates in solution, and the SERS spectra of the different Au nanoparticles allowed to identify the approach that exhibited higher stability when a

protein was conjugated and estimate the one that produces higher SERS intensity, which was the silica encapsulated nanoparticles.

### II.2.vii Ag-RRM-Silica-PEG-Antigen

Silver nanoparticles were synthesized to test them as SERS substrate and determine if they induce a greater enhancement than gold. The functionalization approach that resulted in the highest SERS signal when the different methods were compared was used to functionalize the Ag nanoparticles. Ag nanoparticles were encapsulated in silica, conjugated with cTnI, and characterized. The SERS signal obtained when Ag nanoparticles were used was compared to the signal obtained with Au nanoparticles.

The functionalization protocol was very similar to the protocol of the silica encapsulated Au nanoparticles described before. However, in this case Ag nanoparticles were used and more protein was conjugated. Figure 14 shows the functionalization strategy of the Ag nanoparticles.

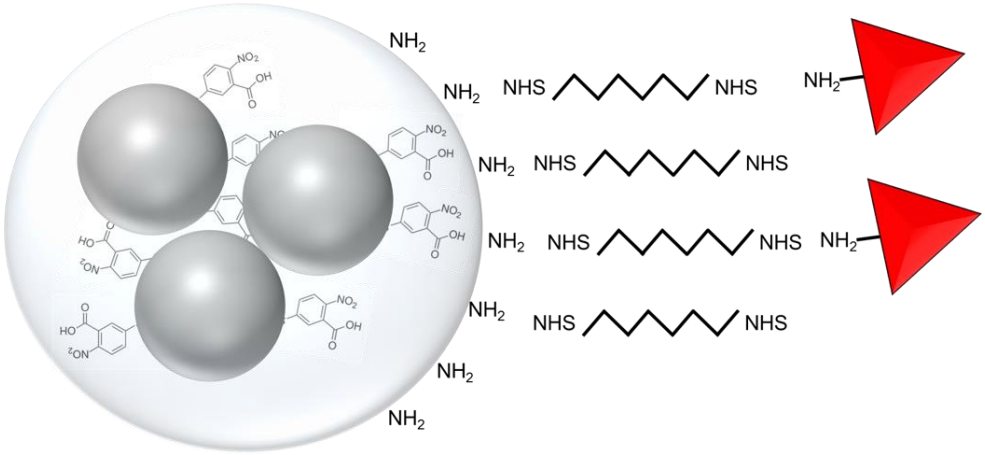


**Figure 14.** Ag-RRM-Silica-PEG-Antigen functionalization strategy. Ag nanoparticles are functionalized with DTNB, aggregated, and encapsulated in silica. Then, an NHS-PEG-NHS linker is used to conjugate cTnI to the silica surface through their amine groups.

TEM images of the nanoparticles were taken to inspect their morphology and the silica encapsulation. As can be observed in Figure 15, the Ag nanoparticles were successfully encapsulated in silica, which can be noticed around them. The number of nanoparticles aggregated inside the silica shell was not very consistent. Monomers, dimers, trimers, tetramers, and larger aggregates were formed in the same batch.

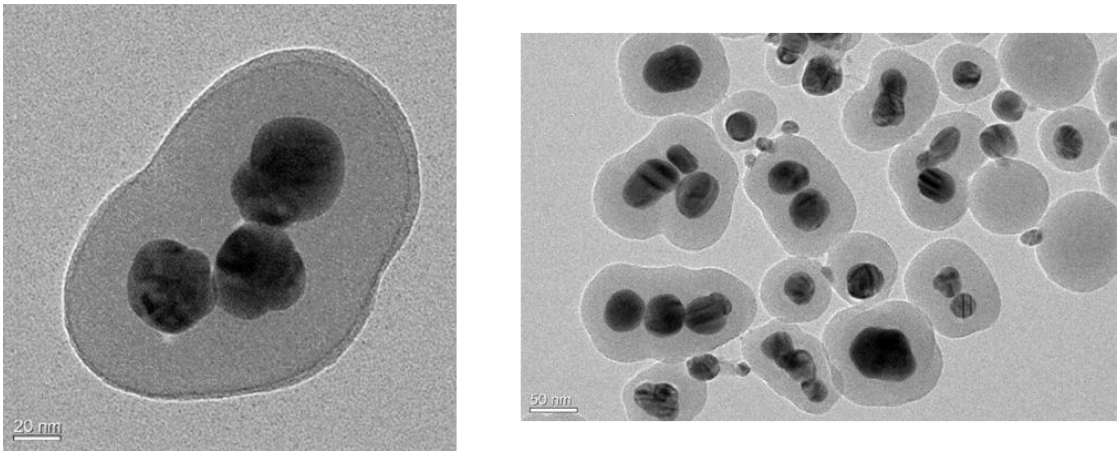


**Figure 15.** TEM images of Ag nanoparticles encapsulated in silica.

The extinction spectrum of the nanoparticles was measured before and after encapsulation. The plasmon peak of the Ag nanoparticles was around 410 nm, as can be seen in Figure 16. After encapsulation, it the extinction spectrum changed, similar to the Au nanoparticles case, to show a second plasmon peak. The second peak indicated that the nanoparticles were aggregated. The size of the nanoparticles was also measured with a Nanosight NTA (Malvern) instrument, and the mean size was determined to be 62 nm for the Ag nanoparticles and 117 nm after they were encapsulated.

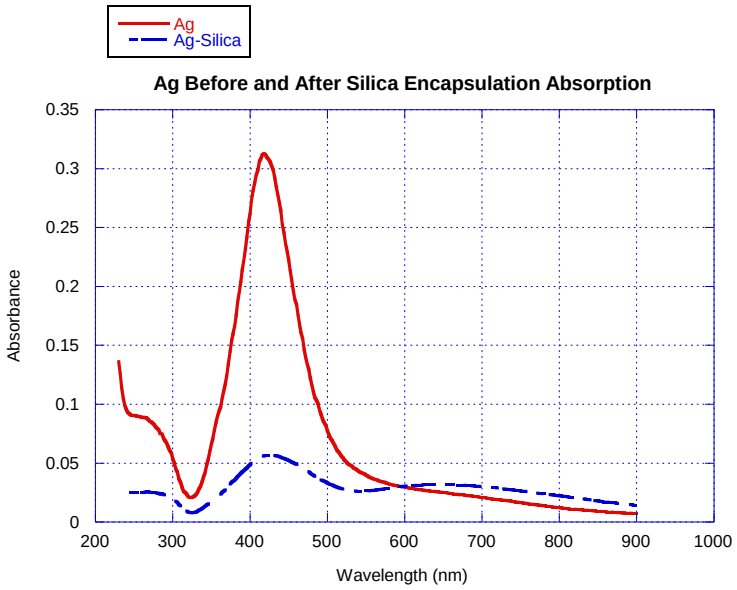


**Figure 16.** Extinction spectrum of Ag and Ag-RRM-Silica. The second peak of the Ag-RRM-Silica spectrum (at approximately 670 nm) indicates controlled aggregation.

The SERS spectrum of Ag functionalized nanoparticles was measured to compare it to the spectrum of Au functionalized nanoparticles. A 780 nm laser (5 mW) was used to take the measurements, and the same volume of similar concentrations of nanoparticles ($4.7 \times 10^{-11}$ M for 40 nm silver nanoparticles and $3.7 \times 10^{-11}$ M for 60 nm gold nanoparticles) was tested. Figure 17 shows the SERS spectra obtained for the two types of nanoparticles used. As can be noted, using Ag nanoparticles resulted in greater SERS signal, about 7 times higher intensity than the Au nanoparticles at 1338 $cm^{-1}$. This result suggests that higher intensities will be obtained at low concentrations if Ag nanoparticles are used, which is desirable for the design of SERS based biosensors that require high sensitivity and low limits of detection.

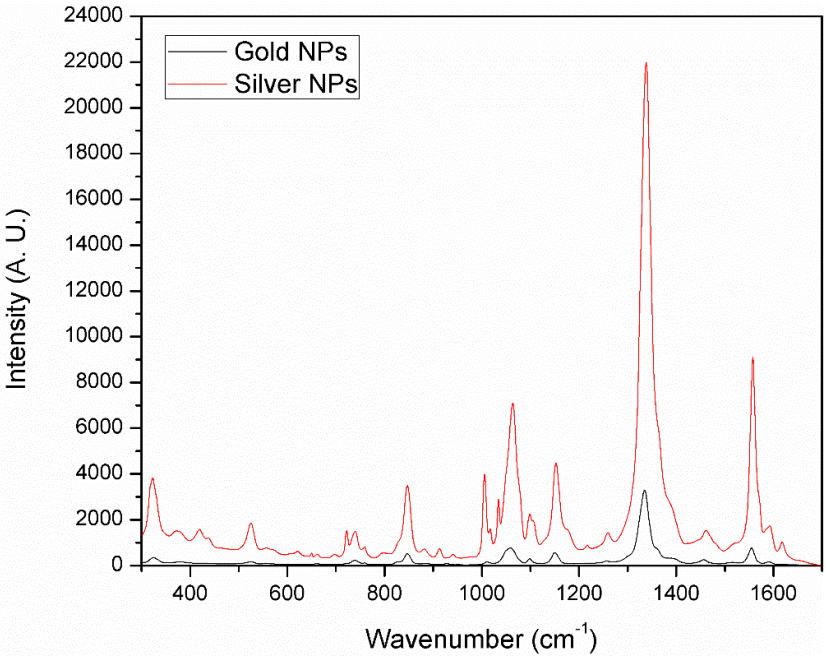


**Figure 17.** SERS signal comparison between functionalized Au and Ag nanoparticles. The use of Ag nanoparticles produced the greatest SERS signal.

### *II.3 SERS Nanoprobe*

After testing different methods of functionalizing nanoparticles to make them stable and SERS active, the approach in which Ag nanoparticles were encapsulated in silica was selected. This functionalization method produced stable nanoparticles with high SERS intensity and the ability to be conjugated with the proteins of interest. In this case, cTnI was conjugated to silica encapsulated Ag nanoparticles, which can be referred as nanoprobes, to analyze if they could be used in assays.

The first versions of the nanoprobe employed the NHS-PEG-NHS linker to attach proteins on the amine active surface of the silica nanoparticles. However, this method resulted in agglomeration of nanoparticles when the functional groups of a linker reacted with amine groups of different nanoparticles. The linker had to be added in excess to

prevent this from happening. To have more control of the amount of linker conjugated on each nanoparticle and avoid crosslinking, the linker silane-PEG-NHS was utilized. The surface of the silica nanoparticles did not have to be amine modified to use this linker, which was another advantage since it increased the stability of the nanoparticles. Figure 18 shows the nanoprobe functionalization strategy.

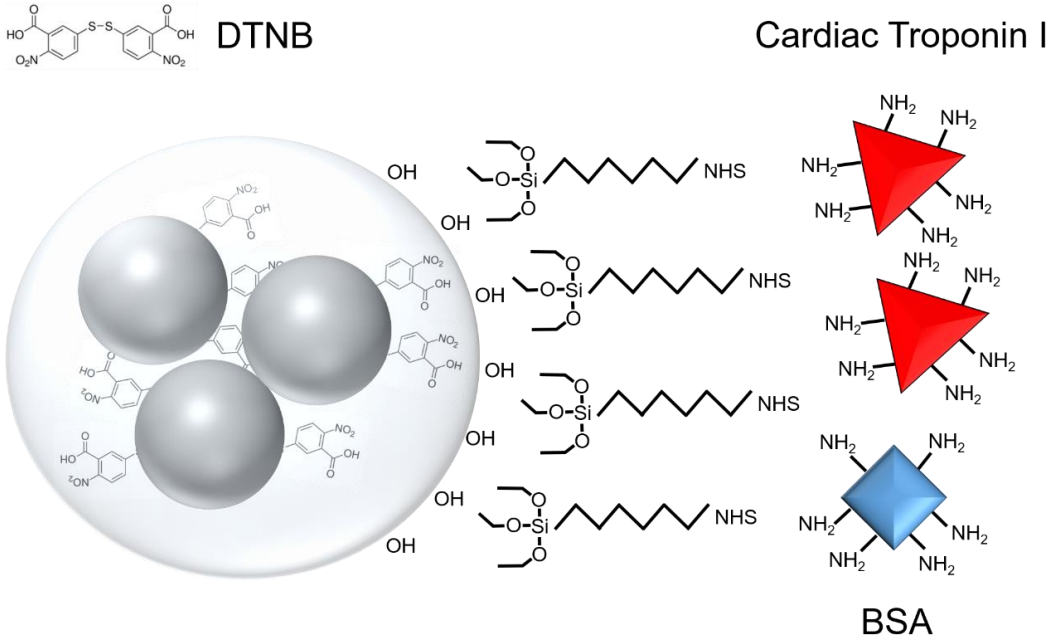


**Figure 18.** Nanoprobe functionalization strategy. Ag nanoparticles were functionalized with DTNB, aggregated, and encapsulated in silica. A silane-PEG-NHS linker was used to attach cTnI to the silica surface.

## II.3.i Materials and Methods

### *II.3.i.a Materials*

Cardiac Troponin I (cTnI) was purchased from GenScript (NJ, USA). Hetero bifunctional 5 kDa PEG linker (Silane-PEG-NHS) was bought from NanoCS (NY, USA). The troponin I (human cardiac specific) enzyme immunoassay test kit was obtained from

GenWay (CA, USA). Hydroxylamine hydrochloride, sodium hydroxide, silver nitrate, tetraethyl orthosilicate (TEOS), (3-Aminopropyl)trimethoxysilane (APTMS), ammonium hydroxide (28%), gold(III) chloride trihydrate ($HAuCl_4$), Bovine Serum Albumin (BSA), TRIS base, Tween 20, 5,5'-Dithiobis(2-nitrobenzoic acid) (DTNB), sodium chloride (NaCl), sodium phosphate, glycerol, ethanol, and isopropanol (IPA) were obtained from Sigma Aldrich (MO, USA).

The size and concentration was measured with a Nanosight NTA (Malvern). The zeta potential was measured on a Zetasizer Nano (Malvern). Absorbance measurements were acquired on a Tecan microplate reader. TEM images were collected on a FEI Morgagni TEM and SEM images on a JEOL JSM-7500F. A Thermo Scientific DXR Raman confocal microscope with a 532 nm laser was used to measure the SERS signal. Samples were excited with 2 mW, an exposure time of 1 s, and 5 exposures per reading. The estimated wavenumber resolution was approximately 5.4 $cm^{-1}$ FWHM.

*II.3.i.b Colloid Synthesis*

As described earlier, silver nanoparticles were synthesized based on the method described by Leopold and Lendl.[75] Briefly, 1 mL of hydroxylamine hydrochloride (1.50 x $10^{-1}$ M) was mixed with 89 mL of sodium hydroxide (3.33 x $10^{-3}$ M) under vigorous stirring. Silver nitrate solution (10 mL, 1 x $10^{-2}$ M) was added drop-wise to the stirring solution. The solution was left stirring for 15 min at room temperature. This nanoparticle solution was then used for the functionalization procedures moving forward as described below.

*II.3.i.c Silica Encapsulation*

The procedure to encapsulate the nanoparticles was based on the method described by Schütz.[88] First, DTNB (250 µL, 1 x $10^{-2}$ M) was added to 5 mL of the synthesized silver nanoparticles to form a self-assembled monolayer (SAM) on the nanoparticles. After overnight incubation at room temperature, the nanoparticles were separated into five microtubes of equal volumes, centrifuged (2700 g, 15 min), redispersed in ethanol (900 µL) and water (65 µL), and combined in a single tube. In order to aggregate the nanoparticles and form hotspots, NaCl solution was added (175 µL, 2 x $10^{-2}$ M), incubated for 30 min, and sonicated. Subsequently, 50 µL of APTMS (0.001% in ethanol) was added to the nanoparticles and incubated for 10 min. After incubation, the nanoparticles were separated into five microtubes, centrifuged, redispersed in a mixture of IPA (1000 µL), DI water (360 µL), and ammonium hydroxide (25 µL, 28%), sonicated for 10 min, and combined in a single tube. Then, 50 µL of TEOS (1% in IPA) was added, and the sample was placed on a stirring rotator. After 30 min, an additional 25 µL of TEOS was added. The nanoparticles solution was left reacting overnight at room temperature in the rotator. Afterwards, they were centrifuged and redispersed in 1 mL of ethanol. Figure 19 shows the nanoprobe synthesis approach.

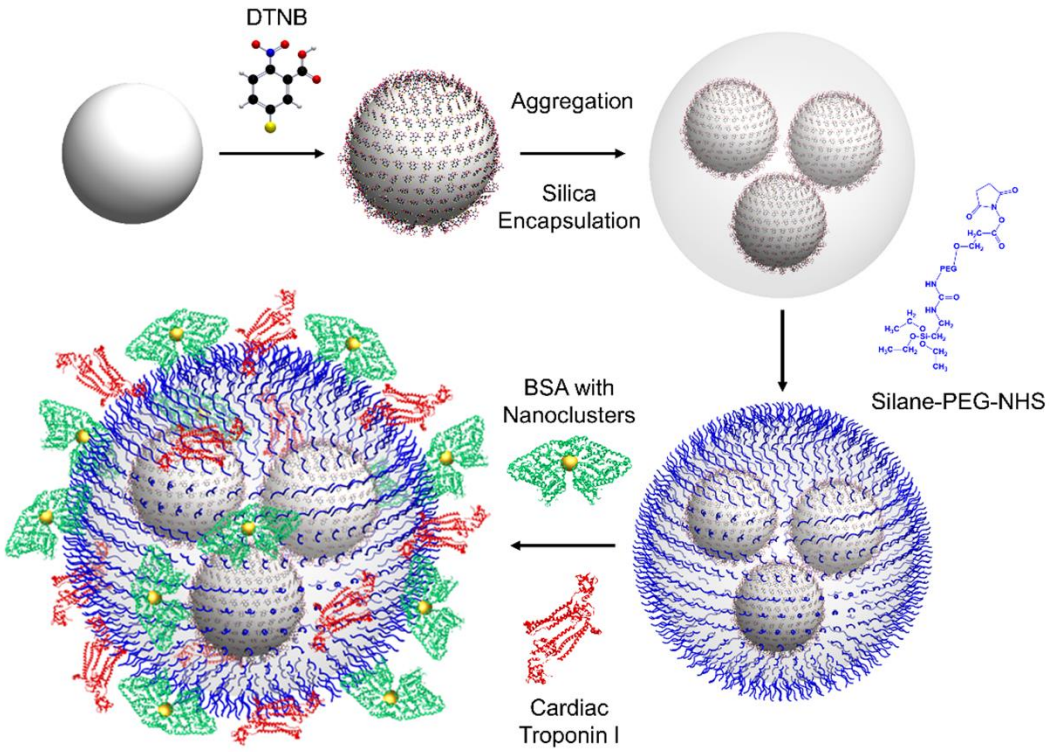


**Figure 19.** Nanoprobe synthesis stages. Ag nanoparticles are created. DTNB was added to form a SAM on the nanoparticles. The nanoparticles were aggregated and encapsulated in silica. After silica encapsulation, a silane-PEG-NHS linker is used to conjugate cTnI and BSA with nanoclusters.

*II.3.i.d Differential Centrifugation*

To decrease the polydispersity of the silica encapsulated nanoparticles, they were separated with a continuous density gradient centrifugation method described by Steinigeweg.[89] In brief, five different glycerol-water mixtures were prepared (30, 35, 40, 45, and 50 vol % glycerol). After preparation, 2 mL of each solution was stacked carefully on top of each other with a syringe starting with the 50 % mixture at the bottom of a 15 mL tube. After stacking all the mixtures, the tube was gently tilted horizontally for 5 min to form a continuous gradient and centrifuged at 2500 g for another 5 min. The silica

encapsulated nanoparticle solution (300 µL) was added on top of the gradient and centrifuged at 2500 g for 45 min. After centrifugation, the gradient solution was separated in sections by extracting about 2 mL for each section. The nanoparticles in each section were washed three times and redispersed in ethanol (200 µL). Two more gradients were used to separate 600 µL of the silica nanoparticles solution. After washing all the sections, the size of the silica encapsulated nanoparticles in each section was measured with the NTA. The sections with nanoparticles of similar size (89 - 90 nm) were combined to form the solution used for further functionalization.

*II.3.i.e Preparation of BSA with Nanoclusters*

BSA nanoclusters were made based on the method described by Xie.[90] In brief, 1 mL of BSA solution (50 mg/mL in water) was prepared and 1 mL of $HAuCl_4$ ($1 \times 10^{-2}$ M) was added under stirring. After two minutes, 100 µL of NaOH (1 M) was added, and the solution was incubated at 37 °C for 12 h. The BSA nanoclusters were washed three times with a Nanosep centrifugal device (Pall Corporation) and resuspended in 1 mL of PBS buffer (pH 7.4).

*II.3.i.f Protein Conjugation*

The heterobifunctional linker silane-PEG-NHS was used to conjugate cTnI and BSA on the nanoparticles. Cardiac troponin I was conjugated on the nanoparticles to give them functionality (similar to the one described by Chon[91]) and to examine its activity after conjugation; however, it can be replaced by any other protein or antibody. To conjugate the proteins silane-PEG-NHS (440 µL, $4 \times 10^{-4}$ M in ethanol/water 95%/5%) was added to 1 mL of the silica encapsulated nanoparticles obtained after the differential

centrifugation step. After reacting for 1 h, the nanoparticles were washed 3 times using a three step process of centrifugation (2000 g, 15 min), redispersion in sodium phosphate (400 µL), and sonication. This solution was added to a mixture of BSA nanoclusters (23 µL) and 10 µg of cTnI. An additional 40 µL of BSA nanoclusters solution was added after 15 min, and the reaction was incubated for 2 h at room temperature. TRIS buffer (550 µL, $2 \times 10^{-2}$ M, pH 7.5) and Tween 20 (5 µL, $8.9 \times 10^{-2}$ M) were added afterwards to quench any reactive groups left. Lastly, the nanoprobes were washed 2 times using centrifugation (900 g, 10 min), redispersion in 1 mL of TRIS and 5 µL of Tween 20, and gentle mixing.

**II.3.ii Characterization**

TEM images of the nanoprobe were collected to analyze and verify the aggregation of silver nanoparticles, silica encapsulation, and the attachment of BSA-nanoclusters. BSA-nanoclusters were used as stabilizers to block spaces after conjugating the antigen and avoid nonspecific binding. In addition, the nanoclusters on the BSA were used as markers to identify the BSA conjugated around the nanoprobes on the TEM images. Figure 20 shows the comparison of the nanoprobes before (A and B) and after attaching cTnI and the BSA-nanoclusters (C and D). As can be noted, nanoclusters surround the silica nanoparticles indicating the attachment of BSA.

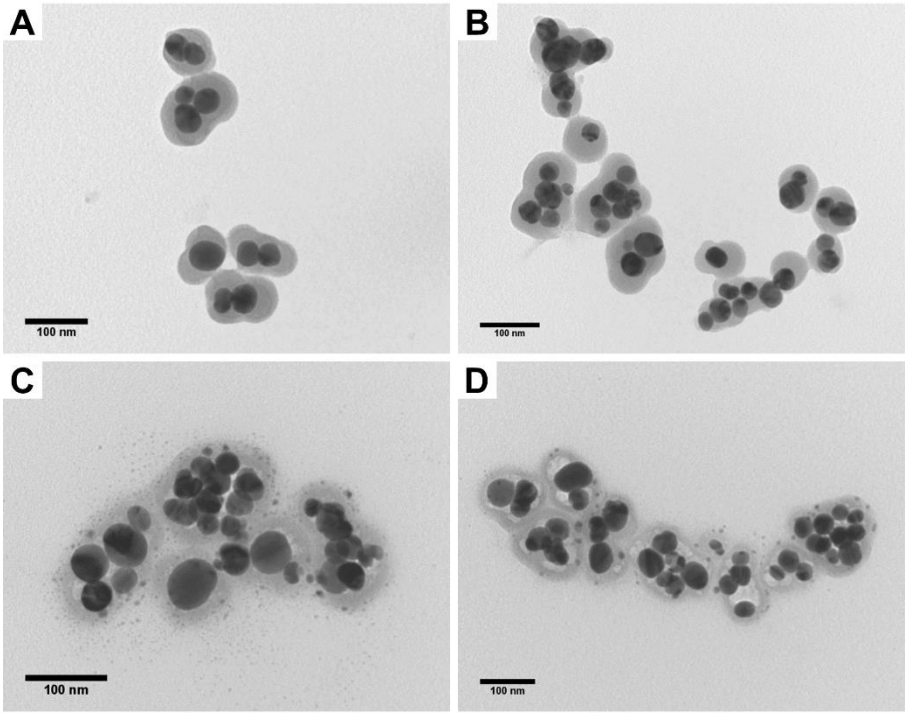


**Figure 20.** (A), (B): TEM images of aggregated Ag nanoparticles encapsulated in silica. (C), (D): TEM images of the silica encapsulated nanoparticles functionalized with cTnI and BSA nanoclusters (observed around the silica shell).

The images also indicate that the nanoprobes are composed of different number of aggregated silver nanoparticles encapsulated in a silica shell with a thickness of approximately 20 nm. The nanoparticles were purposely aggregated to create hot spots between them and make a nanoprobe with a high enhancement factor. Aggregating the nanoparticles with NaCl resulted in variations in the amount of aggregation with nanoprobes containing different numbers of nanoparticles. A glycerol-based differential centrifugation method was used to separate the silica encapsulated nanoparticles with similar weight and reduce the level of polydispersity. However, after differential centrifugation, the collected silica encapsulated nanoparticles still exhibited some degree

of polydispersity with different numbers of aggregated nanoparticles. The resulting degree of polydispersity was not expected to cause inconsistent SERS signal per nanoprobe since it has been reported that in a nanoparticle cluster only one hotspot usually dominates the enhancement and the extra hotspots do not contribute significantly to the SERS signal.[92] The size of the nanoprobe was monitored at different steps of the functionalization process with the NTA as shown in Figure 21. The silver nanoparticles had a mean diameter of 57 nm. These nanoparticles were aggregated and encapsulated in silica. The mean size of these silica nanoparticles was 92 nm. A 5 kDa PEG linker was attached to the silica to link the proteins to the nanoprobe, which increased the nanoprobe overall mean size by 19.5 nm, or rather, the shell thickness by 9.75 nm. The length of a 5 kDa PEG chain on nanoparticles in a brush conformation has been reported to be 9.8 nm[93], which agrees with the results obtained. Finally, conjugating the proteins increased the mean size of the nanoprobe by 13.74 nm to have a final size of 124.8 nm. The increase in thickness of 6.87 nm after adding the proteins is also very similar to the hydrodynamic diameter of 7.4 nm that has been reported for BSA.[94] The standard deviations on each step indicated the level of polydispersity in the nanoprobe size. However, the mean size increases at each step validate the successful functionalization of the nanoprobes.

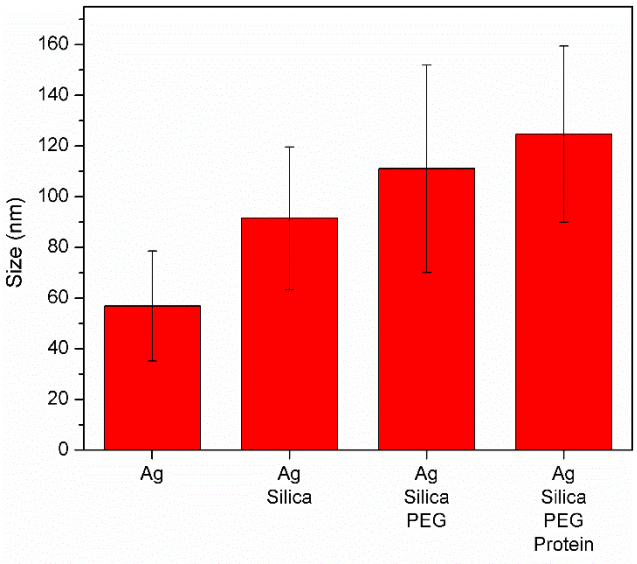


**Figure 21.** Average diameter and standard deviation at different stages of the nanoprobe synthesis process.

The extinction spectrum was also measured at each step to determine the localized surface plasmon resonance (LSPR). The LSPR is related to the aggregation state and the interparticle gap size between nanoparticles.[92] Therefore, the appearance of peaks in the LSPR spectrum can be used as an indication that the nanoparticles are in close proximity or aggregated. Figure 22 shows the different UV/VIS spectra. The silver nanoparticles used had a single extinction peak at 416 nm. However, after the nanoparticles were aggregated a second peak around 575 nm was formed. The overall extinction values decreased after adding PEG and conjugating the proteins because the concentration of the nanoprobes solution decreased as particles were lost in the washing steps. Nevertheless, the two peaks were still observed after completion of all steps in the functionalization process indicating the stability of the silica encapsulated aggregates.

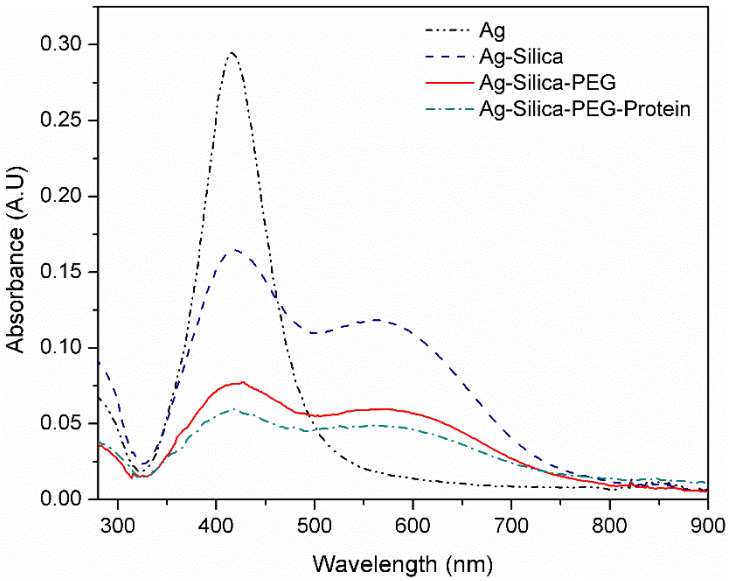


**Figure 22.** Extinction spectrum at different stages of the nanoprobe synthesis process. The second peak (at approximately 575 nm) indicates controlled aggregation.

The zeta potential of the nanoprobe was measured to determine its surface charge at different stages of the functionalization process. This information was used to examine the nanoprobe electrostatic stability and to confirm that the surface was modified. As can be observed in Figure 23, the charge of the silver nanoparticles increases from -41 mV to -31 mV when they are encapsulated in silica. After attaching the PEG linker, the charge further increases to -20 mV, which can be attributed to the charge of the linker reactive group on ethanol before it reacts with a protein. After the proteins react with the functional groups, the charge decreases to its final value. The stability of a nanoparticle usually depends on a combination of electrostatic and steric effects, and it can be referred to as electrosteric stability.[95] The use of a 5 kDa PEG linker and the attachment of cTnI and BSA served as steric stabilizers. The final zeta potential of the nanoprobe in a TRIS buffer

solution (pH 7.5) was -34 mV. This surface charge suggests the nanoprobe was electrosterically stable.

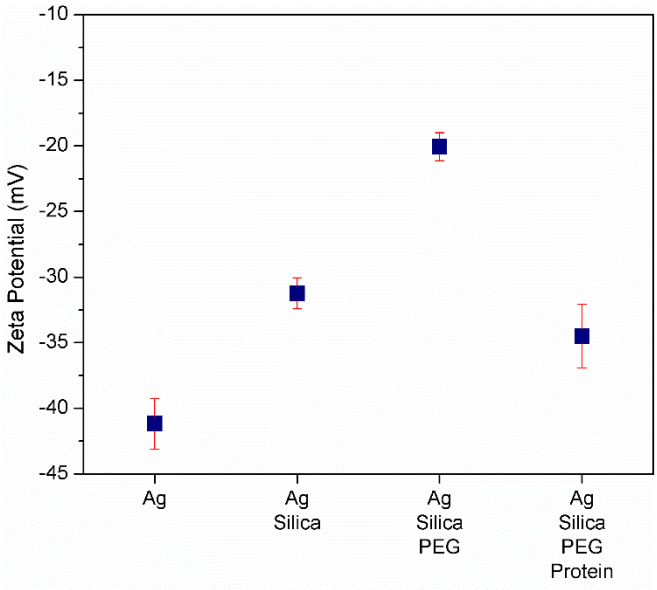


**Figure 23.** Zeta potential at different stages of the nanoprobe synthesis process.

A cardiac Troponin I ELISA kit was used to confirm that the conjugated cTnI can react with its antibodies after it is attached to the nanoprobe. The test also allowed approximation of the amount of cTnI proteins conjugated on a nanoprobe. Figure 24 shows the kit standard curve and the measured cTnI concentration when 100 µL of 2.81 pM and 5.63 pM of nanoprobe was tested. The kit measurements and approximate calculations, using 26 kDa as the cTnI molecular weight, indicate there were an average of 112 cTnI proteins per nanoprobe (see SI for calculations). It should be noted that the nanoprobe absorbs at the wavelength used on the ELISA kit measurements; however, its contribution to the measured absorbance was minimal since a very low volume and concentration of nanoprobe was used.

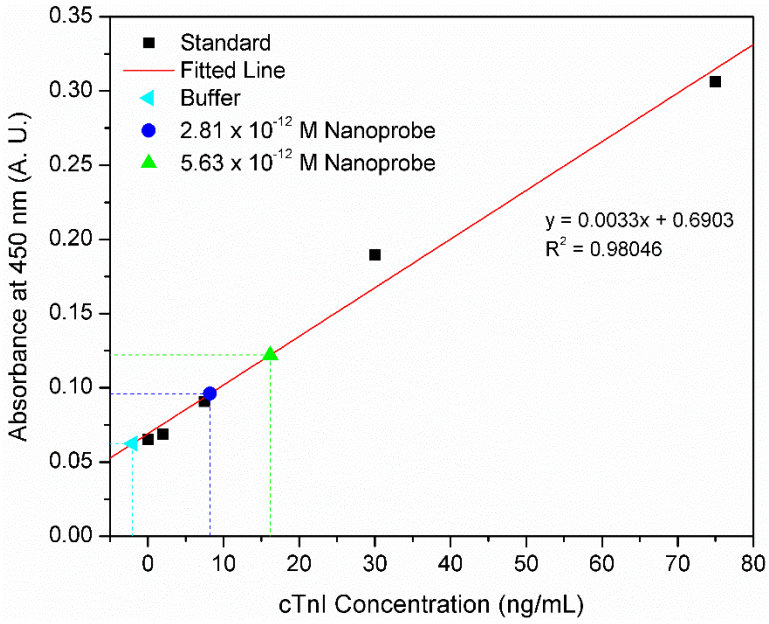


**Figure 24.** ELISA kit results used to determine the amount of cTnI functionalized on specific concentrations of nanoprobe. Based on standard samples measurements a concentration curve with a fitted line was obtained to predict measured concentrations.

The SERS spectrum of the nanoprobe was measured to analyze its signal. Figure 25 shows the peaks of the nanoprobe, which correspond the SERS spectrum of the RRM DTNB. As can be noted, the spectrum has several major peaks that can be monitored, specifically 1336, 1558, 1064, 1153, and 849 $cm^{-1}$. Most of these vibrational peaks correspond to the nitro group stretching, or the aromatic ring stretching modes (see Table 3). The narrow peaks of the spectrum allow to simultaneously measure different RRM spectra with peaks at different wavenumbers, and thus perform multiplexing measurements.

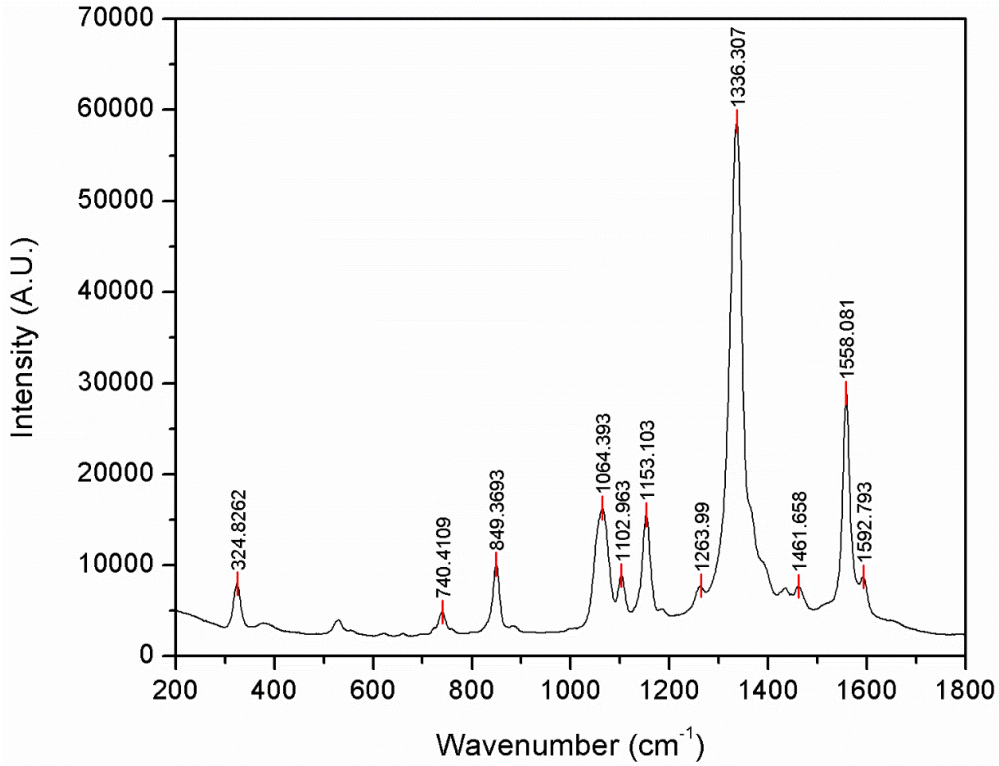


**Figure 25.** SERS spectrum of nanoprobe. The SERS spectrum corresponds to the Raman reporter molecule DTNB, which forms a SAM on the Ag nanoparticles.

**Table 3.** DTNB Assignment Peaks.

| Peak ($cm^{-1}$) | Assignment | Reference |
|---|---|---|
| 1336 | Symmetric $NO_2$ stretching | 96-97 |
| 1558 | Aromatic ring stretching mode | 96-97 |
| 1064 | Aromatic ring modes | 96-97 |
| 849 | Nitro scissoring vibration | 96 |

### *II.4 Different Functionalities*

The synthesized nanoprobes can be functionalized with different proteins or antibodies to give them the desired functionality. The conjugation strategy is the same for most proteins if they contain the targeted functional groups. The most common functional group is amine since it is present in the N-terminus of each polypeptide chain and in the side chain of lysine. The linker functional group used to conjugate proteins to the nanoprobe is NHS. Therefore, almost any protein can be conjugated without changing the linker functionality.

One of the main advantages of SERS is its multiplexing capability. Several nanoprobes can be detected simultaneously with the same excitation laser if the appropriate RRM are used. For multiplexing to work, RRM with peaks at different locations need to be utilized. Three RRMs (DTNB, MBA, and TFMBA) were selected to create nanoprobes with a different SERS spectrum. Figure 26 shows the spectrum of each nanoprobe. As can be observed on the spectrum with the combined nanoprobes, the narrow peaks of each nanoprobe can be detected. These three nanoprobes can be conjugated with antibodies for cTnI, myoglobin and CK-MB to develop an assay that can detect the three biomarkers at the same time.

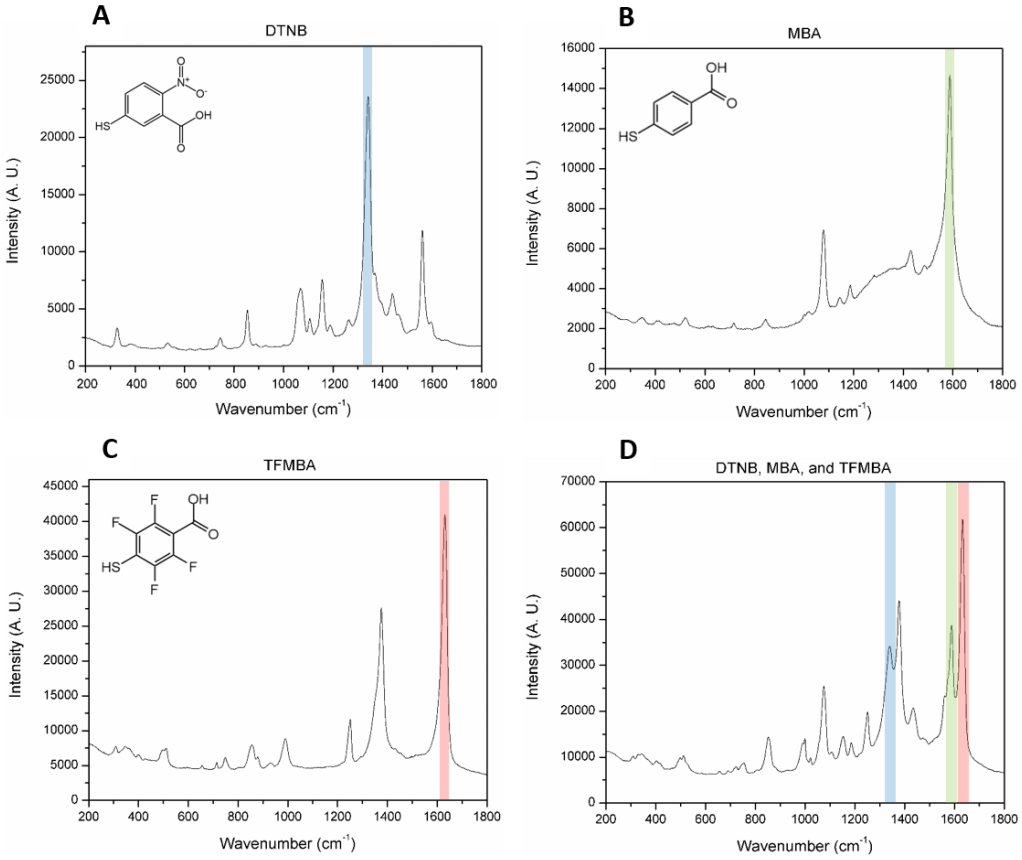


**Figure 26.** SERS spectrum of nanoprobes functionalized with different RRM. (A) SERS spectrum of nanoprobe with DTNB. (B) SERS spectrum of nanoprobe with MBA. (C) SERS spectrum of nanoprobe with TFMBA. (D) SERS spectrum of a solution with the three different nanoprobes combined.

### *II.5 Nanostars*

Gold nanostars were created to be used as alternative SERS active nanoprobes in the developed assays. Nanostars have been reported to be good SERS substrates due to the hotspots formed at their sharp edges. They provide the greatest enhancement when they are excited with a 780 nm laser. The nanostars were functionalized with RRM, encapsulated in silica, and conjugated with antibodies. They were also characterized to monitor the functionalization process and determine their SERS signal.

### II.5.i Protocol

A 20 nm citrate reduced Au colloid was synthesized first to be used as seed for the nanostars synthesis. To make the 20 nm Au colloid, 500 mL of DI water was added to a clean round bottomed flask with 50 mg of sodium tetrachloroaurate. The solution was heated until boiling. Then, 0.075 g of sodium citrate in 7.5 mL of DI water was added to the solution. The solution was boiled for 15 min and allowed to cool afterwards. Continuous stirring was maintained throughout the process.

The protocol to synthesize gold nanostars was based on the method described by Yuan.[98] Briefly, 100 µL of the prepared citrate Au (Avg. size: ~12 nm, A520: 2.81) was added to 10 mL of 0.25 mM auric chloride ($HAuCl_4$) solution (1.70 mg in 20 mL DI water) and 100 µL of 3 mM silver nitrate ($AgNO_3$) in a 20 mL glass vial at room temperature under moderate stirring. After 5 min, 50 µL of 100 mM ascorbic acid was added, and the solution was left stirring for 15 min. To make the nanoparticles SERS active, 1 mL of nanostars solution was mixed with RRM, incubated overnight, and redispersed in ethanol after washing. The nanostars were then encapsulated in silica by adding APTMS (10 µL, 0.001% in ethanol) to the solution, incubating for 10 min, washing, and redispersing them in IPA (1 mL), water (360 µL), and ammonium hydroxide (25 µL, 28%). After that, TEOS (10 µL, 1% in IPA) was added two times in an hour, incubated overnight, washed, and redispersed in ethanol. To conjugate antibodies on the nanoparticles, silane-PEG-NHS was added (400 µL, 2 mg/mL). The nanoparticles were washed and redispersed in sodium phosphate (400 µL, pH 7.4) to add 20 µL of cTnI antibody (1 mg/mL) and incubate the solution for 2 hrs. BSA was also added (20 µL, 50 mg/mL) to prevent nonspecific binding.

The nanoparticles were finally washed two times and redispersed in TRIS (1 mL, pH 7.5) and Tween 20 (5 µL, 1%). In Figure 27, the nanostars functionalization strategy is presented.

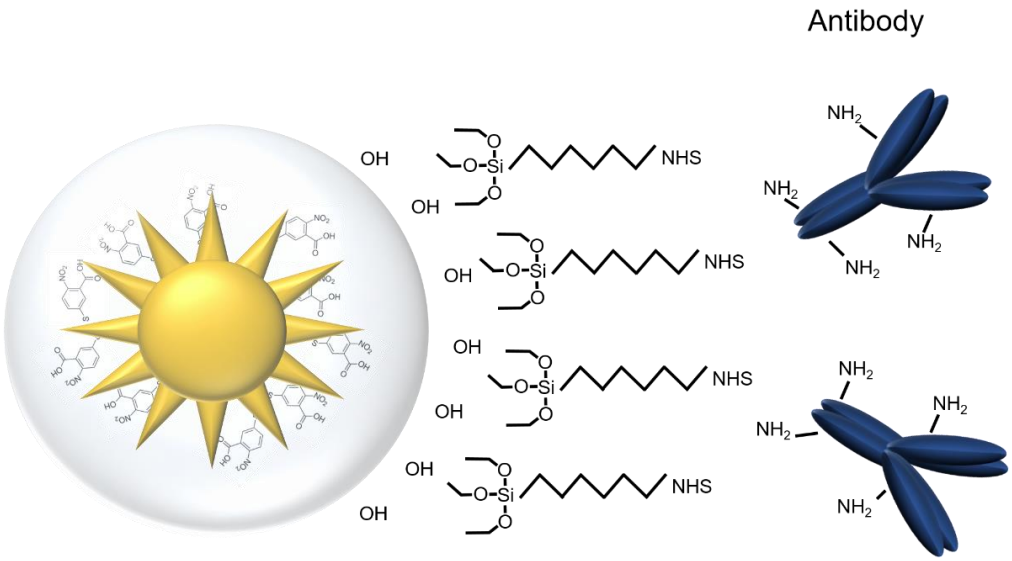


**Figure 27.** Nanostar functionalization strategy. DTNB is attached to synthesized nanostars. Then, a silane-PEG-NHS linker is used to conjugate antibodies to the silica surface.

### II.5.ii Characterization

The extinction spectrum was measured at three stages of the functionalization process (before functionalization, after silica encapsulation, and after protein attachment). As can be observed in Figure 28, the normalized extinction spectrum of the nanostars is red shifted after encapsulation and protein conjugation. The changes in the extinction spectrum is an indication that encapsulation was successful. It is important to note that in the absorbance measurements, the functionalized nanostars samples were more concentrated than the nanostars sample. Therefore, in the normalized spectrum the second

peak is more prominent than the first peak. Since the concentration of the nanostars sample was low, the two peaks can be clearly observed in the spectrum. Even though the spectra appear different because of the concentrations used in the measurements, the red shift of the second peak can be distinguished clearly.

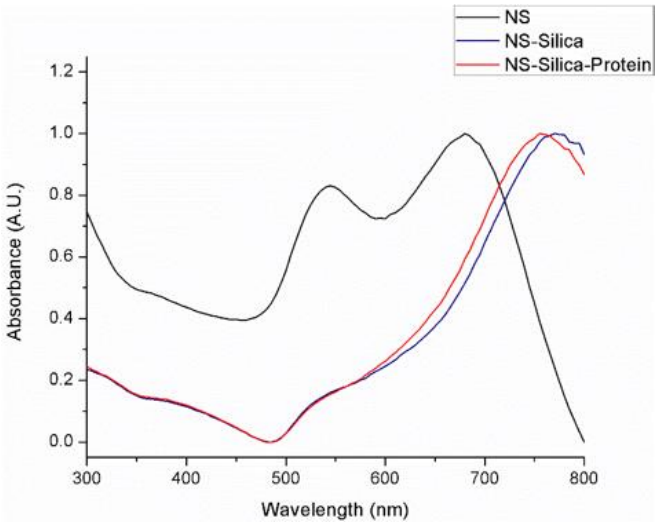


**Figure 28.** Nanostar extinction spectrum at different stages of the functionalization process.

The size of the nanostars was also monitored with a DLS instrument as they were functionalized. Figure 29 shows the increment in size as a silica layer was added and antibodies were conjugated. The size of the synthesized nanostars was approximately 126 nm, and after encapsulation it increased to 152 nm. Thus, the silica thickness was about 12.8 nm. The size of the nanoparticles further increased to 180 nm after attaching the PEG linker and the antibodies. The increase in thickness of 14.1 nm can be attributed to 9 nm of the 5 kDa PEG linker[93] plus approximately 5 nm of the conjugated antibodies, which implies that the functionalization was successful.

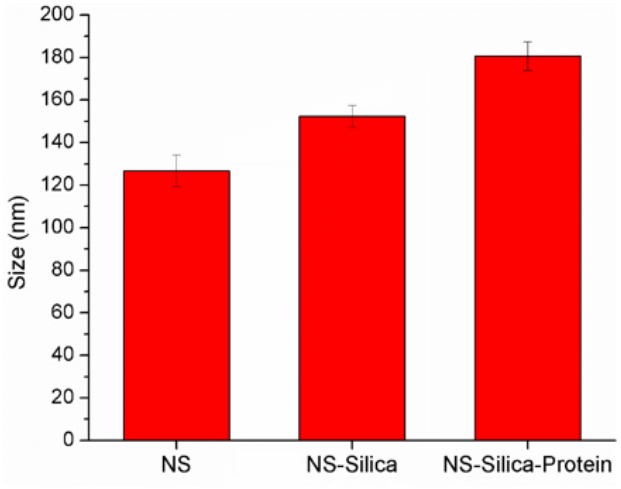


**Figure 29.** Nanostar average size at different stages of the functionalization process.

SEM images of the functionalized nanostars were also obtained. Figure 30 shows an image of several silica encapsulated nanostars. In the image, the branches of the nanostars can be distinctly noticed. The silica around the nanostar makes the edges and tips of the branches appear soft. The size of the nanostars (around 150 nm) also matches the size measured with the DLS.

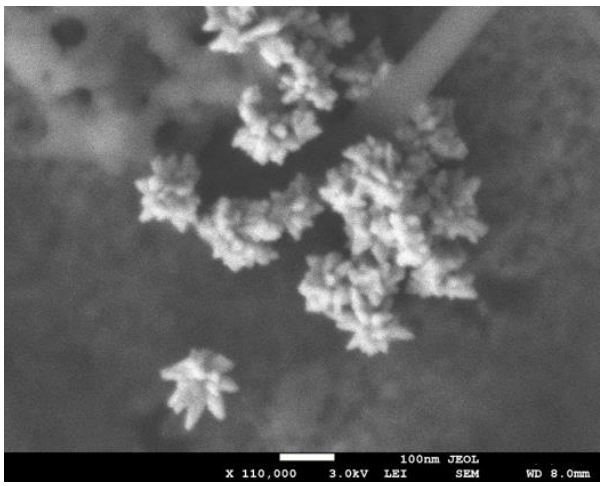


**Figure 30.** SEM image of nanostars encapsulated in silica.

The SERS signal of the nanostars was measured with a Sierra Series spectroscopic reader from Snowy Range Instruments (780 laser) to analyze it. As can be observed in Figure 31, the functionalized nanostars exhibited the expected SERS spectrum of the RRM DTNB. The characteristic peaks of the SERS spectrum could be distinguished clearly, and the signal intensity was high (about 18000 counts). This means that the nanostars could be used as SERS active nanoprobes for the development of biosensors.

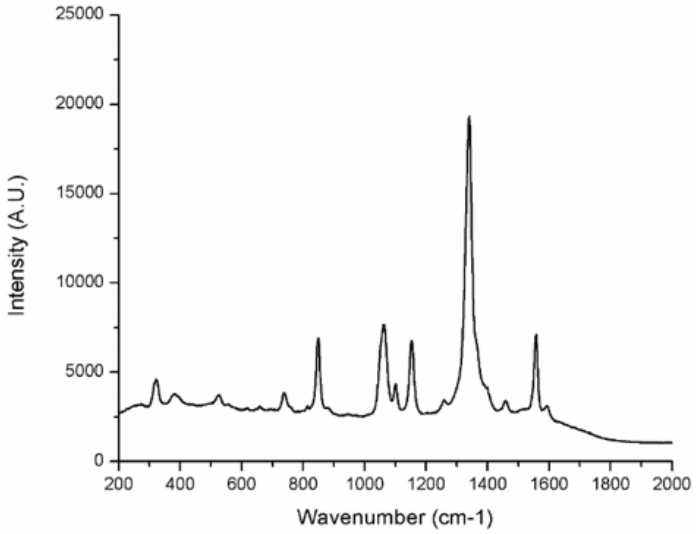


**Figure 31.** Nanostar SERS signal obtained with a Sierra from Snowy Instruments.

### *II.6 Magnetic Particles*

Magnetic nanoparticles were synthesized and functionalized to use them as components of the assays tested. These magnetic nanoparticles were not functionalized to be SERS active. They were conjugated with antibodies and other compounds or proteins to make them stable and prevent non-specific binding. The functionalized magnetic nanoparticles were also characterized.

### II.6.i Protocol

Superparamagnetic iron oxide nanoparticles (SPIONs) were synthesized based on the method described by Lee.[99] Briefly, ferric chloride hexahydrate (500 mg, 1.85 mmol) and ferrous chloride tetrahydrate (184 mg, 0.925 mmol) was added to deoxygenated DI water (30 mL) that had been degassed by bubbling with nitrogen gas for 20 min. Then, 7.5 mL of ammonium hydroxide solution (28% in water) was added under nitrogen gas while stirring vigorously for 30 min. The remaining salt was removed by applying an external magnetic field to attract the particles and discard the supernatant. DI water (30 mL) was added to the black precipitate, and the mixture was stirred gently to redisperse the particles. The particles were washed three times with water.

The SPIONs were encapsulated in silica for further functionalization. To do this, APTMS (10 µL, 0.001% in ethanol) was added to 1 mL of SPIONs, and the solution was incubated for 10 min. After that, the supernatant was removed by separating the nanoparticles with a magnet, and they were redispersed in IPA (1 mL), water (360 µL), and ammonium hydroxide (25 µL, 28%). Subsequently, TEOS (10 µL, 1% in IPA) was added two times in one hr. The solution was incubated overnight in a rotator, washed, and redispersed in ethanol. Silane-PEG-NHS (400 µL, 2 mg/mL) was added to the solution to be used as a linker to attach the antibodies. After incubating the solution for one hr and washing the nanoparticles three times, 20 µL of cTnI antibody (1 mg/mL) was added. BSA (20 µL, 50 mg/mL) was also added after 15 min to block unreacted groups. The nanoparticles solution was incubated 2 hrs and washed two times with TRIS base (1 mL,

pH 7.5) and 5 µL Tween 20 (1%). Figure 32 shows the schematic of the functionalized magnetic nanoparticles.

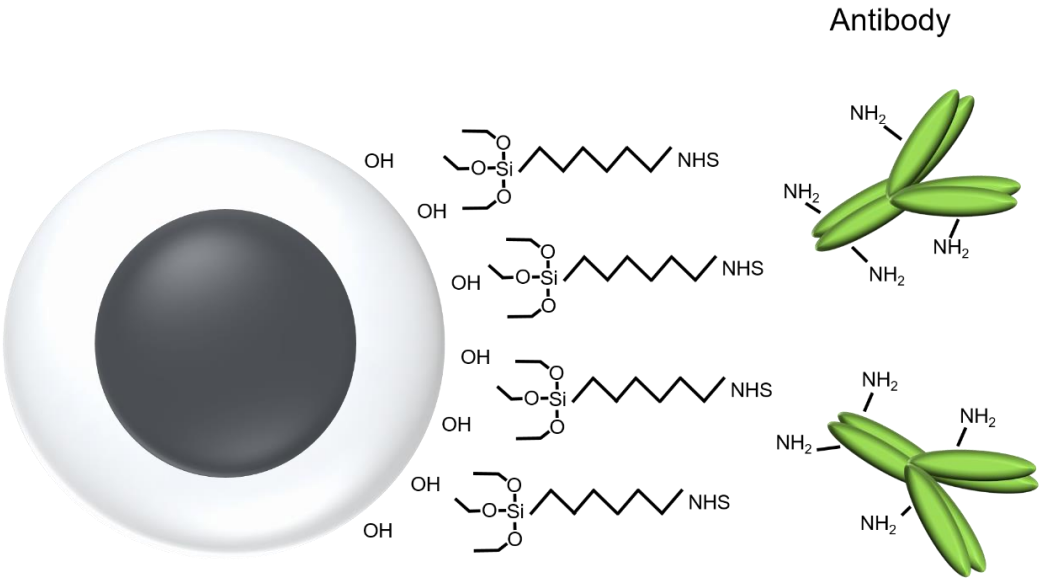


**Figure 32.** SPIONs functionalization strategy. The SPIONs are encapsulated in silica, and a silane-PEG-NHS linker is used to attach the antibody to the silica surface.

### II.6.ii Characterization

The size of the functionalized SPIONs was measured with a DLS (Malvern) instrument. The nanoparticles were approximately 168.7 nm after they were encapsulated in silica and the antibodies were conjugated. The extinction spectrum of the SPIONs was also measured. The extinction values were decreasing with increasing wavelength, and the spectra of the SPIONs before and after functionalization were very similar. To test if the magnetic nanoparticles could be magnetically collected, they were flowed on a microchannel with a magnetic area. However, most nanoparticles flowed past the

magnetic area when they were injected at 1 µL/min. This suggested that the response of the SPIONs to the applied magnetic field was not strong enough.

The size of a magnetic particle can have an effect in its response to an applied magnetic field.[100] Usually, larger particles are more strongly attracted to a magnetic field than smaller particles. Therefore, 1 µm magnetic particles were used to functionalize them and use them instead of the SPIONs. Dynabeads MyOne coated with streptavidin were obtained from Thermo Fisher Scientific. Since these magnetic particles were coated with streptavidin, biotinylated antibodies were used to conjugate them via the streptavidin-biotin bond. After attaching the antibody, BSA was added to block free spaces and avoid nonspecific interactions. Figure 33 shows the 1 µm functionalized magnetic particle.

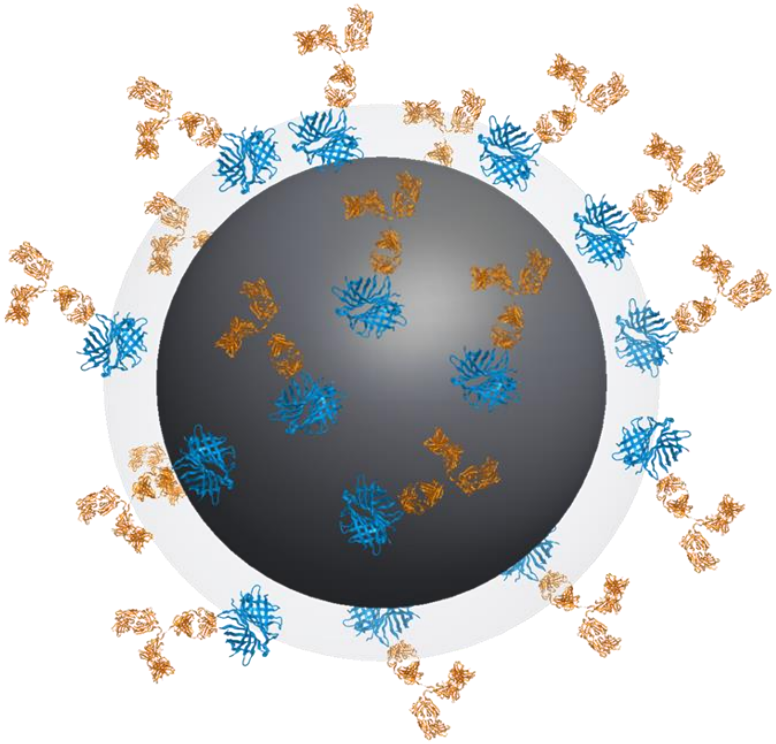

**Figure 33.** Dynabeads MyOne coated with streptavidin to attach biotinylated antibodies. The diameter of the magnetic particle is 1 µm.

### *II.7 Chapter Summary and Conclusions*

In this chapter, several nanoparticle functionalization approaches were examined. The goal was to develop SERS active nanoparticles that (1) exhibit intense SERS signal, (2) are stable, and (3) are conjugated with a protein or antibody that makes them functional. The stability of the different approaches (summarized in Table 4) was used as the first criteria to select the best approach. The extinction spectra was measured in each case to test for aggregation, which usually indicates if the nanoparticles are stable. The first two functionalization approaches (Au-RRM-Antigen and Au-RRM-CAPEG-Antigen) were not stable as they exhibited aggregation. In the third approach (Au-RRM-PEG-Antigen), the nanoparticles did not aggregate, but they were sticking to the wall of the microtube. In the fourth approach (Au-RRM-Silica-PEG-Antigen), the Au nanoparticles were aggregated in a controlled manner; therefore, they exhibited stability.

**Table 4.** Summary of functionalization approaches and their aggregation state.

| Approach | Aggregation (Extinction) |
|---|---|
| 1: Au-RRM-Antigen | Aggregated |
| 2: Au-RRM-CAPEG-Antigen | Aggregated |
| 3: Au-RRM-PEG-Antigen | Non-aggregated/Wall binding |
| 4: Au-RRM-Silica-PEG-Antigen | Non-aggregated (controlled) |
| 5: Au-RRM-Silica-PEG-Antigen (modified 4 with Ag) | Non-aggregated (controlled) |
| 6: Au-RRM-Silica-PEG-Antigen (modified 5 with linker) | Non-aggregated (controlled) |

The SERS intensity of the nanoparticles was also considered in the selection process. From the first four approaches, the fourth approach (Au-RRM-Silica-PEG-

Antigen) produced the most intense SERS signal. The fifth functionalization approach (Ag-RRM-Silica-PEG-Antigen) was very similar to the fourth; the only difference was that Ag nanoparticles were used instead of Au nanoparticles. In addition, a 532 nm laser was used as an alternative to the 780 nm laser to measure the SERS signal, which produces a more intense signal when silver nanoparticles are measured. In the sixth approach (Ag-RRM-Silica-PEG-Antigen), a different linker (Silane-PEG-NHS) than the fifth approach was employed. This linker allowed better control over the functionalization process. The sixth functionalization approach was selected to develop the nanoprobe and use it as an assay component. After making the nanoprobe, it was characterized to monitor the functionalization process and test its functionality.

As an alternative approach, SERS active nanostars were synthesized and considered as potential assay components. They were encapsulated in silica, functionalized with cTnI, and characterized. However, they were not selected because the nanoprobes produced a more intense SERS signal with the 532 nm laser. Magnetic nanoparticles or SPIONs were also synthesized and functionalized with antibodies to use them as capture nanoparticles in the assay.

# CHAPTER III

# NANOPARTICLE COLLECTION METHODS FOR SERS MEASUREMENTS

## *III.1 Need for Nanoparticle Collection*

One of the main challenges of SERS measurements is controlling their signal repeatability and performance since these can be affected by variations in substrate preparation or hot spots formation, which can be difficult to control.[81, 92] The consistent collection of aggregated substrates in a specific area for SERS measurement can also have a significant effect on the repeatability. Therefore, an effort has been made to develop methods and techniques to produce consistent substrates and allow fine control over aggregation and collection for measurement.[101] In general, SERS substrates are aggregated chemically, magnetically, or mechanically. Chemical methods of aggregation include adding solutions to change the electrostatic stability of the nanoparticles and induce aggregation.[102] In addition, nanoparticles can be aggregated by functionalizing them with compounds, biomolecules, DNA strands, or other components that link them together.[103] Some groups have used magnets to aggregate or collect magnetic nanoparticles in specific areas to measure their SERS signal.[104] SERS substrates have also been aggregated and collected in microchannels[105], agglomerated silica particles[106], and filter membranes[107]. However, the challenge of obtaining precise and sensitive measurements still exists, and improvements in nanoprobe synthesis and collection methods will greatly enhance the quality of SERS measurements. Typical requirements for high performance assays usually demand detection limits at the femtomolar (fM) level or below with a precision of less than 15 % CV.[108-109]

*III.2 Centrifugation Wells Collection*

One of the first methods used to collect the functionalized nanoparticles for SERS measurements was based on centrifugation. A device that allowed to place the sample on a well, centrifuge it, and measure the SERS signal on the well was designed and built. A sample with SERS active nanoparticles could simply be added to a microcentrifuge tube and centrifuged to collect the nanoparticles on the bottom. However, to measure the SERS signal on a confocal microscope, the bottom part of the centrifuge tube would need to be cut to be able to focus on the nanoparticles. This could affect the sample and thus the SERS measurement. In contrast, the developed collection method contained a well inside the microcentrifuge tube that could be removed to perform the SERS measurements. Figure 34 shows the device built.

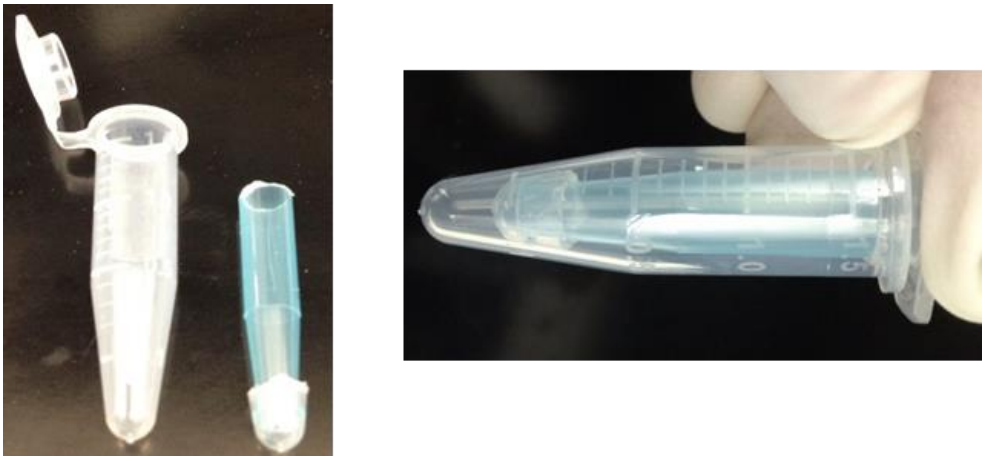

**Figure 34.** Device built to collect nanoparticles with centrifugation. The sample is placed inside the blue tube. Then, the microcentrifuge tube is centrifuged. After centrifugation, the blue tube is removed to measure the SERS signal on the small well.

The device was composed of a microcentrifuge tube, the cut bottom part of another microcentrifuge tube (which created the well), and a cut 1 mL pipette tip. It was assembled

by inserting the pipette tip to the well (as seen in Figure x). These two parts fitted tightly when they were joined. Then, this assembly was inserted in a regular microcentrifuge tube. The sample was added inside the pipette tip assembly. The microcentrifuge tube was then centrifuged (2800 rcf). The centrifugation force pulled the nanoparticles to the bottom of the well. After centrifugation, the pipette tip assembly with the sample was removed. The supernatant was discarded and the pipette tip was separated from the well (which contained the nanoparticles). The well was then placed under the confocal microscope to measure the SERS signal from the collected nanoparticles.

Different concentrations of SERS active nanoparticles were collected and tested on the centrifugation wells. Figure 35 demonstrates the images of several concentrations of nanoparticles collected on the wells. As can be observed, the nanoparticles were spread throughout the area and aggregated differently. A point where the nanoparticles were aggregated in each well was selected to measure the SERS signal. Figure 36 shows the SERS intensities obtained at specific concentrations. A volume of 200 µL of the nanoparticles solution was used for the measurements. Three different measurements of the same concentration were tested to calculate the standard deviation. The standard deviations obtained indicate that the collection of nanoparticles on the centrifugation wells is inconsistent. The intensities of the four lower concentrations tested show an increasing SERS signal trend as the concentration increases. Nevertheless, after a specific concentration the signal fluctuates and does not exhibit a pattern.

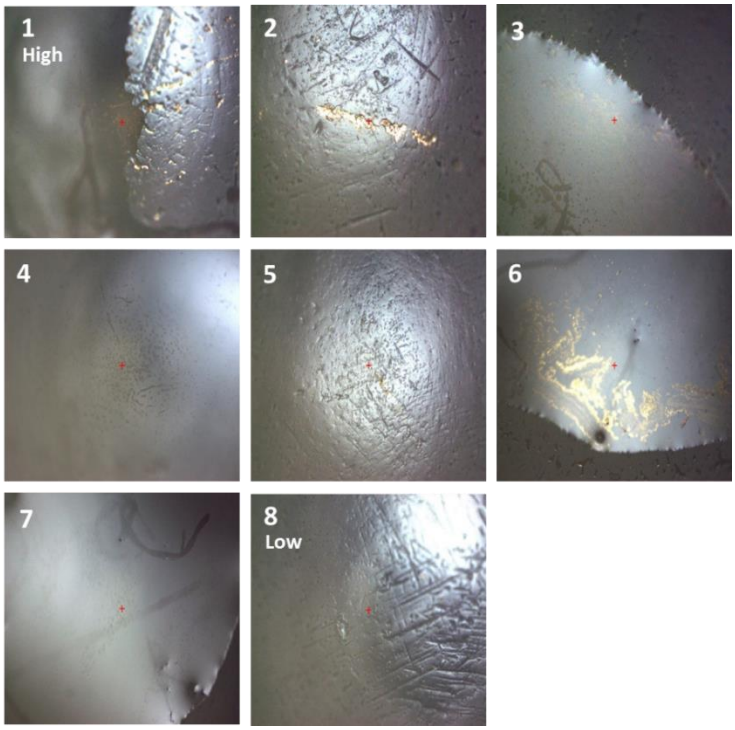


**Figure 35.** Images of nanoparticles collected on the bottom of the wells with the centrifugation microtube.

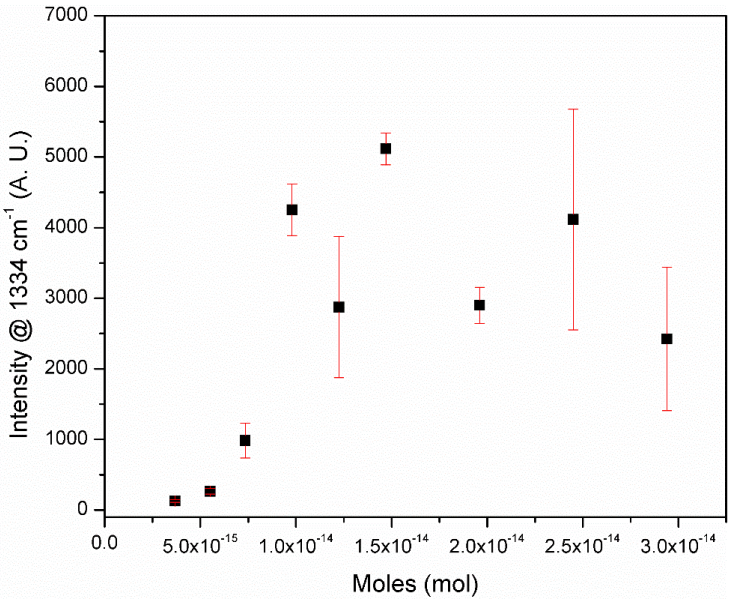


**Figure 36.** SERS signal concentration curve of functionalized nanoparticles collected and measured on the wells of the centrifugation microtube device.

This collection method offers a simple approach to collect nanoparticles using centrifugation and measure their SERS signal. However, the collection is not consistent and the nanoparticles aggregate differently, which affects the measurements repeatability.

### *III.3 Magnetic Collection*

A method based on magnetic force was also explored for the collection of nanoparticles. To use this method, magnetic nanoparticles were synthesized and functionalized. In addition, a magnet or an area with magnetic field was incorporated inside a microchannel or close to it. The magnetic nanoparticles would then be inserted in the microchannel, and they would be attracted and collected on the area with the magnetic field as they flow through. Several magnetic nanoparticles and magnetic field areas were tested to optimize the collection method.

#### III.3.i Magnetic Pads

One of the magnetic collection areas tested was the magnetic pads inside the microchannel. Nickel (Ni) 50 µm by 50 µm square pads (200 nm thick) were deposited onto a glass slide, and a PDMS microchannel was bound to the glass slide with the pads to contain them. To analyze if the magnetic pads could collect nanoparticles a magnetic nanoparticles solution was added to the microchannel as the collection areas were monitored under a microscope.

The pads fabrication process is described in detail by Marks.[110] Briefly, glass slides were spin-coated with lift-off resist (LOR). After exposure and development, the Ni pattern was visibly transferred onto the slides. Chromium (100 nm thick) and copper (50 nm thick) were deposited on the pattern as the adhesion layer. Then, nickel (200 nm thick)

was deposited as the third and final magnetically responsive layer. After deposition, the photoresist layer was removed by placing the glass slide into a chemical stripper at 80 °C. The 100 µm thick microchannel was constructed via soft lithography. To do this, an uncured PDMS solution (10:1) was poured over a silicon wafer mold and cured at 65 °C for 2 hrs. After that, the PDMS microchannel was bound to the Ni pads patterned glass slide by plasma etching treatment. The nickel pads were magnetically activated by placing two attractive neodymium magnets on the sides of the microchannel and pads. Figure 37 shows the magnetic pads.

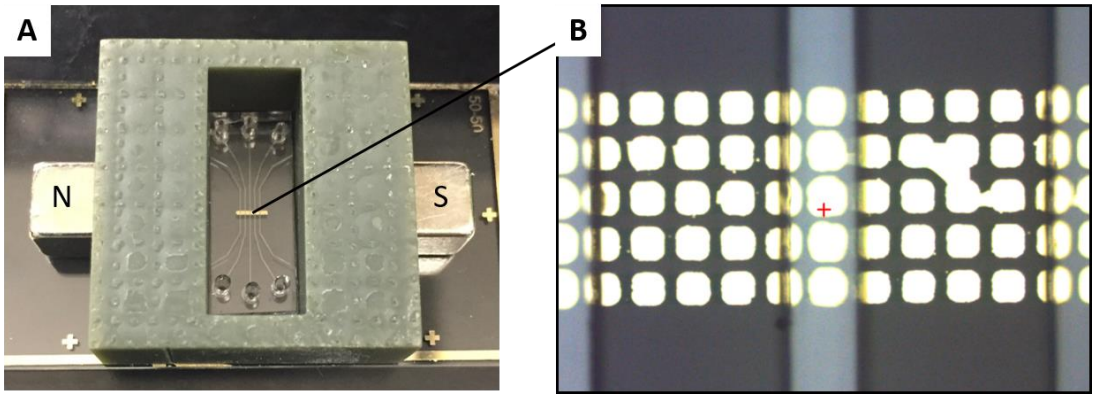


**Figure 37.** Microfluidic channel with nickel magnetic pads (B). Two permanent magnets need to be placed as shown in (A) to create the magnetic field on the pads. Each pad is 50 µm x 50 µm and 200 nm thick.

A solution of functionalized magnetic nanoparticles was injected to the microchannel with Ni pads at different flow rates. The induced magnetic field propagates down the magnetic pads, and the field is strongest at the centers and edges of the Ni magnetic pads.[110] Therefore, the nanoparticles were expected to be collected on top of the pads as they passed through them. Figure 38 shows images of the pads as the solution of magnetic nanoparticles was flowing through them at different rates. The pads were

observed for 10 min as the fluid was pumped to the microchannels. In all the cases nanoparticles flowed through the pads without stopping, indicating that the magnetic force was not stronger than the flow to collect them. It is important to note that even though most nanoparticles passed through the pads, some of them were collected at the pads, especially when the flow was low. However, losing some nanoparticles could negatively affect the response of a sensor that depends on the effective collection of all the nanoparticles for quantification. Another concern with this design was the large area that would need to be probed to measure the SERS signal of the collected nanoparticles. Five 50 µm by 50 µm pads would need to be mapped, which could take considerable time depending on the selected resolution.

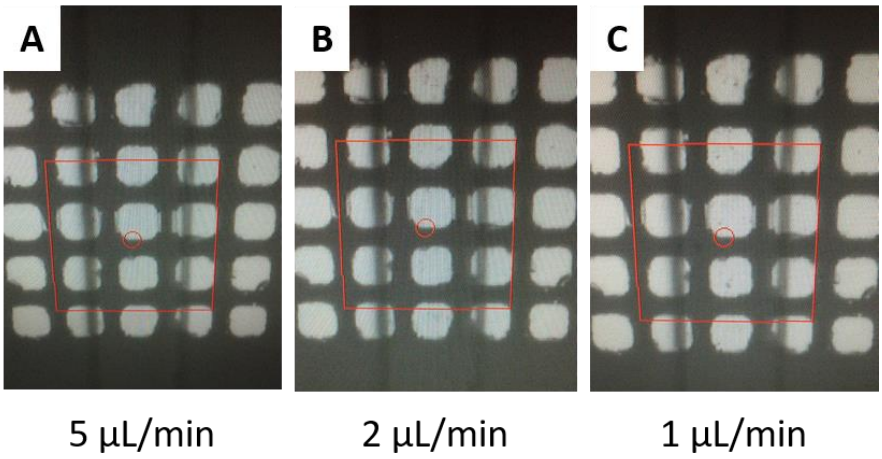


**Figure 38.** Images of the pads when magnetic particles (SPIONs) were flowing through them at different rates. (A) No nanoparticles can be detected on the pads. (B) Some nanoparticles can be detected on the top pad. (C) Some nanoparticles can be observed on the first four pads.

In order to increase the magnetic force between the particles and the pads, larger magnetic particles (1 µm diameter) were used. These magnetic particles were considerably

more magnetic than the original ones. They could be collected in seconds if a magnet was placed next to a microtube containing a solution of them where it could take hours for a solution of magnetic nanoparticles in the same case. A solution of 1 µm magnetic particles was added to the pads at 1 µL/min to observe if all the particles were collected. Figure 39 shows an image of the pads and the collected particles. As can be noted, most particles were aggregated between pads in the horizontal direction and some of them on top of the pads. The use of larger magnetic particles improve the collection considerably compared to the case when the smaller nanoparticles were used. Although more particles were collected, some of them passed through the pads and were lost, which is not desirable. In Figure 39 particles can also be observed on the microchannel above the pads area. In addition, the collection of the particles was not consistent as they were not localized on top of the pads.

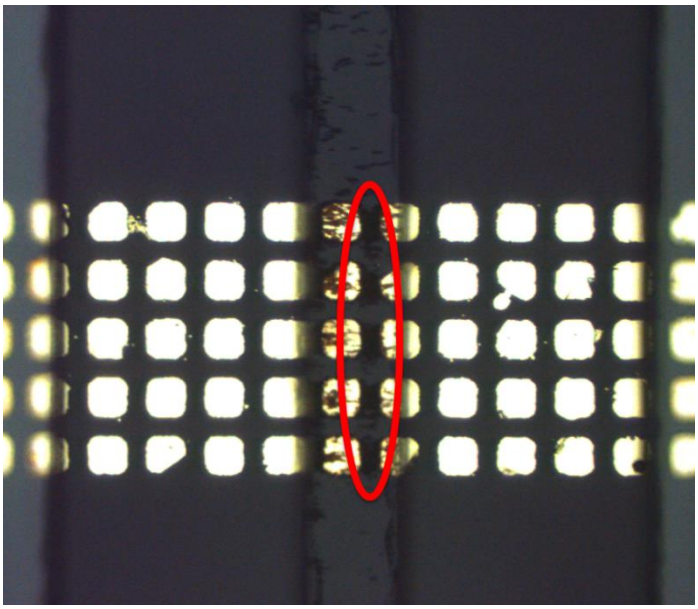

**Figure 39.** Magnetic particles (Dynabeads, 1 µm) collected as a solution with them is injected through the pads. Some particles are aggregated between the pads or the sides of the microchannel. Other particles are not collected and pass through the magnetic pads.

In addition to the square magnetic pads, another design was tested in which only one 200 µm diameter circular pad was used to collect magnetic particles (see Figure 40). The design intended to focus the particles in a small area. A small collection area would reduce the SERS measurements collection time or allow to probe more particles. However, in this case, the magnetic force of the circular pad was not strong enough to collect all the magnetic particles with a flow rate of 1 µL/min. Similarly to the previous design, some particles passed the circular pad when they were introduced. Figure 40 presents the collection of the particles on the circular pad.

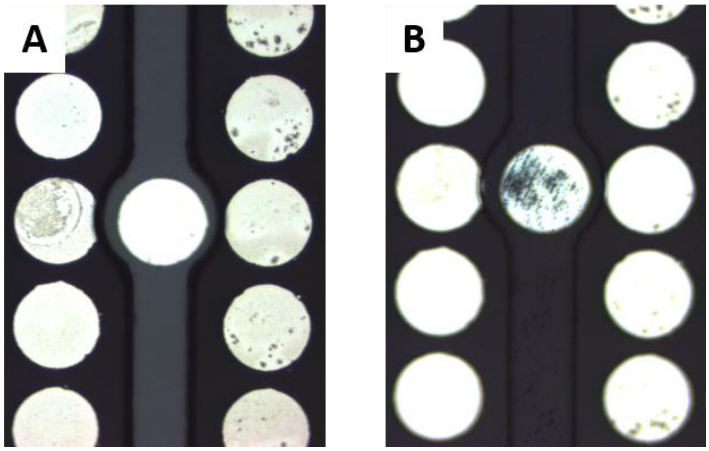


**Figure 40.** Microfluidic channel with single circular nickel pad (200 µm diameter**)**. (A) Dry microchannel. (B) Magnetic particles injected through the microchannel and collected on the circular pad.

Nickel pads were patterned on a microchannel to create a magnetic field and collect magnetic particles on top of them. As magnetic nanoparticles and particles flowed through them at low flow rates some of them were collected, but others were not. The collection of large magnetic particles was considerably better than the smaller nanoparticles. However, the collection was not consistent and it had a high dependence in the flow rate.

### III.3.ii Magnet below Microchannel

The use of a magnet below a microchannel was another approach tested to create a magnetic area for collection of magnetic particles. In this case, a microchannel with an inlet and outlet was bonded on a glass slide, and a 3 mm diameter magnet was positioned below the glass slide and the microchannel. Magnetic particles were flowed through the microchannel to analyze their collection.

A silicon wafer mold with the microchannels design was created first to fabricate the microchannels. To produce the mold a silicon wafer was washed with acetone, then

IPA, and next with water. After drying it with air, it was placed on a hot plate for 1 min at 65 °C, 2 min at 120 °C, and allowed to cool for 5 min. Then, it was paced on a spin coater, and 3 mL of SU8 photoresist was poured to the wafer. The spin coater was turned on with the appropriate settings. After that, the wafer was transferred to a hotplate to heat it for 6 min at 65 °C and 15 min at 95 °C. The mask with the design was positioned over the wafer, and both were inserted on the UV exposure box. A long pass filter was placed on top of the mask before turning the UV box on. After the UV exposure, the wafer was placed on the hotplate for 1 min at 65 °C and 5 min at 95 °C. The wafer was placed on a glass dish with SU8 developer, and it was swirled for 7 min. The wafer was then washed with IPA and dried with air. Finally, the wafer was heated for 1 min at 65 °C and 5 min at 120 °C.

The microchannels were created by mixing PDMS polymer and curing agent in a 10:1 ratio. Subsequently, the solution was poured on a petri dish on top of the silicon wafer mold. The petri dish was placed on a desiccator for 45 min to remove all the bubbles. Then, the dish was transferred to an oven to bake the PDMS for 20 min at 80 °C. The PDMS with the design was cut with a razor and separated from the mold. A glass slide and the PDMS design were placed on the plasma cleaner. After that, they were bonded to make the microchannels. Finally, the 3 mm diameter magnet was placed below the glass slide. Figure 41 demonstrates the microchannels with the magnet below.

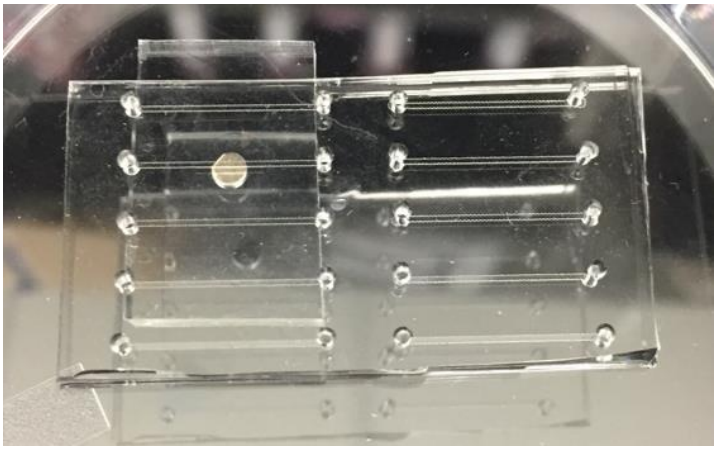

**Figure 41.** Microchannels with permanent magnet (3 mm diameter) placed below.

A solution with 1 μm magnetic particles was flowed through the microchannel to examine the collection area and asses if all the particles were collected. The solution was injected with a syringe and a microtube at a flow of 5 μL/min, and the magnetic area was monitored under a confocal microscope as the solution was flowing. In Figure 42 the magnetic nanoparticles can be observed as they are collected on the microchannel above the magnet. At the tested flow rate most particles were collected and very few flowed through the magnetic area. Some particles moved slowly on the magnetic area as the fluid was injected, but the flow force was not greater than the magnetic force, and thus the particles were not transported by the flow. The particles were transported by the flow only when the last volume of the injected solution passed thorough the magnetic area.

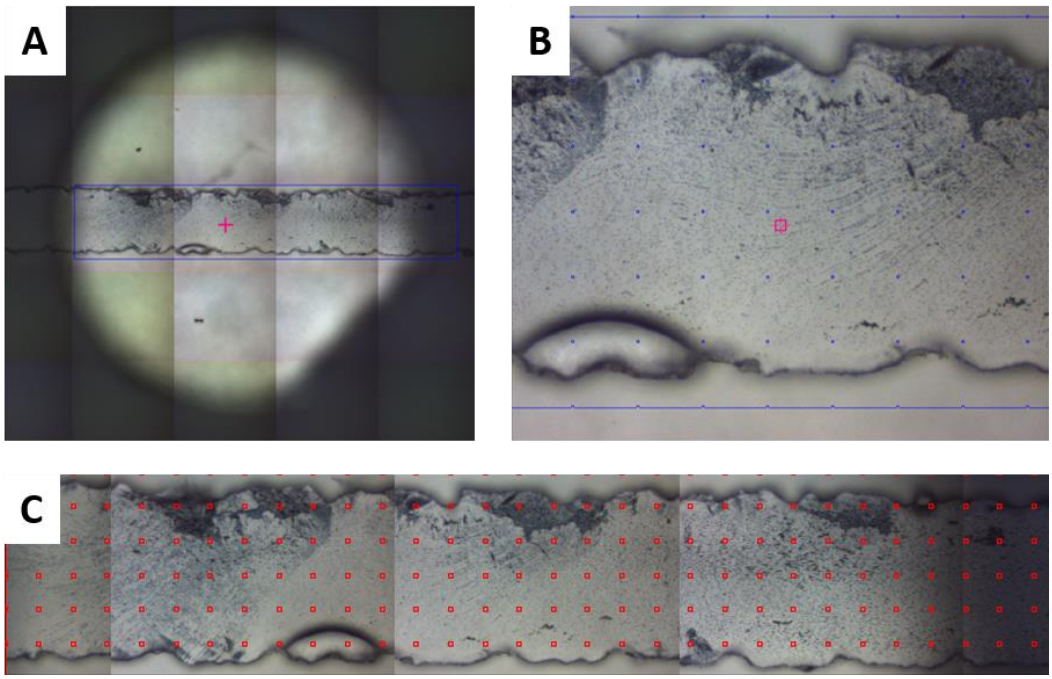


**Figure 42.** Images of magnetic particles collected on the microchannel. (A) Area above the permanent magnet where the magnetic particles are collected. (B) Zoom of the collection area. (C) Defined points in collection area to measure the SERS signal.

Although most magnetic particles were collected on the magnetic area, the area was too large to measure the SERS signal of most of the collected particles. Usually, a SERS reading takes 5 sec, and it has a spot size of 2.1 µm. Therefore, to probe several particles a map is defined with the number of points and distance between them that will be used to automatically measure the signals. Ideally, most particles would be measured in a short amount of time (approximately 10 min or less depending on the application). Nevertheless, if the particles are spread in a large area a significant amount of time would be needed to probe a considerable number of them, which is not desirable in many cases.

## *III.4 Membrane Collection*

A method to consistently collect nanoparticles on a specific area without losing any of them is desired to potentially improve the quality of SERS measurements. Besides chemical and magnetic approaches, mechanical methods can be employed to aggregate nanoparticles. Membranes with controlled pore sizes have been utilized in many applications to separate solutes in a solution based on their size. In this chapter, the use of a membrane to separate and collect nanoparticles was explored. Several designs were created and analyzed to determine their potential to collect nanoparticles for SERS measurements.

### III.4.i Plastic Wells

A device was built to contain a membrane and place the sample to be analyzed. This membrane collected SERS active nanoparticles when liquid containing the nanoparticles was aspirated through it. Multiple concentrations were passed through the membrane to analyze their collection and SERS signal.

The device was composed of two plastic squares and two rubber squares with a hole in the center and three smaller holes on the sides at identical positions to pass screws through them. The device was assembled in a specific order (as can be observed in Figure 43). First, a rubber square was placed on top of a plastic square with their holes aligned. Then, an aluminum oxide 20 nm pore size membrane was positioned on the center to cover the middle hole. After that, the second rubber square was placed over the membrane with its holes aligned. The second plastic square was aligned and situated above the rubber

square. Finally, three screws were passed through the side holes to fasten the squares and sandwich the membrane.

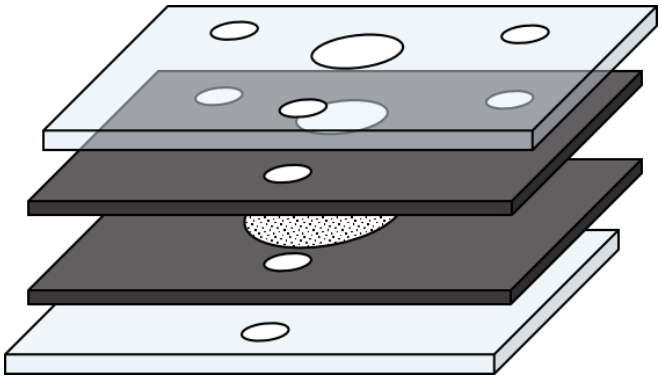

**Figure 43.** Device with membrane to collect nanoparticles. The 20 nm pore membrane is sandwiched between two rubber and plastic pieces with a hole in the center to collect the nanoparticles and three holes around it to insert screws and fasten the pieces.

The hole in the center of the assembly created a well with the membrane as the bottom. The solution with SERS active nanoparticles was added to this well (100 µL). Then, a tube connected to vacuum was placed below the hole and the membrane to aspirate the liquid through the membrane. As the liquid on the well was aspirated, the nanoparticles were trapped on the pores of the membrane. Since the sandwiched membrane was pressed between the rubber squares, the membrane was sealed around the holes. This prevented the liquid from leaking outside the well.

Several concentrations of SERS active nanoparticles were collected in the device. Then, the SERS signal was measured at selected points of the membrane. Figure 44 shows the SERS signal obtained at 1334 $cm^{-1}$ for the concentration curve. The curve shows an expected response with increasing SERS values for increasing concentrations. The measurements were collected three times to calculate the coefficient of variations (CVs).

From 1.7 pM to 13.9 pM the CVs were greater than 10%, with values as high as 43% CV. In addition, the signals from concentrations below 3.5 pM could not be distinguished. These results suggest that the reproducibility and ability to measure low concentrations with this method would need to be further improved to be used in the development of a biosensor. The utilization of lower volumes and a smaller collection area could facilitate SERS mapping, which could contribute to signal improvement.

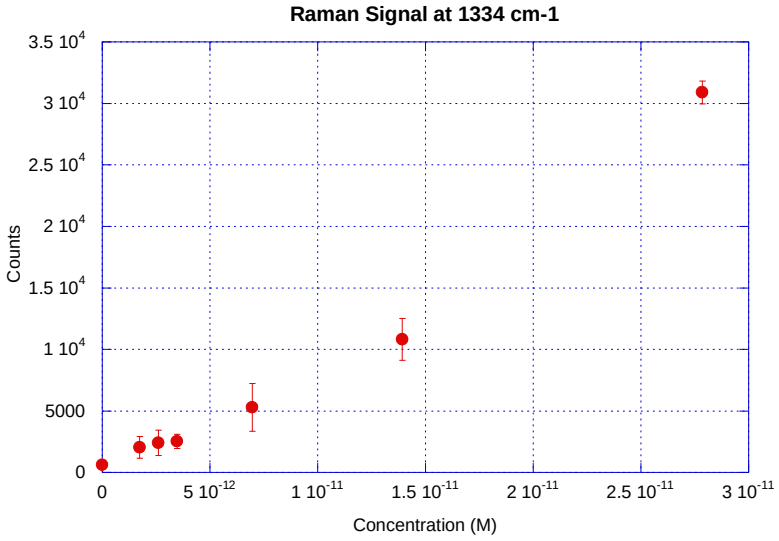


**Figure 44.** SERS signal concentration curve of functionalized nanoparticles collected on the sandwiched membrane.

### III.4.ii Multiple PDMS Wells

Another filter-based collection device was designed and built to perform multiple measurements simultaneously. The device was based on the previous design in which a membrane was sandwiched between rubber and plastic structures with holes. It was tested by examining how nanoparticles were collected on the membrane.

The device was constructed with PDMS slabs. Three PDMS slabs of different thickness were created by mixing PDMS polymer and curing agent in a 10:1 ratio. For the bottom slab, 22.5 mL of PDMS polymer was mixed with 2.5 mL of curing agent (25 mL total). For the middle layer, 9 mL of PDMS polymer was mixed with 1 mL of curing agent (10 mL total). For the top layer, 18 mL of PDMS polymer was mixed with 2 mL of curing agent (20 mL total). Each of the mixed solutions was added to a petri dish and left under vacuum for 40 min to remove air bubbles. After that, they were placed in an oven for 30 min at 80 °C. Once the PDMS circle slabs were cured, the middle slab was aligned and positioned over the bottom slab to make multiple holes through them with a 1 mm hole punch at specific locations. Then, 5 mm holes were punched on the top slab at the same locations where the holes were made on other two slabs. This layer would form a well where the solution tested would be added. Before bonding the three layers, the filter membrane was placed between the holes of the bottom and middle layers. The membrane was cut into pieces large enough to cover the 1 mm hole. After all the holes had filter membranes of them, the layers were bonded by plasma treating them and joining them. Figure 45 shows the PDMS collection device.

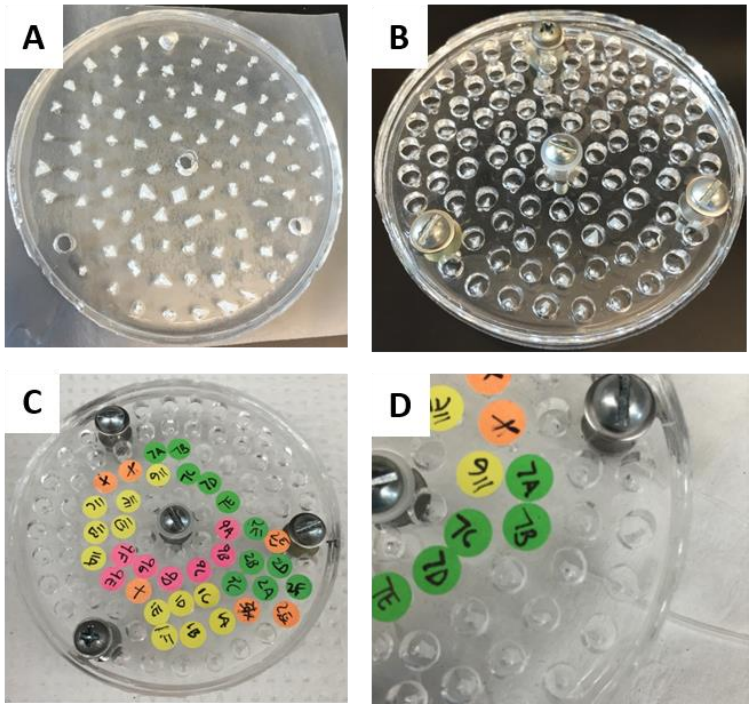


**Figure 45.** PDMS collection device created by sandwiching pieces of a 20 nm pore membrane between two PDMS slices with holes in them to place the sample on top and suction it from the bottom.

The SERS active nanoparticles samples were introduced to the wells to collect the nanoparticles. The liquid on the wells was aspirated and passed through the filter membrane by connecting a tube to the bottom layer hole and applying vacuum. The nanoparticles collected on the membrane were examined with a confocal microscope to analyze how consistent they were collected. Figure 46 shows different wells explored. As can be noted, the collection was inconsistent. The nanoparticles were aggregated differently in the wells, which is not desirable because it affects reproducibility. Furthermore, sometimes the membrane was bent, and this caused the liquid to be aspirated under it as opposed of flowing through it. A rigid bottom layer with same size holes could solve this problem and make the collection method more reproducible.

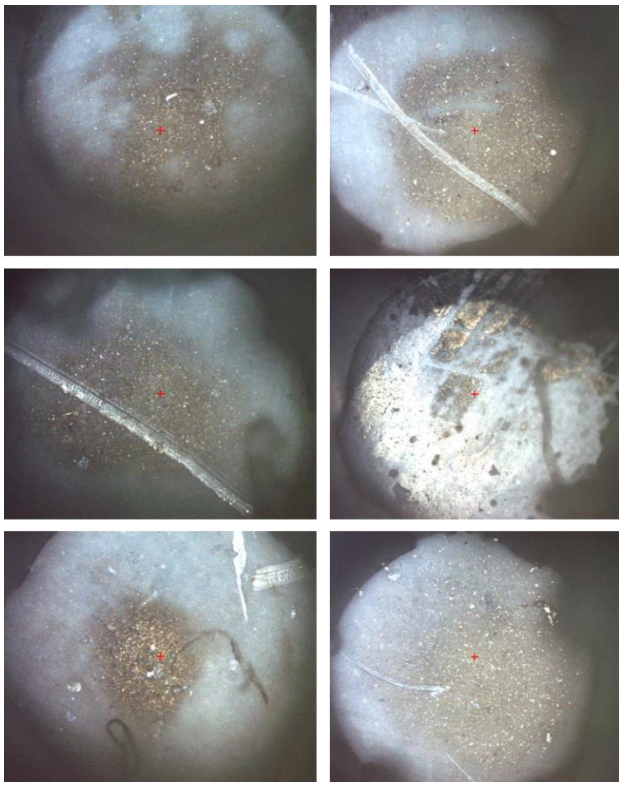

**Figure 46.** Collection of nanoparticles in different wells of the PDMS collection device. The nanoparticles are inconsistently aggregated on the membrane.

### *III.5 Membrane Collection Device*

Another device was built to collect nanoparticles with a filter membrane. However, this design addressed problems that previous designs exhibited. The collection device was composed of a rigid base with consistent holes. The holes were small enough to allow mapping in 15 min. Furthermore, the intersection between the hole and the membrane was sealed, which prevented leaks. Finally, this design allowed the testing of multiple samples without the need of a tube to apply suction. These improvements permitted the collection device to detect low limits of detection in a repeatable manner.

The device shown in Figure 47 was fabricated to consistently collect and aggregate functionalized nanoprobes and measure their SERS signal. The collection slide has holes and an aluminum oxide membrane with 20 nm pores. Since the membrane adheres to PDMS and PDMS to the acrylic slide without any adhesive, a PDMS layer was placed between the slide and the membrane to seal the membrane around the holes and avoid any liquid to be suctioned at any other point but the holes. The collection slide was built by drilling 457.2 µm holes on an acrylic slide, punching holes of similar size on the PDMS layer, and stacking the membrane on top of the PDMS layer. A CNC machine was used to drill the holes on the slide in a repeatable manner. The main priority was to consistently create sealed holes with the same diameter.

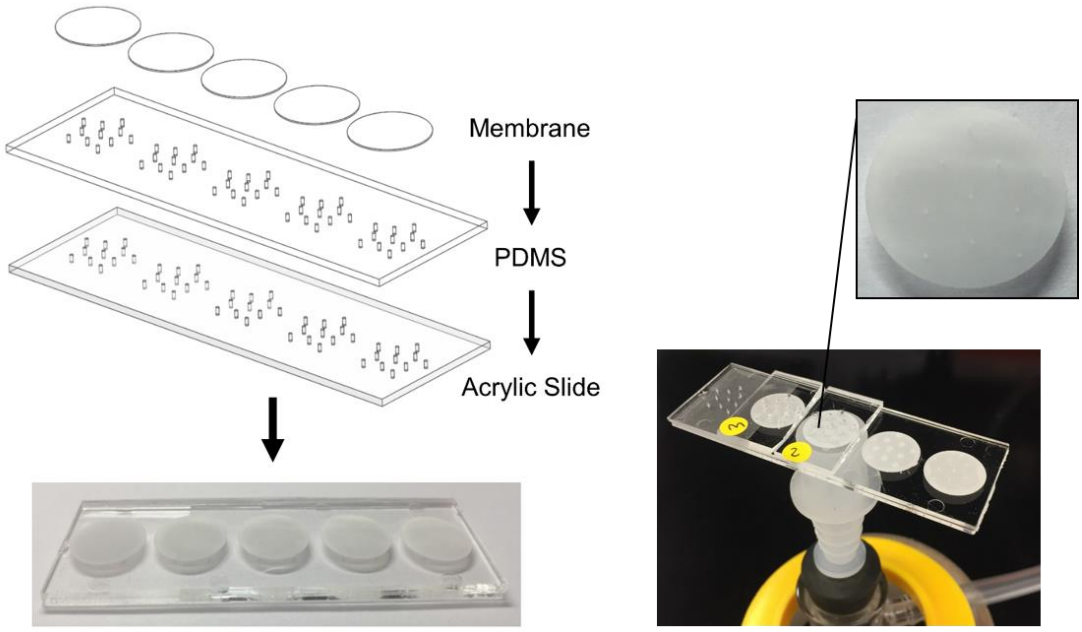


**Figure 47.** Collection device. The device was built by placing a PDMS layer on top of an acrylic plastic slide, making holes through them (approximately 300 µm diameter), and placing a 20 nm pore membrane on top. The sample was placed on top of the membrane, and vacuum was applied at the bottom of the slide.

### III.5.i Materials and Methods

*III.5.i.a Materials*

UVT acrylic microscope plastic slides were acquired from Ted Pella, Inc. (CA, USA). A polydimethylsiloxane (PDMS) Sylgard 184 kit was bought from Ellsworth Adhesives (WI, USA). Whatman inorganic membranes Anodisc 13 (0.02 μm pore size, 13 mm diameter) were obtained from GE Healthcare Life Sciences (PA, USA).

*III.5.i.b Collection Device Fabrication*

A collection device was fabricated and built starting with the use of acrylic plastic slides (25 mm x 75 mm). A specified pattern of holes were drilled on two acrylic slides with a CNC machine. A thin layer of PDMS (2 mm) was created by mixing 20 mL of the silicone elastomer solution with 2 mL of the curing agent, adding the mixture to a big petri dish, leaving it in vacuum for 50 min, and heating it at 80 $^{o}$C for 45 min. A piece of the PDMS (25 mm x 75 mm) was cut and placed in the middle of the two plastic slides with their holes aligned. A dispensing needle (0.009 in inner diameter) was passed through the holes on the slides to pierce the sandwiched PDMS and create consistent holes on it. The top slide was carefully removed to avoid misaligning the PDMS slide and the bottom slide. Finally, 20 nm Anodisc filters were placed on top of the PDMS surface to cover the holes.

*III.5.i.c Collection Method and SERS Measurement*

The SERS signal of the nanoprobe was measured on the collection device. To do this, 10 μL of the sample was placed on top of the membrane above the hole, and vacuum (approximately -0.06 MPa) was applied with a tube below the slide to suction the liquid through the membrane and holes. After they were collected, the collection area was

focused on the Raman microscope and an 11 by 10 point grid with a step size of 40 µm and 45 µm respectively was defined to measure the SERS spectrum at each point. The intensity peak values at 1336 $cm^{-1}$, which is a peak of the Raman reporter DTNB, of the measured spectra were used to plot maps and averaged to determine a value for the tested concentration.

### III.5.ii Testing the Membrane Collection Method

*III.5.ii.a Testing the Nanoprobes in the Collection Device*

Figure 48 shows the SEM images of the collection device with nanoprobes collected on the membrane. As can be observed, the nanoprobes are collected only on the areas in contact with the holes. When a low concentration of nanoprobes is passed through the membrane, they are spread throughout the area and the pores can be observed in the SEM image (Figure 48A-B). However, when a higher concentration of nanoprobes is analyzed, they cover all the area and form a thicker layer as they are stacked on top of each other (Figure 48E-F). The main function of the collection device is to gather together the nanoprobes in a small area and have the concentration of nanoprobes as the only changing variable in a SERS measurement. An effort was made to make the holes consistently and keep the aggregation area as similar as possible for each measurement.

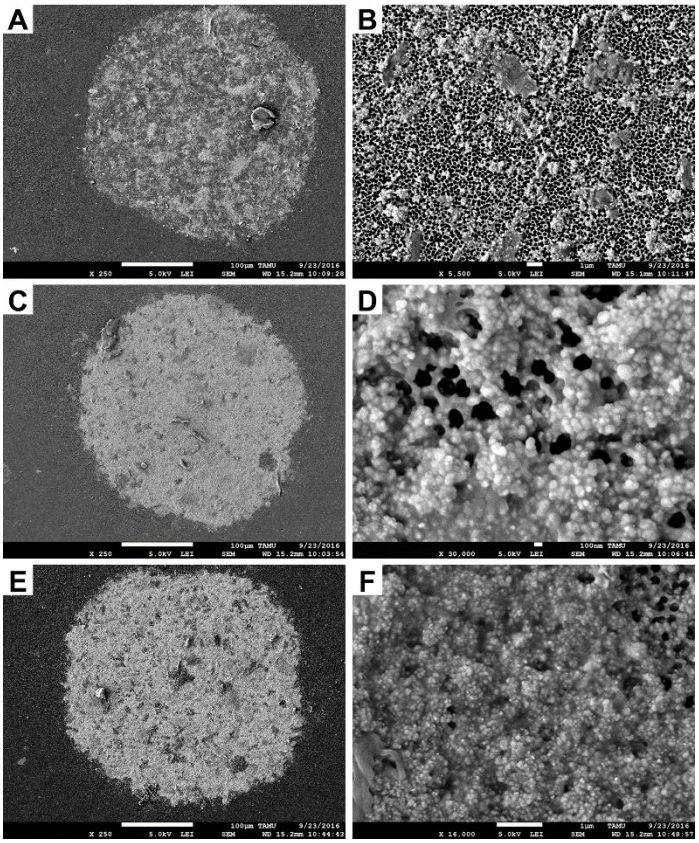


**Figure 48.** SEM images of nanoprobes aggregated on the collection device. Low concentration: (A), (B) zoom. Medium concentration: (C), (D) zoom. High concentration: (E), (F) zoom.

After gathering the nanoprobes with the collection device, the area was focused in the Raman microscope, and the SERS spectrum was measured at defined points on the collection area. SERS maps were plotted by using the intensity at 1336 $cm^{-1}$ of all the spectra. Figure 49 shows the maps of the SERS intensity at 1336 $cm^{-1}$ as different amounts of nanoprobe were analyzed on the collection device. As can be observed, the signal is mainly detected on the holes of the device. The signal increases with increasing concentration and reaches a maximum at 7.03 pM. At the blank measurement no signal is observed.

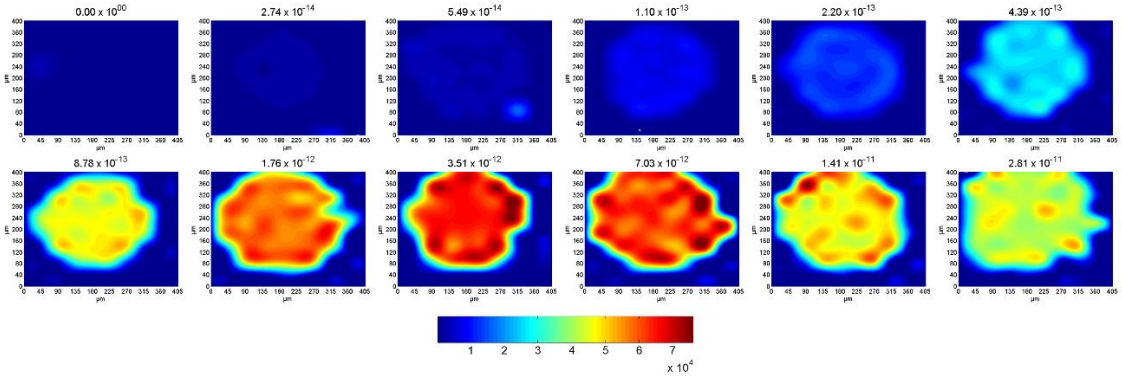


**Figure 49.** SERS intensity maps of different concentrations of nanoprobe collected on the collection device. To plot the maps, the SERS spectrum was measured at different points covering the collection spot (11 x 10 points, 40 µm and 45 µm step size respectively). Then, the peak values at 1336 cm-1 were used to obtain an intensity value for each grid point.

The intensities at the specific wavenumber of interest of all the spectra measured in the grid to plot each map were averaged to obtain a single value for each collection spot. These values were then plotted with their corresponding concentration of nanoprobe used when 10 µL was tested. Three different measurements with the same amount of nanoprobe were tested to calculate the standard deviation. Figure 50 shows the curves obtained when different peaks of the nanoprobe spectrum were used to obtain a value for each measurement. The four peaks analyzed exhibited a similar trend as the concentration changed. In addition, as can be observed in the logarithmic plot, there is a portion that can be used to calculate a linear function to predict the concentration. At higher concentrations, the SERS signal flattens out and on average appears to decrease slightly but is effectively flat given the increase in standard deviation. This standard deviation increase is likely due to the membrane saturating and more proteins, specifically BSA-nanoclusters absorbing at the laser wavelength used for SERS excitation (532 nm), present

in the measurement area. It is expected that different concentration curves will be obtained if the dimensions of the hole are changed, which means that the collection device could be optimized for the desired response given a particular application.

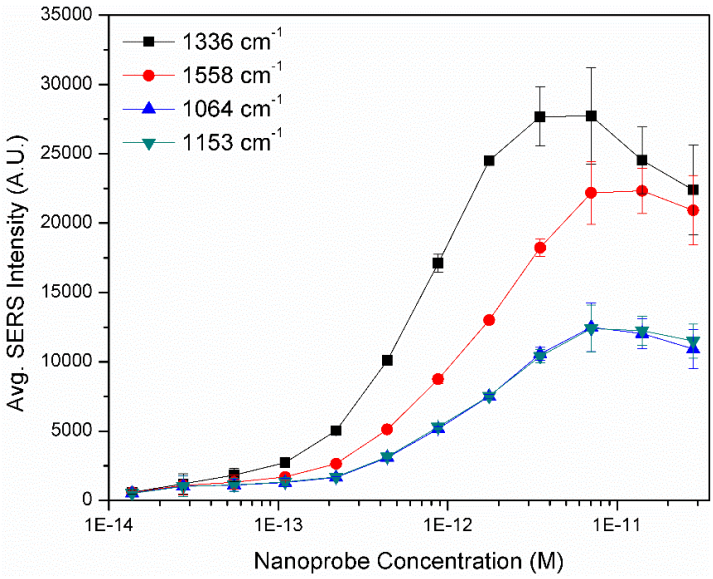


**Figure 50.** SERS values obtained for each concentration of nanoprobe tested when four different peaks of the DTNB spectrum were analyzed. Each point is the mean of the SERS intensity values at the specific wavenumber measured at different points on the nanoprobe collection area when 10 µL of the corresponding nanoprobe concentration was analyzed.

*III.5.ii.b Comparison of Nanoprobes with Ag-DTNB Nanoparticles*

The SERS signal concentration curve of the nanoprobe on the collection device was compared with the SERS signal concentration curve of Ag nanoparticles functionalized only with DTNB (Ag-DTNB). The same concentrations were used to test them in the collection device. As can be noted in Figure 51 the minimum concentration of nanoprobe that can be detected is about an order of magnitude lower than the concentration of Ag-DTNB nanoparticles. The LoD of the nanoprobe and Ag-DTNB nanoparticles of

the raw spectra measured on the collection device was calculated to be 16.2 fM and 517 fM respectively. The collected spectra at each measurement point was also baseline subtracted using an algorithm based on a method described by Ning[111] before averaging the intensities at 1336 $cm^{-1}$ to obtain a value for each concentration. The LoD calculated with the baselined data improved to 12.9 fM for the nanoprobe and 190 fM for the Ag-DTNB nanoparticles. The smaller LoD of the nanoprobe can be attributed to the consistent enhancement produced even after the nanoprobes are spread on the collection area at low concentrations. In each nanoprobe there are about 2 or more silver nanoparticles encapsulated in silica that interact with each other to form hotspots and enhance the signal of the DTNB molecule. In comparison, all the Ag-DTNB nanoparticles are aggregated on the membrane to form less controlled hotspots as they are not encapsulated. When the concentration is low, these nanoparticles spread on the collection area and less or no hotspots occur.

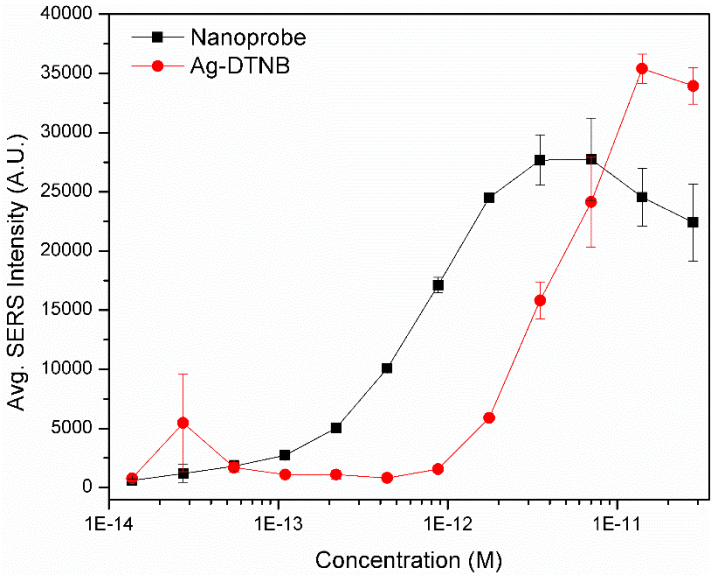


**Figure 51.** Comparison of signal obtained when the same concentrations of nanoprobe and Ag nanoparticles functionalized with DNTB were tested on the collection device.

The coefficient of variation (CV) was also calculated for the replicate measurements of nanoprobe and Ag-DTNB nanoparticles gathered with the collection device to determine how precise this method can be. As can be observed in Figure 52, for nanoprobe concentrations between 0.1 pM and 3.5 pM their CVs were less than 10 % when raw data was analyzed. However, when baselined data was used for analysis, CVs were less than 10 % for concentrations between 27.4 fM and 1.76 pM. At higher and lower concentrations, their CVs were greater than 10 %, and this can be attributed to the previously discussed saturation for the higher concentrations and approaching the LoD for the lower concentrations. The CVs of the Ag-DTNB nanoparticles were more variable, with most CV values of less than 10 % obtained for concentrations higher than 0.43 pM (see Figure 52).

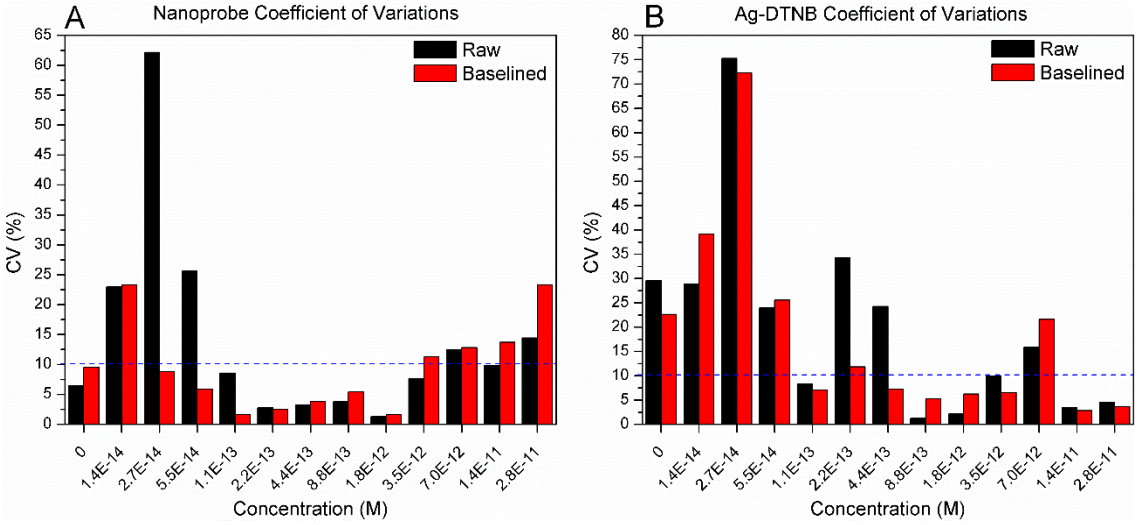


**Figure 52.** Coefficient of variations (CVs) of three replicate measurements at different concentrations of nanoprobe and Ag-DTNB measured with the collection method. (A) Nanoprobe CVs when raw or baselined spectra were used to calculate values. (B) Ag-DTNB CVs when raw or baselined spectra were used to calculate values.

### *III.6 Chapter Summary and Conclusions*

In this chapter, several nanoparticle collection methods were designed, tested, and analyzed to determine an approach to consistently collect and measure SERS active nanoprobes. The first method tried consisted in using centrifugation to collect the nanoparticles. A device that facilitated the sample placement, centrifugation, and measurement was built; however, the collection was inconsistent. Magnetic collection was another method explored to gather magnetic particles at specific locations. A solution with magnetic nanoparticles was added into a microchannel with 50 µm by 50 µm magnetic square pads inside to test their collection ability. The magnetic nanoparticles were flowed at different flow velocities, and it was observed that most nanoparticles passed through the magnetic collection area. Magnetic particles of larger diameter (1 µm) were used to improve the collection, but many particles were still not collected. In an alternative

method, a 3 mm diameter magnet was placed below a microchannel to collect the magnetic particles. More particles were collected with this method, but the collection area was very large to measure the SERS signal.

A filter membrane with 20 nm pores was used to collect the nanoparticles in several subsequent approaches. A device was created with plastic and rubber squares that sandwiched the membrane and contained a hole in the middle to place the sample. The problem with this approach was the large collection area and the difficulty of assembling the device for every measurement. To improve this concept, PDMS slabs with holes were used to sandwich the membrane. This design allowed to test multiple samples simultaneously. Nevertheless, the flexibility of the bottom structure caused it to bend, which promoted leaks of the tested solution through the holes that resulted in inconsistent collection. A modified design was built with a solid base and consistent 300 μm holes that improved the collection efficiency. This collection device was tested by collecting different concentrations of nanoprobe. Nanoprobe samples (10 μL) were detected with less than 10 % coefficient of variation (CV) across a range from nearly 27.4 fM to 1.7 pM using the described collection method.

# CHAPTER IV

# ASSAY DEVELOPMENT

## *IV.1 Assay Formats*

Assays are used to quantify the concentration of analytes in a sample. They are usually composed of antibodies or proteins that can selectively bind to the analyte of interest, even in the presence of multiple elements in a sample. An antibody can also form a strong bond with its analyte. These unique properties of antibodies are exploited to design assays. Several assay formats have been developed in which the procedures and the manner antibodies are used differ to obtain the desired results. The four main assay formats are: direct assay, indirect assay, sandwich assay, and competitive binding assay. Each assay format can be further customized by selecting the detection method, order of steps, and additional variables that affect the assay response.

### IV.1.i Direct Assay

The direct assay is a simple format with very few steps. In this format, the sample to be analyzed that contains the analyte of interest is incubated in a solid surface (plate or particle). The analyte then adsorbs to the surface to coat it. After this, a blocking solution is added to block available spaces in the solid surface. Subsequently, antibodies that bind to the analyte and are tagged with the detection compound (fluorescent dye, enzymes, etc.) are introduced to the solid surface. These antibodies bind to the analyte adsorbed on the solid surface. Then, the unbound antibodies are washed or removed from the capture area, and the signal produced by the labeled antibodies is measured. The signal is directly

proportional to the amount of antibody present. Figure 53 presents how the direct assay works. Advantages of this format include the minimal steps required to perform the assay.

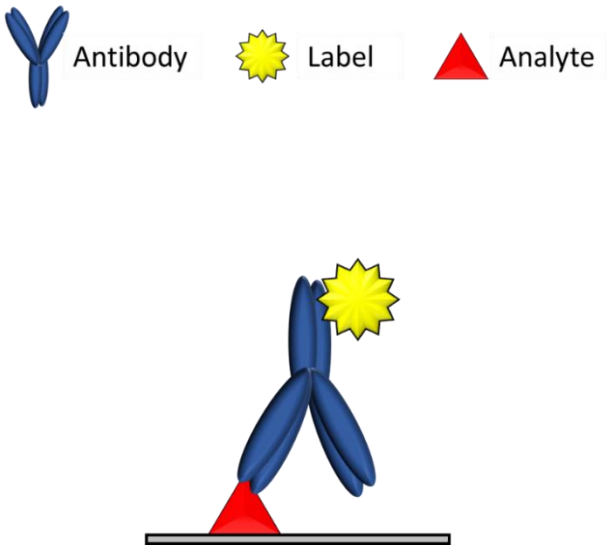


**Figure 53.** Direct assay format schematic. The analyte is adsorbed to the surface. Then, its labeled antibody binds to it and produces the signal.

### IV.1.ii Indirect Assay

Another format very similar to the direct assay is the indirect assay. In this format, the analyte of interest is also incubated and adsorbed on a solid surface. After the analyte is adsorbed, the surface is blocked, and the antibody of the analyte is added. This antibody, or primary antibody, binds to the analyte on the solid surface. However, in contrast with the direct assay format, in this format the primary antibody is not labeled. Another species-specific antibody, or secondary antibody, that is conjugated with a fluorophore or an enzyme is used to generate the measured signal. The secondary antibody, which binds to antibodies from the species of the primary antibody, binds to the primary antibody bound to the analyte. Figure 54 shows how the indirect assay works. An advantage to this format

is that several secondary antibodies can be bound to a primary antibody; therefore, the signal can be amplified and the sensitivity can be increased. Disadvantages of this format include an extra incubation step and the possible cross-reactivity of the secondary antibody that can cause background signal.

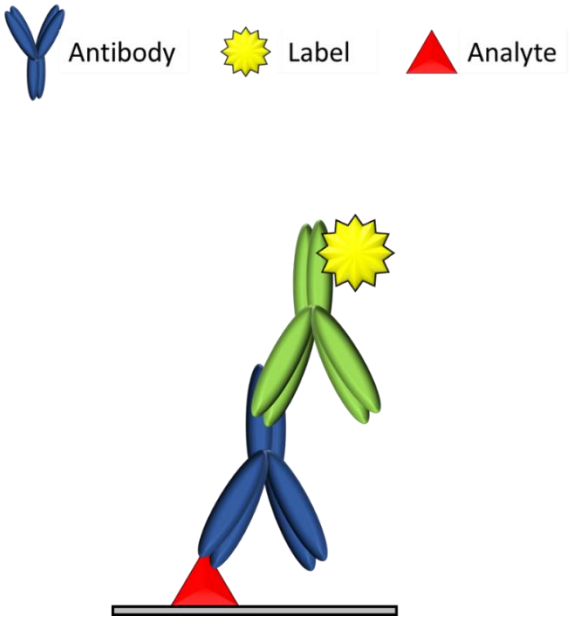


**Figure 54.** Indirect assay format schematic. The analyte is adsorbed to the surface. Then, its antibody (primary) binds to it. After that, another labeled antibody (secondary) binds to the primary antibody to produce the signal.

### IV.1.iii Competitive Binding Assay

The competitive binding assay format is based on the competition between labeled analyte and the analyte in the sample of interest for antibody binding sites. This assay is usually used to measure small analytes. Since only one antibody is used in this format, competitive binding assays are also used when antibody pairs of an analyte do not exist. In this format, the antibody is usually attached on a solid surface. Then, a known amount of labeled analyte and the sample containing the analyte that will be measured are mixed

with the antibodies on the surface. Figure 55 shows the steps of a competitive binding assay. According to the law of mass action, the amount of free labeled analyte at a specific time will depend on the total amount of labeled analyte, total amount of sample analyte, total amount of antibody, and the association and dissociation rate constants of the analytes with the antibody. Therefore, when the concentration of sample analyte is high, less labeled analyte will be bound to the antibodies and more will be in the supernatant. In contrast, when the concentration of the sample analyte is low, more labeled analyte will be bound to the antibodies and less will be in the supernatant. The relationship between the signal and the analyte of interest concentration depends on which sample of the labeled analyte is measured. If the labeled analyte bound to the antibody is measured the signal will be inversely proportional to the analyte of interest concentration. However, if the labeled analyte in the supernatant is measured the signal will be directly proportional.

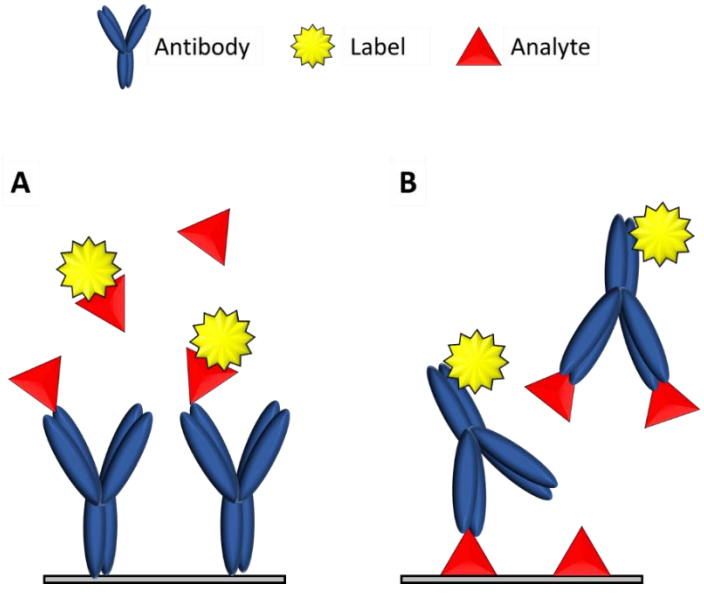


**Figure 55.** Competitive binding format schematic. (A) The analyte competes with a labeled analyte for antibody binding sites. (B) The analyte binds to its labeled antibody. Then, any antibody with free binding sites binds to analyte conjugated on the surface.

In an alternative version of the competitive binding assay, the analyte is attached to a solid surface. Then, a known amount of labeled antibody and the sample interest are mixed and added to the surface. In this case, the analyte in the sample of interest will bind and occupy binding sites of the labeled antibody. If free antibody binding sites are available, the labeled antibody will bind to the analyte on the surface. As a result, the amount of labeled antibody free or on the surface will be depend on the amount of analyte in the sample. Additional modifications can be made to the competitive binding format, such as sequentially adding any of the components. Advantages of competitive binding assays include the flexibility of the detection methods, high sensitivity, the use of only one antibody, and the ability to perform the measurements in complex samples.

**IV.1.iv Sandwich Assay**

The sandwich assay format is the most commonly used assay because it tends to be more sensitive and selective than other formats. In this format, two antibodies are used: the capture antibody and the detection antibody. Each antibody binds to a different site or epitope of the analyte. In a sandwich assay, the capture antibody is attached to a solid surface (well or particle). The surface is blocked to prevent non-specific binding. Then, the analyte is introduced to the area with the capture antibody. After some time, the analyte binds to the capture antibody, and the detection antibody is added. The detection antibody can be labeled with the detection compound (fluorescent dye, enzyme, etc.) or a labeled secondary antibody that binds to the detection antibody can be used. The detection antibody also binds to the analyte bound to the capture antibody. Consequently, the analyte is sandwiched between the two antibodies. Figure 56 shows the sandwich assay format.

As the concentration of analyte increases more labeled detection antibody is bound on the solid surface, and the signal obtained from the sandwich assay is proportional to the amount of analyte present. If a known amount of labeled detection antibody is added and the supernatant is measured, the signal is inversely proportional. Among the advantages of this assay format are its sensitivity, specificity, and flexibility of detection method.

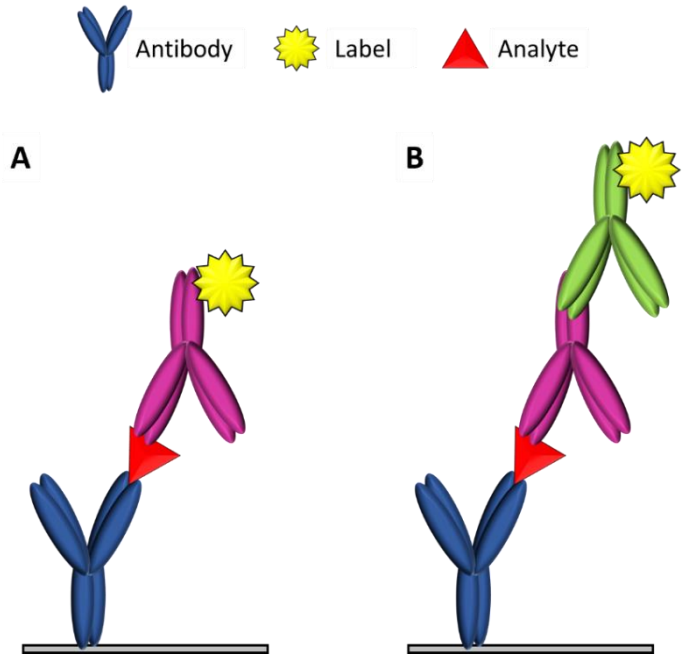


**Figure 56.** Sandwich assay format schematic. (A) The analyte is sandwiched between its capture and detection antibodies. The detection antibody is labeled to produce the signal. (B) The analyte is sandwiched between its capture and detection antibodies. Then, another labeled antibody binds to the detection antibody to produce the signal.

### *IV.2 Selecting the Assay Format*

An assay to detect cardiac biomarkers could have been developed in the different assay formats. To select the assay type to be used, the requirements of the biosensor and the characteristics of the assay formats were considered. The main requirements for the development of a cardiac biomarkers assay are high sensitivity, precision, and a fast

response. As discussed before, the assay formats differ in the steps, number of antibodies, and the way the analyte is detected. Each of them have advantages and disadvantages that affect the assay performance and its ability to meet the desired requirements.

### IV.2.i Direct and Indirect Assay

In direct and indirect assays, the analyte of interest is adsorbed on a surface to detect it. Since the sample to be analyzed by the biosensor is composed of multiple proteins and other compounds, they will also be adsorbed on the surface. The surface then needs to be blocked to prevent the nanoprobes functionalized with detection antibodies to adsorb to the surface. The lack of control of which proteins or compounds and how many of them are adsorbed on the surface can increase the nonspecific binding of the nanoprobes and thus negatively impact the sensitivity and precision of the assay. In addition, the incubation time required for a blocking step after introducing the sample with the analyte would increase the assay detection time. For the indirect assay, having different proteins or antibodies on the surface could also increase the possibility of nonspecific binding caused by the interaction of the secondary antibody with them.

The adsorption of a protein on a surface is usually dominated by the surface energy, electrostatic interactions, and hydrophobic interactions.[112] The bonds associated with adsorption are not as strong as covalent bonds, and can be disrupted by changing the pH, salt concentration or the addition of washing reagents. Since a washing step is required in both assay formats to separate the bound and unbound detection nanoprobes, the wash could also remove the adsorbed analyte of interest, which would cause inaccurate measurements. Furthermore, when the assays are translated to a microfluidic point-of-care

platform, the defined binding surface area would have to be composed of a different material than the channel walls to avoid adsorption in undesired sections. The failure potential associated with the direct and indirect assay formats prevented their selection as the formats for the development of an assay to detect cardiac biomarkers.

### IV.2.ii Competitive Binding Modeling

The competitive binding assay format can be designed in several versions to create a SERS based assay. The different versions of this format can be classified according to the order in which the reagents are mixed. For example, in the case in which an antibody is attached to the surface of a particle and the competitor is a SERS active nanoprobe functionalized with the analyte of interest on its surface, the following are the mixing possibilities: (1) simultaneous mixing - the nanoprobe and the sample with the analyte are mixed simultaneously with the antibody; (2) sequential saturation - the sample with the analyte is mixed with the antibody first, then the nanoprobe is added so it can bind in the available binding sites; (3) sequential displacement - the nanoprobe is mixed with the antibody first, then the sample with the analyte is added to displace the bound nanoprobe.

A model was created to predict and analyze the behavior of the sequential displacement competitive binding format. Specifically, the model calculated the free and bound amount of nanoprobe in the presence of different concentrations of analyte. The reagents concentrations and rate constants used were input in the equations of the model to obtain the predicted results.

To create the model, the steps, components, and mechanisms of the sensor were defined. The sensor would consist in the filtration part, where the blood sample is filtered

to obtain the plasma with the analytes; the recognition part, where the analytes react in the assay; and the transduction part, where an element of the assay concentration is measured and converted to a quantitative value. Antibodies, functionalized nanoprobes, and the analyte of interest would be the three components of the assay. The assay would have a sequential displacement competitive binding format. In a competitive binding assay, the unknown concentration of an analyte of interest can be determined by measuring the concentration of the competing ligand, in this case the functionalized nanoprobes, that are free or bound to the receptor.

In the envisioned sensor, recognition would occur in a microchannel. The antibodies or receptors would be attached to a surface inside the microchannel. In order to separate the flow in sections and control the assay reaction time, the microchannel would have three micro-valves that divide the channel in three sections: the assay or recognition section, the transduction section, and the waste section (see Figure 57). To prepare the sensor, the first step would be to add a small volume of functionalized nanoprobes solution to the microchannel. The transduction and waste micro-valves would be closed to allow the nanoprobes bind to the receptors in the assay section. After a period of time, the waste micro-valve would be opened to flush the liquid out of the assay section and leave the nanoprobe-antibody complexes ready for the next step.

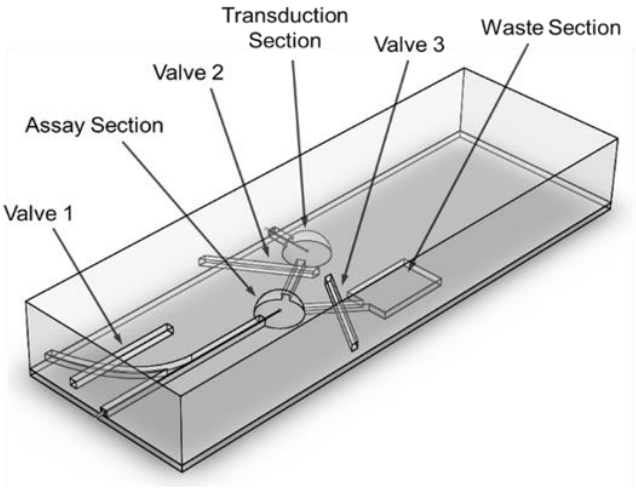


**Figure 57.** Envisioned microchannel in which the sequential displacement assay occurs in the model. The channel has three sections: assay section where the reaction occurs, transduction section where the SERS signal is measured, and waste section. It also has valves to control the flow of reagents.

To perform the test, a sample of blood would be obtained and filtered to separate the red blood cells from the plasma. The plasma would then be flowed to the assay section, where the competitive binding reaction would occur and the analyte of interest would displace the bound nanoprobes. The amount of nanoprobes that would be displaced would be proportional to the amount of analyte of interest present. After a specific time, the transduction micro-valve would be opened for a short time to separate the bound and free nanoprobes. Then, the micro-valve would be closed again and the free nanoprobes would be collected on the transduction section. Finally, the signal would be measured at the nanoprobes collection spot and processed to obtain the concentration of the analyte of interest. Table 5 shows the steps of the sensor and the equations used to model the system.

**Table 5.** Sequential displacement assay steps and equations used to model the system.

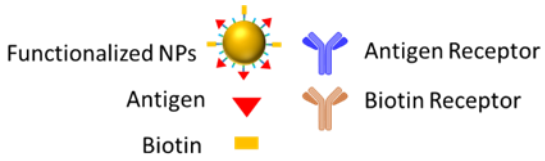


| Sensor Stage | Equations in Model | Time |
|---|---|---|
| Initial State 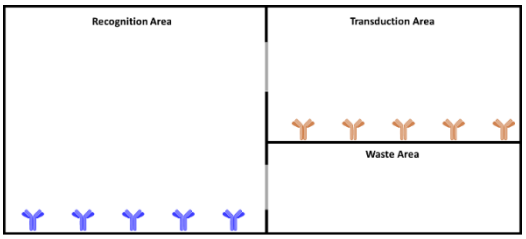  | No equations | |
| Part I: Loading NPs 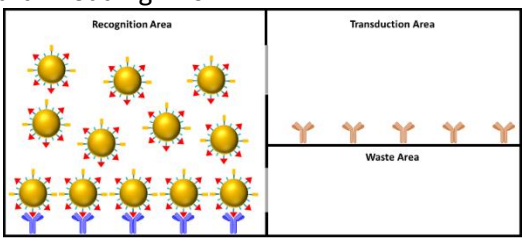  | $CR + CL \underset{k2}{\overset{k1}{\leftrightarrow}} CRL$<br>$\frac{dCRL(t)}{dt} = k1 * CL(t) * CR(t) - k2 * CRL(t)$<br>$CR(t) = CR(0) - CRL(t)$<br>$CL(t) = CL(0) - CRL(t)$ | 60 min |
| Part II: NPs separation 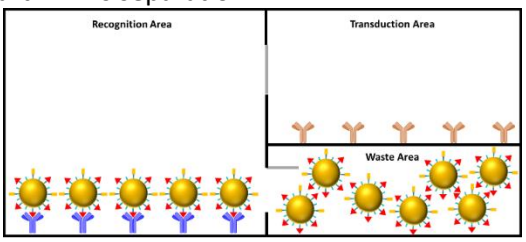  | $CRL \overset{k2}{\rightarrow} CR + CL$<br>$\frac{dCRL(t)}{dt} = -k2 * CRL(t)$ | 1 min |
| Part III: Waiting for analyte of interest 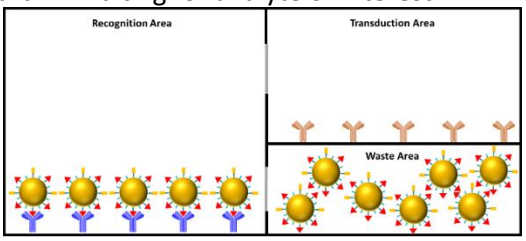  | No equations | 1 min |

**Table 5.** Continued

| Sensor Stage | Equations in Model | Time |
|---|---|---|
| Part IV: Competitive binding 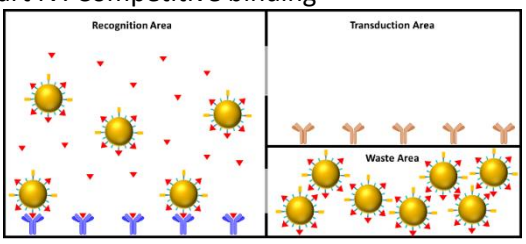  | $CR + CL \underset{k2}{\overset{k1}{\leftrightarrow}} CRL$<br>$CR + CI \underset{k4}{\overset{k3}{\leftrightarrow}} CRI$<br>$\frac{dCRL(t)}{dt} = k1 * CL(t) * CR(t) - k2 * CRL(t)$<br>$\frac{dCRI(t)}{dt} = k3 * CI(t) * CR(t) - k4 * CRI(t)$<br>$CR(t) = CR(0) - CRL(t) - CRI(t)$<br>$CL(t) = CL(0) - CRL(t)$<br>$CI(t) = CI(0) - CRI(t)$ | 15 min |
| Part V: Competitive binding separation 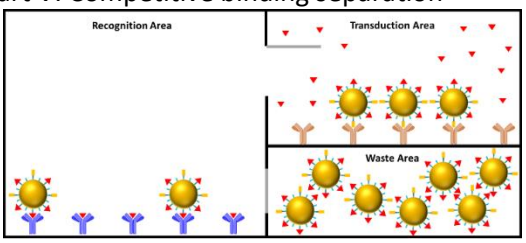  | $CRL \overset{k2}{\rightarrow} CR + CL$<br>$\frac{dCRL(t)}{dt} = -k2 * CRL(t)$ | 3 min |
| Part VI: After competitive binding 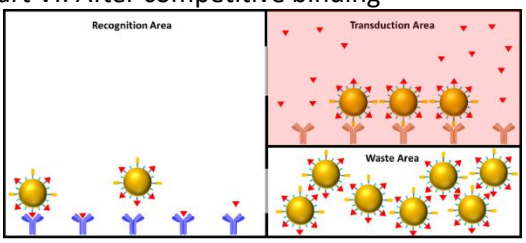  | No equations | 2 min |

The equations that describe the model at the different stages of the sensor are derived from the law of mass action and the law of conservation of mass (shown in Table 5). Since all the stages of the sensor are connected, the equations that describe the behavior of the sensor components in each stage are coupled with the equations that describe the behavior in previous and future stages. A final value (the amount of nanoprobes measured

after the sensor reaction with an amount of analyte of interest present) is obtained after all the equations are solved for each stage. Matlab was used to solve the ordinary differential equations of the system, couple the equations, and plot the responses to predict the concentration of NPs or the receptor-NPs complex at each point in time (see Figure 58).

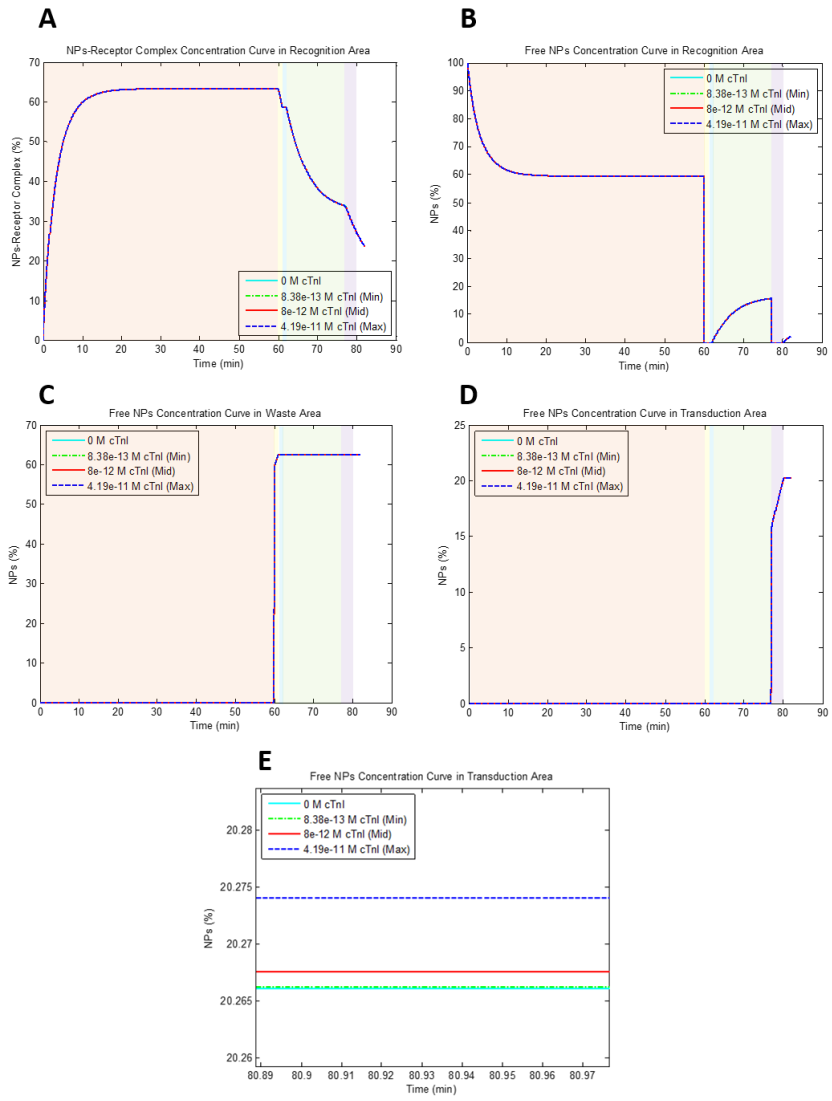


**Figure 58.** Model results that predict the amount of NPs in each section at each point in time for different concentrations of analyte tested. (A) Nanoparticles bound to antibodies in recognition section. (B) Free nanoparticles in recognition section. (C) Nanoparticles in waste section. (D) Nanoparticles in transduction section. (E) Zoom of nanoparticles in transduction section at the end of the assay.

As can be observed in Figure 58, the percentage of nanoprobes or antibody-nanoprobes complexes at the defined areas (recognition area, transduction area, and waste area) is calculated for each point in time. The theoretical response of the sensor was calculated for four different concentrations of the analyte of interest: 0 M (blank), 8.38 x $10^{-13}$ M (minimum), 8 x $10^{-8}$ M (medium), and 4.19 x $10^{-11}$ M (maximum). These values were selected because they are in the clinical cTnI concentration range of interest. The difference between the response when no analyte was present and when the maximum concentration of analyte was present can be observed in Figure 58E. As can be noted, the difference is approximately 0.008 % of the initial concentration of nanoprobes used (54.9 nM) or 4.4 pM (difference between 11.130 nM and 11.126 nM). This value was obtained after optimizing the concentration values used of antibodies and nanoprobes to obtain the largest difference. The difference between the minimum and maximum concentrations is minimal compared to the actual concentration of nanoprobes that would be measured (about four orders of magnitude lower). This suggest that this assay version could be susceptible to errors that can affect the sensitivity or precision as any slight change could cause the same difference in signal. In other words, the signal to noise ratio (SNR) would probably be very small. Therefore, additional versions were considered to develop the biosensor.

**IV.2.iii Kinetic Rate Constants**

The law of mass action is used to describe the behavior of reactants in a solution. Specifically, it states that the rate of a chemical reaction is directly proportional to the concentrations of the reactants.[113] This interaction can be expressed as:

**Equation 4**

$$RL \underset{kd}{\overset{ka}{\rightleftharpoons}} R + L$$

In this expression, R is the receptor, L is the ligand, RL is the receptor-ligand complex, ka is the association rate constant ($M^{-1}$ $s^{-1}$), and kd is the dissociation rate constant ($s^{-1}$). The association rate constant kd is the amount of complexes formed per second in one molar solution of ligand and receptor and is used to describe the rate of complex formation. The dissociation rate constant kd is the fraction of complexes that dissociate per second and is used to describe the stability of the complex. The rate of change at time t of this reaction can be written as: [113]

**Equation 5**

$$\frac{d[RL]}{dt} = ka[R][L] - kd[RL]$$

At equilibrium the ratio of the two rate constants gives the equilibrium association constant Ka, which represents the ratio of bound to unbound ligand and receptor. This is also known as the affinity constant and can be expressed as: [114]

**Equation 6**

$$Ka = \frac{ka}{kd} = \frac{[RL]}{[R][L]}$$

The inverse of the equilibrium association constant is the equilibrium dissociation constant Kd, which measures the tendency of a complex to reversibly dissociate into its components and can be written as: [114]

**Equation 7**

$$Kd = \frac{kd}{ka} = \frac{[R][L]}{[RL]}$$

The rates are related to the time the ligand is free or bound to the receptor. When a ligand gets sufficiently close to the binding site of a receptor it will bind and form a complex. The ligand will eventually dissociate when the random thermal movements of the complex produce enough energy to break the bond and allow the ligand escape.[113] The average amount of time that a ligand will spend as part of a complex is the mean-life and is: [115]

**Equation 8**

$$t_{mean} = \frac{1}{kd}$$

The time at which half of the initial amount of complexes have dissociated is the half-life and can be calculated by: [115]

**Equation 9**

$$t_{1/2} = \frac{0.693}{kd}$$

The mean-life and half-life are useful parameters that should be considered when designing assays. Table 6 present the half-life of different dissociation rate constants. As can be observed, complexes in a reaction can last from micro-seconds to days. This suggests that if receptors with a high kd are used in sandwich assay formats, they would dissociate in the washing steps and thus cause measurements errors. Similarly, if receptors with a very low kd are used in sequential displacement competitive binding formats a long time would be required to break the complexes.

**Table 6.** Half-life of dissociation rate constants.

| kd ($s^{-1}$) | $t_{1/2}$ |
|---|---|
| $1 \times 10^{-6}$ | 8 days |
| $1 \times 10^{-5}$ | 19.2 h |
| $1 \times 10^{-4}$ | 1.9 h |
| $5 \times 10^{-4}$ | 23.1 min |
| $1 \times 10^{-3}$ | 11.5 min |
| $5 \times 10^{-3}$ | 2.3 min |
| $1 \times 10^{-2}$ | 1.1 min |
| $1 \times 10^{-1}$ | 6.9 sec |
| $1 \times 10^{1}$ | 69.3 msec |
| $1 \times 10^{5}$ | 6.9 μsec |

When a nanoprobe is functionalized with multiple analytes its dissociation constant will be different than the original analyte-receptor kd. This occurs because the probability of the nanoprobe to dissociate is reduced by the presence of additional analytes close to the receptor. The functional affinity or avidity of the nanoprobe is an accumulation of the affinities of individual interactions. The dissociation constant of cTnI with a specific antibody has been reported to be approximately $5.6 \times 10^{-4}$ $s^{-1}$.[116] However, it is predicted that the dissociation constant of a nanoprobe functionalized with cTnI will have a lower kd and thus have a slower half-life. This means that it would take a long time for the complexes to dissociate and reach equilibrium in a saturation displacement competitive binding assay, which explains the small difference predicted in the model as different amounts of cTnI were tested. It takes approximately five times the half-time to reach equilibrium after the ligand and receptor are mixed.[114] This would also negatively affect

the simultaneous mixing competitive binding assay as it would take a long time to reach equilibrium and measure the free nanoprobe proportional to the amount of cTnI present. In contrast, the sequential saturation competitive binding assay would not be affected by the half-time of cTnI and its antibody since the nanoprobes would only bind on the free binding sites, and after a couple minutes the free nanoprobes would be collected to measure them. Therefore, based on the model results, the dissociation rate constant, and half-time analysis of the complexes formed, it can be concluded that the sequential saturation version would probably be the best format to design a competitive binding assay to detect cTnI.

### IV.2.iv Selection between Sandwich and Sequential Saturation Competitive Binding Assays

After considering the different formats to design and develop an assay to detect cTnI, several of them were rejected and only two were identified as the most promising options. The assay can be designed in the sequential saturation competitive binding and sandwich assays formats. Both formats have different advantages and disadvantages that were considered to move forward in the assay development.

Both formats have the same number of steps: (1) mixing of analyte in the sample with the antibodies, (2) incubation of analyte and antibodies, (3) addition of functionalized nanoprobe, (4) incubation, (5) separation, (6) collection of nanoprobes, and (7) measurement. The main advantages of the competitive assay over the sandwich assay is that it only uses one antibody. The sandwich assay format requires antibody pairs that bind to different epitopes of the analyte. A main disadvantage of competitive binding assays is

that it is essential to control the concentrations of reagents used as any variations could affect the response.[33] Although it would be ideal to control the reagents concentrations used for sandwich assays too, its response is not as sensitive to changes in concentrations used. Competitive binding assays can produce sensitive measurements; however, sandwich assays are considered the most sensitive and specific of all the assay formats when they are optimized and designed appropriately.[33] As a result, the sandwich assay format was selected as the format to develop the cardiac biomarkers biosensor.

### *IV.3 Sandwich cTnI SERS-Based Assay*

A SERS-based sandwich assay was designed and developed to detect cardiac biomarkers. The main components of the assay included the functionalized nanoprobe synthesized to produce a specific SERS signal, a magnetic particle functionalized with the capture antibody, and a device to collect the nanoprobes for measurement. Figure 59 shows the assay procedure steps. First, the sample with the analyte of interested is mixed with the magnetic particles, and they are incubated for approximately 20 min. Then, the nanoprobe is added, and the components are incubated for another 15 min. Subsequently, a magnet is used to separate the magnetic particles and extract the supernatant. After collecting the supernatant, buffer is added to the magnetic particles to wash them. The magnetic particles are separated again to collect the buffer. The collected supernatant is then passed through a membrane in the collection device to aggregate the nanoprobes on a specified area. Finally, specific points in the area are defined to measure the SERS signal. The monitored SERS peaks of the measurements are averaged to obtain an intensity value for the sample tested.

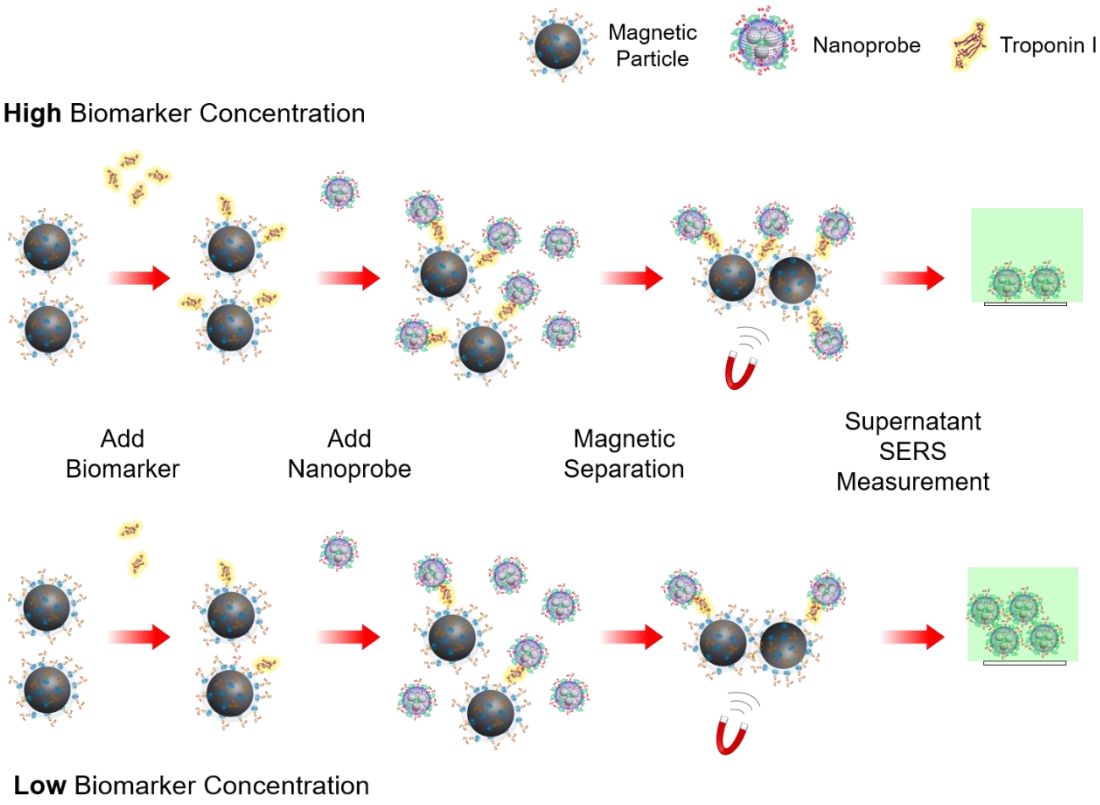


**Figure 59.** SERS-based sandwich assay procedure. The analyte is incubated with the magnetic particles. Then, the nanoprobe is added and incubated. After that, the particles are separated to collect the free nanoprobe and measure it.

### IV.3.i First Tests

To test the cTnI sandwich assay two concentrations were examined: one with cTnI (2000 ng/mL) and the other without (0 ng/mL). In this case, the magnetic particles were collected on the membrane to measure the SERS signal of the nanoprobes attached on them when cTnI was present.

The first step of the assay was to add 30 µL of cTnI in PBS or only 30 µL of PBS on a wellplate with 5 µL of magnetic particles. They were incubated for 30 min on a shaker at room temperature. Then, 10 µL of nanoprobe solution was added, and the solution was

incubated for another 30 min. After incubation, a magnet was placed on the bottom of the well to attract the magnetic particles and collect the supernatant. To wash the particles, 30 µL of TRIS was added. This step was repeated one time. Finally, 10 µL of the magnetic particles solution was passed through the collection device to measure a SERS map.

Figure 60 shows the assay responses of the two different cases (blank and cTnI). The top images show the aggregated magnetic particles on the membrane with the defined points where the SERS signal was measured (blue marks). The bottom graphs are the corresponding SERS intensity maps (intensity value at 1333 cm-1 peak for each spectrum) obtained at the 110 different points.

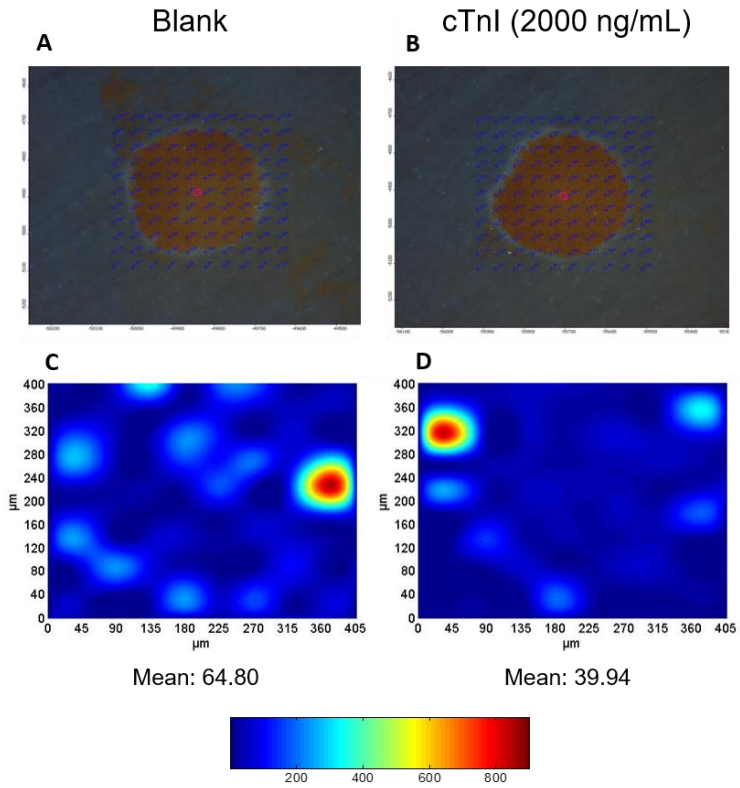


**Figure 60.** Sandwich assay results. Collected magnetic particles (A) and SERS intensity map (C) of blank sample. Collected magnetic particles (B) and SERS intensity map (D) of sample with cTnI (2000 ng/mL).

As can be observed, no significant difference was noticed between the two cases. Also, the SERS signal intensity of the few spots on the map was low (less than 1000 a.u.). SEM images of the tested magnetic particles were obtained to examine if nanoprobes were attached to them. In Figure 61, the nanoprobes (small white dots) can be observed on the magnetic particles in both cases. The nanoprobe attaching to the particles when no cTnI was present is an indication that nonspecific binding occurred.

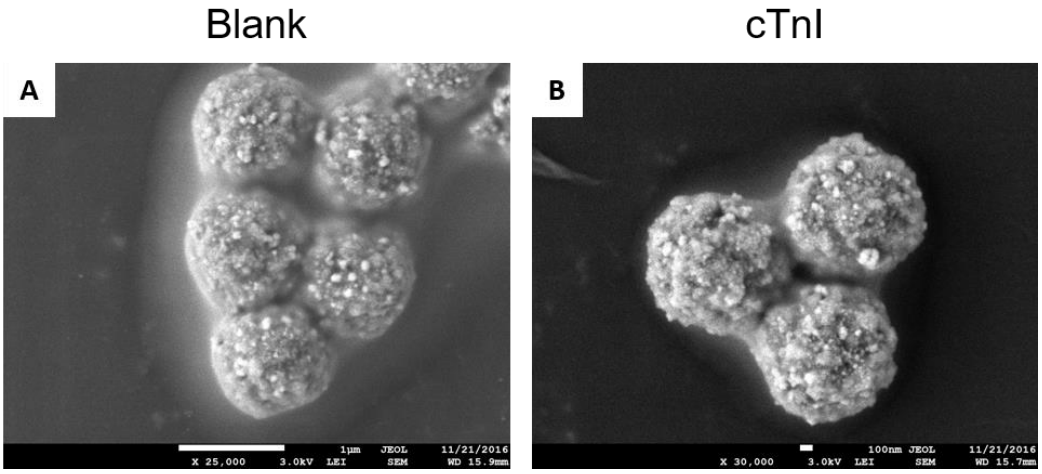


**Figure 61.** SEM images of the magnetic particles after the assay. (A) Magnetic particles of blank sample. (B) Magnetic particles of cTnI (2000 ng/mL) sample. The small white dots are nanoprobes.

Another similar test was performed; however, in this case more BSA was added to the particles after functionalization to block free spaces and avoid nonspecific binding. Also, three different amounts of magnetic particles were tested to determine if this variable had an effect in the assay response.

In this assay, 30 µL of cTnI in PBS or 30 µL of only PBS was added to wells with different amounts of magnetic particles: 0.1 µL, 1 µL, and 2 µL. The solution was incubated for 20 min on a shaker at room temperature. Then, 2 µL of nanoprobe was added

and incubated for another 20 min. The particles were magnetically separated to wash them two times. Subsequently, they were redispersed in 30 µL of PBS and aggregated on the collection device to measure their SERS signal.

The results of the assays at the two different cases can be seen in Figure 62. A slight increase of signal was noticed from the blank case to the cTnI case when 1 µL and 2 µL of magnetic particles were used. However, the difference was very small. The opposite response was obtained when 0.1 µL was used, which was not expected. It is important to note that only small spots of SERS signal were observed in the maps, usually in the edge of the collection area. Furthermore, the addition of extra BSA to prevent nonspecific binding did not improve the signal, which suggested that other techniques would have to be examined.

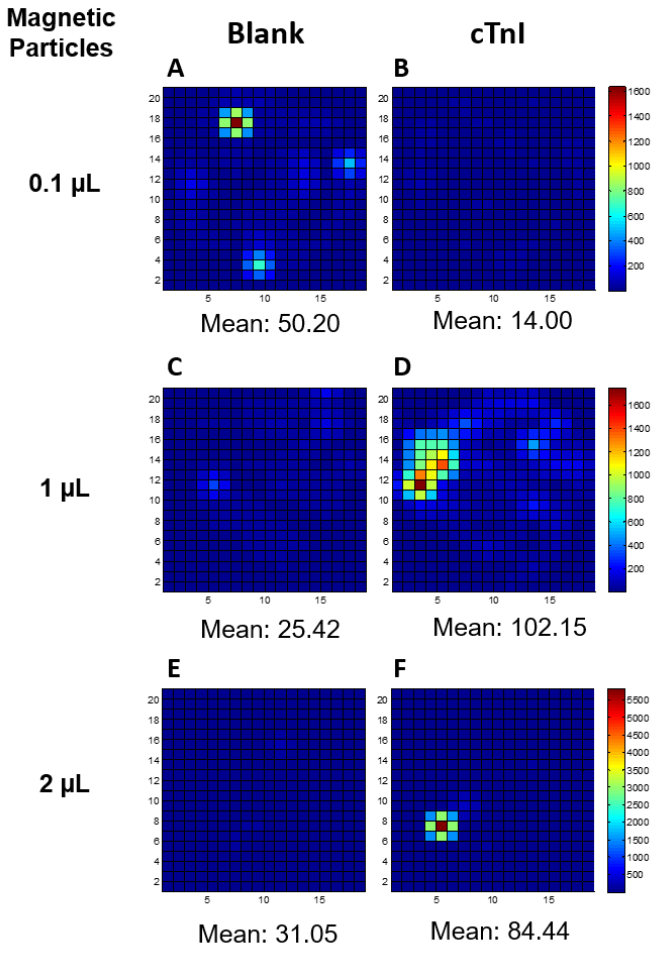


**Figure 62.** SERS intensity maps of sandwich assays with different concentrations of magnetic particles. In (A), (C), and (E) a blank sample was tested. In (B), (D), and (F) a sample with cTnI was tested.

### IV.3.ii Use of Streptavidin/Neutravidin to Reduce Nonspecific Binding

Streptavidin and neutravidin were used in the antibody bioconjugation process as another method to prevent nonspecific binding and have more control over the amount of antibodies conjugated on the nanoprobe and magnetic particles. Magnetic particles coated with streptavidin were used to attach biotinylated antibodies. Similarly, the surface of the nanoprobe was coated with neutravidin to conjugate the biotinylated antibody sandwich

pair. Covering the surface of the nanoprobe and magnetic particles with streptavidin/neutravidin stabilized them without the need to cover them with antibody and BSA as previously done. In previous conjugation techniques, antibody and BSA had to be added in excess of the amount of NHS-active PEG present on the nanoprobes to avoid crosslinking since the proteins have more than one amine groups. Adding neurtravidin in excess prevented crosslinking, nonspecific binding, and permit the attachment of the desired amount of antibody.

The assay procedure was similar to the previous tests. Briefly, the samples to be tested (blank and cTnI or low cTnI and high cTnI) were added to wells with different amounts of magnetic particles (1 µL, 2 µL, or 5 µL). They were incubated for 20 min on a shaker at room temperature. Then, 2 µL of nanoprobe was added and incubated for another 20 min. After this, the particles were washed two times and resuspended in 30 µL of PBS. In two assays, the magnetic particles were aggregated on the collection device to measure their SERS signal. However, in one assay 5 µL of the supernatant solution was passed through the collection device to aggregate the nanoprobes that did not bind and measure their SERS signal.

Figure 63 shows the SERS intensity maps of the different cases: blank and cTnI (1666 ng/mL) for 2 µL and 5 µL of magnetic particles used and low cTnI (1 ng/mL) and high cTnI (10 ng/mL) for 1 µL of magnetic particles used. A slight decrease of signal was observed from the high cTnI to the low cTnI cases when 1 µL of magnetic particles was used, which was expected. However, the difference was minimal. A similar response was observed for the 2 µL of magnetic particles case when blank and cTnI were tested. It was

noted that the SERS map intensity was low at the center of the collection spot and high around the spot. In the case where the supernatant was measured and 5 µL of the magnetic particles were used, the results were also as anticipated because the blank sample resulted in higher signal than the sample with cTnI. This should happen because the amount of nanoprobe on the supernatant is inversely proportional to the amount of cTnI added. Even though all the results followed the expected trend, the difference in SERS signal was not very high (the largest intensity difference was 1061 a.u. between blank and cTnI when the supernatant was measured). This suggested that optimization of the assay would be needed to improve the response.

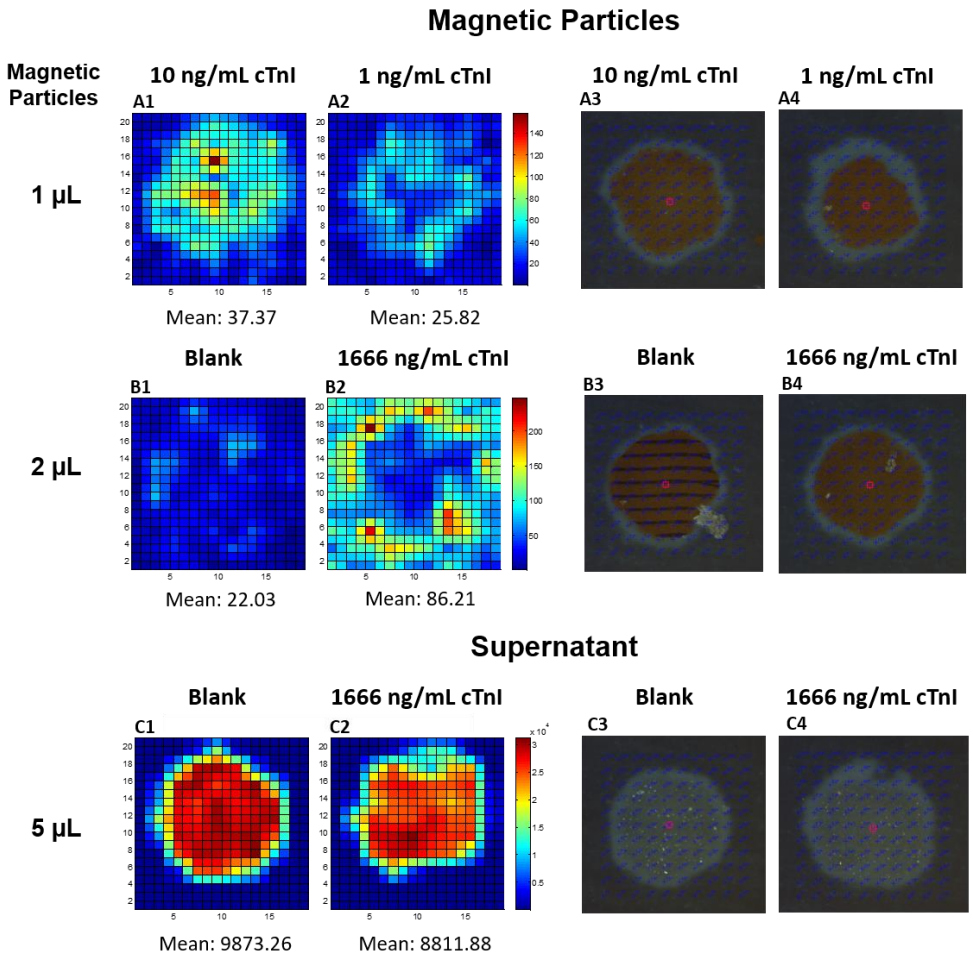


**Figure 63.** SERS intensity maps and collection images. Assay responses of two different cases: blank and cTnI samples when 2 and 5 µL of magnetic particles were used, and high (10 mg/mL) and low (1 ng/mL) cTnI samples when 1 µL was used. (A1), (A2), (B1), (B2) show the SERS intensity maps of the aggregated magnetic particles on the membrane. (C1) and (C2) show the SERS maps of the aggregated supernatant.

### IV.3.iii Antibody Selection Pair Test

Monoclonal antibodies bind to a specific region or epitope of their antigen. For many antibody clones, the amino acids of the antigen they target have been identified. This information as well as empirical tests are used to determine the antibody pairs that target the antigen at different regions in order to be used in sandwich assays. In an effort

to find the sandwich pair that resulted in the largest difference between blank and cTnI different antibodies combinations were tested.

Three different antibody clones were used to test different combinations. Two antibodies were biotinylated, and other two were not. Table 7 shows the capture and detection antibodies combinations. After bioconjugating the antibodies on the magnetic particles (with streptavidin) or the nanoprobe (with neutravidin or with NHS linking), they were used to test a blank sample and a sample with cTnI (100 ng/mL).

**Table 7.** Capture and detection antibodies combinations.

| Capture Antibody on Magnetic Particle | Detection Antibody on Nanoprobe |
|---|---|
| 19C7-Biotin | 560 |
| 4C2-Biotin | 19C7 |
| 4C2-Biotin | 560 |
| 4C2-Biotin | 19C7-Biotin |

In the assay, 30 µL of the sample was added to 15 µL of magnetic particles. They were incubated for 30 min on a shaker at room temperature. Then, 2 µL of nanoprobe was added and incubated for another 30 min. The supernatant was collected as the particles were washed two times and redispersed in 30 µL of PBS. Then, 5 µL of the supernatant solution was passed through the collection device to measure the SERS signal.

The assays results are shown in Figure 64. As can be noted, the pair that demonstrated the largest difference between the blank and cTnI cases was the 4C2-biotin – 560. The 4C2-biotin – 19C7 pair also demonstrated a difference between the two tested

cases. In contrast, the 19C7-biotin – 560 sandwich pair resulted in the opposite expected result as the supernatant SERS signal of the blank case was lower than the signal of the cTnI case. The 4C2-biotin – 19C7-biotin pair resulted in almost no difference. These results implied that the 4C2-biotin – 560 pair should be used for further tests of the sandwich assay.

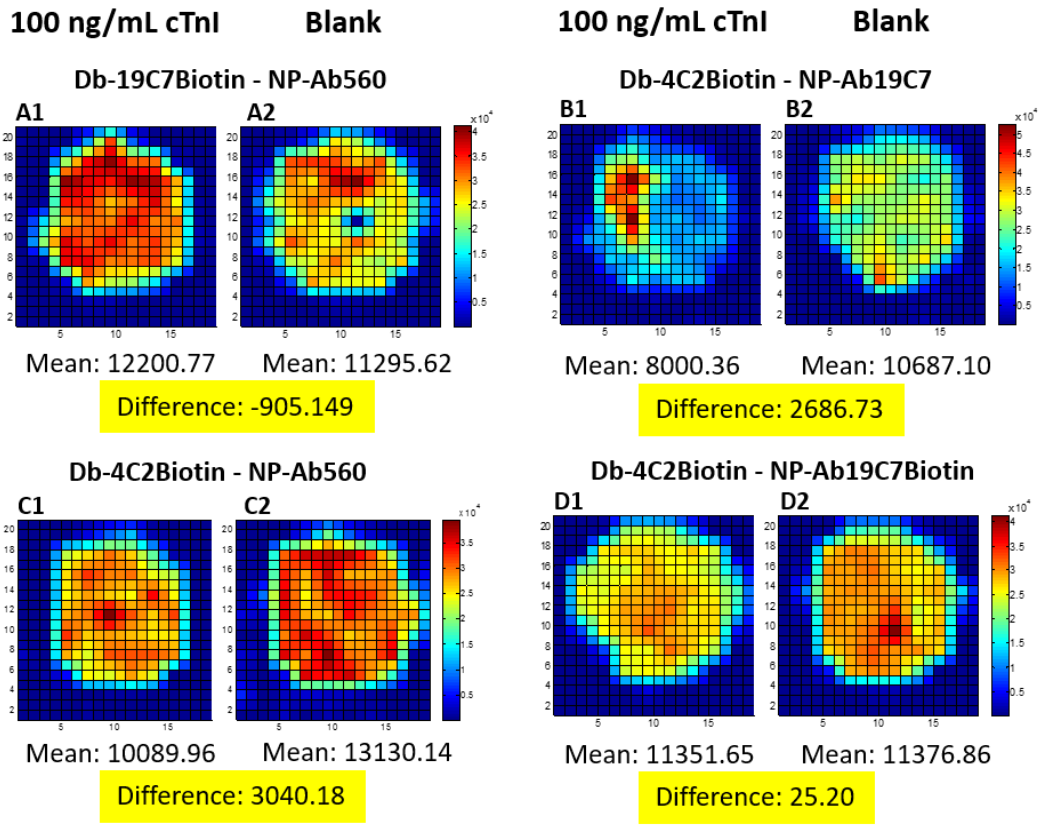


**Figure 64.** SERS intensity maps of collected nanoprobes when 100 ng/mL cTnI (for A1, B1, C1, and D1) and blank samples (for A2, B2, C2, and D2) are tested using distinct sets of capture-detection antibodies. The difference between the mean values of the two samples tested for each set was calculated to determine the pair that resulted in the greatest difference.

The sandwich pair that resulted in the largest difference was used to test several cTnI concentrations. To do this, 30 µL of the samples (100, 50, 10, 5, 1, 0.5, 0.2, 0.02, and

0 ng/mL) were added to wells with 15 µL of magnetic particles. The samples was incubated for 20 min. Then, 1 µL of nanoprobe was added to incubate them for another 20 min. After washing two times, 2.5 µL of the supernatant was passed through the collection device to measure the SERS signal.

The concentration curve obtained for the tested sandwich pair was not as expected. As can be seen in Figure 65, no significant trend was detected. In the ideal case, the SERS values decrease with increasing concentration of troponin. Several factors, including nonspecific binding, the amount of the assay components used, the activity of the antibodies, or the condition of the cTnI protein sample tested, could have caused the response obtained.

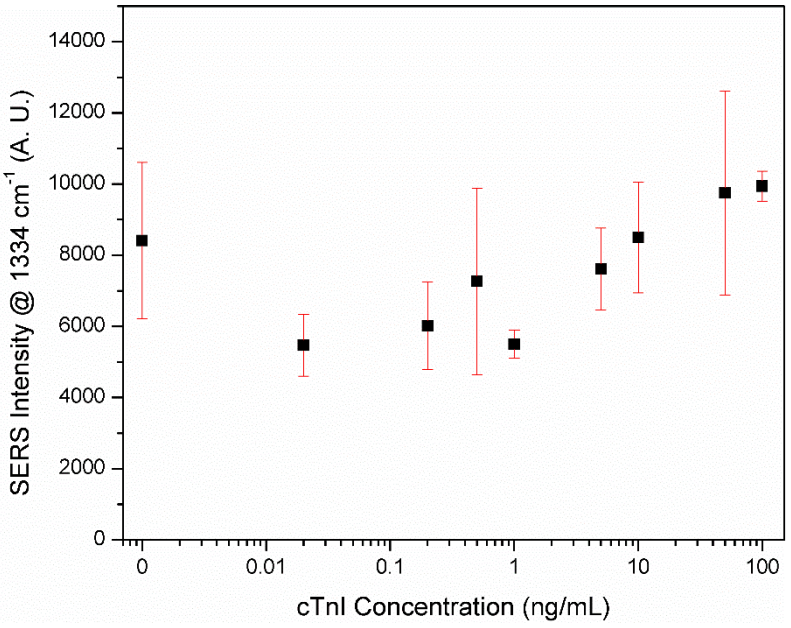


**Figure 65.** SERS-based sandwich assay concentration curve obtained when magnetic particles were conjugated with the 4C2-biotin antibody and nanoprobes with the 560 antibody.

### IV.3.iv Troubleshooting with ELISA Kit

A cTnI ELISA kit obtained from GenWay (CA, USA) was used to analyze some of the components of the developed assays. It was expected that by comparing the results from the kit with the results obtained by using components of the developed SERS-based assay problems could be identified. Specifically, prepared cTnI samples of several concentrations were tested on the kit and compared with the standard samples. In addition, the functionalized magnetic particles were used, instead of the kit wellplate, in conjunction with the enzyme labeled antibody solution from the kit to test samples.

The steps for the tests were based on the kit assay procedure. First, 100 µL of standards and the samples to be analyzed were added to the wells. Then, 100 µL of enzyme conjugate reagent was added, mixed, and incubated for 90 min at room temperature. After incubation, the mixture was removed, and the wells were washed 5 times with deionized water. Subsequently, 100 µL of TMB reagent was added into each well and incubated for 20 min at room temperature. To stop the reaction, 100 µL of stop solution was added. Finally, the absorbance at 450 nm was measured. To test the magnetic particles the previous steps were performed on a well with 10 µL of magnetic particles. Two magnetic particles functionalized with the 19C7-biotin and 4C2-biotin antibody clones respectively were tested. The particles were washed by using a magnet to collect the particles on the well and remove the supernatant. Table 8 and Table 9 show the samples and concentrations tested for the different cases.

**Table 8.** Samples and results from the ELISA kit tests.

.

| Sample | Concentration (ng/mL) | Volume Added (µL) | Absorbance |
|---|---|---|---|
| Standard 1 | 0 | 100 | 0.0544 |
| Standard 2 | 2 | 100 | 0.0578 |
| Standard 3 | 7.5 | 100 | 0.0604 |
| Standard 4 | 30 | 100 | 0.1050 |
| Standard 5 | 75 | 100 | 0.1671 |
| cTnI | 0 | 100 | 0.0570 |
| cTnI | 0.2 | 100 | 0.0560 |
| cTnI | 1 | 100 | 0.0552 |
| cTnI | 10 | 100 | 0.0651 |
| cTnI | 100 | 100 | 0.1706 |

**Table 9.** Samples and results from the ELISA kit tests using magnetic particles.

| Sample | Concentration (ng/mL) | Volume Added (µL) | MNPs-19C7 Absorbance | MNPs-4C2 Absorbance |
|---|---|---|---|---|
| Standard 1 | 0 | 100 | 0.0664 | 0.0528 |
| Standard 3 | 7.5 | 100 | 0.1270 | 0.0550 |
| Standard 5 | 75 | 100 | 0.8366 | 0.0598 |
| cTnI | 0 | 100 | 0.5424 | 0.5846 |
| cTnI | 10 | 100 | 0.6964 | 0.5919 |
| cTnI | 600 | 100 | 3.9038 | 1.4960 |

Figure 66 shows the results obtained when the standards and the prepared recombinant cTnI solutions were tested with the kit and the magnetic particles. As can be seen in Figure 66A, for the samples tested with the kit the absorbance increases with increasing cTnI concentrations. However, when the magnetic particles were used instead of the kit coated wells the results were different for the standard and the prepared cTnI samples. The absorbance values of the prepared recombinant cTnI samples were higher than the standards for similar concentrations (see Figure 66B, and Figure 66C). In

addition, the difference of antibody clonality had an effect in the response obtained. For the magnetic particle functionalized with 4C2 antibody minimal absorbance change was observed for increasing concentrations of the standard samples. Conversely, absorbance values increased with increasing concentrations of the standard sample for the magnetic particles functionalized with the 19C7 antibody clone, suggesting that cTnI binds specifically to the particles. The flat response obtained when the 4C2 antibody was used can be explained if the antibody from the kit (labeled with the enzyme) attaches to the same cTnI epitope as the 4C2 antibody conjugated on the magnetic particles.

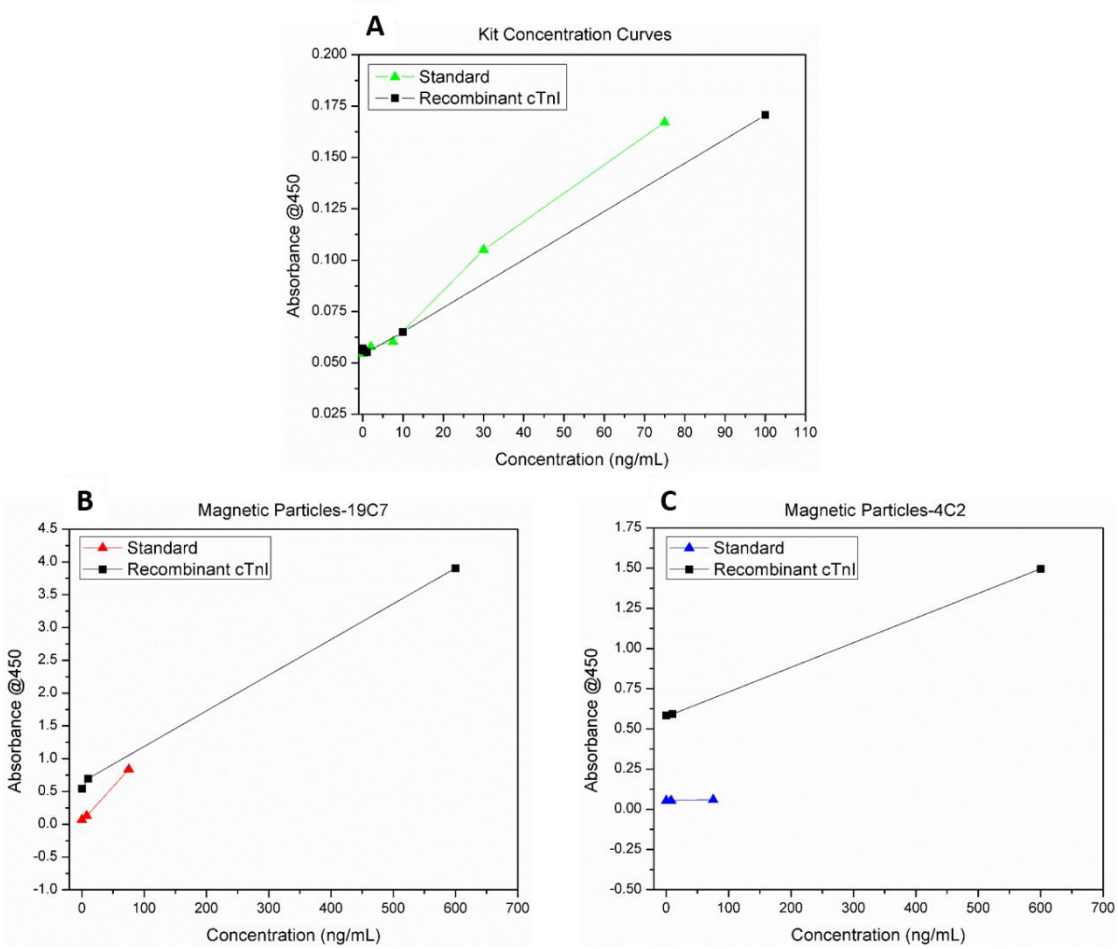


**Figure 66.** ELISA kit results. (A) Concentration curve obtained when the standards and prepared cTnI samples were tested with the kit. (B) and (C) are the concentration curves obtained when magnetic particles (conjugated with (B) 19C7 antibody and (C) 4C2 antibody) were used with the kit to test the standards and prepared cTnI samples.

An important result to note is the different values obtained for the two different blanks on the magnetic particles tests. In Figure 67 the measured blank values of the standard and the prepared cTnI sample (PBS buffer only) tested on the magnetic particles can be compared. The values of the PBS buffer are considerable higher than the blank standard, and this occurs without any cTnI present in the sample. This implies that antibodies attach to the magnetic particles without the presence of cTnI and after blocking

them with BSA. The fact that a low signal was obtained with the blank standard suggests that the solution contains something that prevents nonspecific binding. This also suggests that for future tests BSA or another compound needs to be added to the cTnI sample solution to prevent nonspecific binding. The results obtained in previous assay tests could have been affected by not adding anything to the tested samples that prevents nonspecific binding.

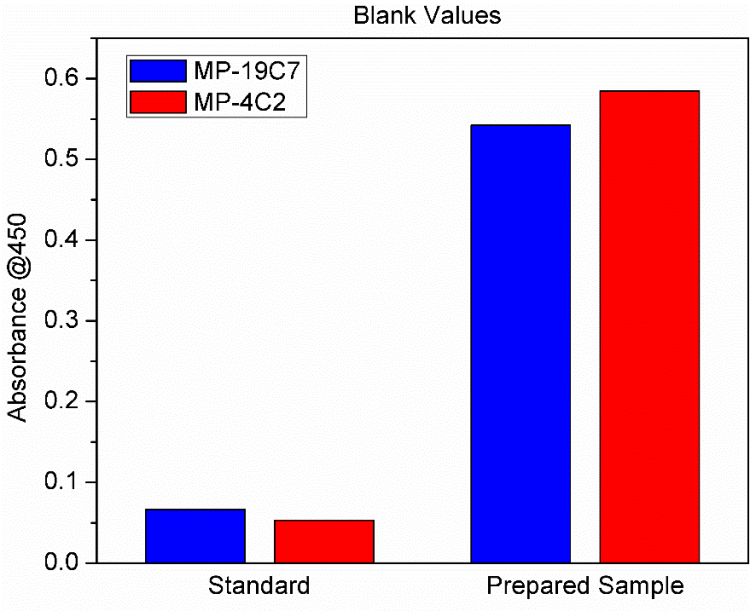


**Figure 67.** Comparison between a standard blank sample and a prepared blank sample. The samples were tested with an ELISA kit using two antibodies (19C7 and 4C2).

### IV.3.v Addition of BSA to Dilution Buffer

The previous results demonstrated that the composition of the dilution buffer used to prepare cTnI samples has a significant impact in the assay response. Nonspecific binding can be reduced considerably if the dilution buffer contains stabilizing agents that prevent it. Therefore, different buffers were prepared, tested, and compared with the

standard blank sample of an ELISA kit to assess their ability to prevent nonspecific binding and be used as dilution buffers for the preparation of assay samples.

BSA and Tween 20 are commonly used in assays to reduce nonspecific binding. Also, the sodium chloride concentration can have an effect in the antibody binding reaction. As a result, PBS and TRIS buffers with several concentrations of BSA, Tween 20, and sodium chloride were prepared. Table 10 shows the composition of the different buffers made.

**Table 10.** Dilution buffers composition.

| Buffer | BSA (%) | Tween 20 (%) | NaCl (M) |
|---|---|---|---|
| PBS | 0 | 0 | 0.15 |
| PBS 1 | 1 | 0.05 | 0.15 |
| PBS 2 | 2 | 0.10 | 0.30 |
| PBS 3 | 3 | 0.10 | 0.50 |
| TRIS | 0 | 0 | 0 |
| TRIS 1 | 1 | 0.05 | 0.15 |
| TRIS 2 | 2 | 0.10 | 0.30 |
| TRIS 3 | 3 | 0.10 | 0.50 |

The ELISA kit employed previously was utilized to test the effect of the buffers on the signal. The assay protocol was the same as described before. Magnetic particles functionalized with two different cTnI antibodies (19C7, 4C2) were used for the tests instead of the kit wells. The samples tested were the prepared buffers plus the blank standard for comparison.

Figure 68 shows the absorbance values obtained for each sample (identified with the percentage of BSA present). As can be noted, in all cases, except the PBS and TRIS

buffers without BSA or Tween 20, the signal was the same as the standard blank sample. This indicates that any of the buffers with different formulations of BSA and Tween 20 could be used as dilution buffers, but buffers without BSA and Tween should not be used. The results were similar for magnetic particles functionalized with different antibodies.

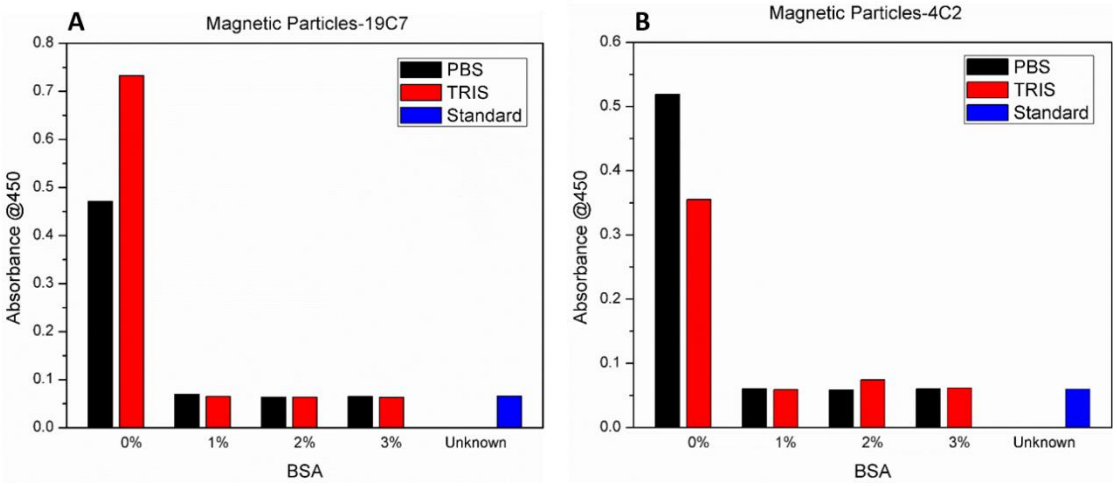


**Figure 68.** Dilution buffers effects on the measured signal. The blank samples were tested with an ELISA kit. Only when dilution buffer without BSA was utilized nonspecific binding occurred.

Since no BSA or Tween 20 was used to prepare cTnI samples in previous assay tests, the assay was tested again with cTnI samples prepared in dilution buffer containing 1% BSA and 0.05 Tween 20 (PBS 1 buffer). The cTnI samples (30 µL of 0, 1, and 621 ng/mL) were incubated with 5 µL of magnetic particles (conjugated with 4C2-biotin antibody) for 20 min at room temperature. Then, 2 µL of nanoprobe (conjugated with 19C7-biotin antibody) was added and incubated for another 20 min. The particles were washed, and 2.5 µL of the supernatant was collected on the collection device to measure the SERS signal.

The assay results, shown in Figure 69, indicate that the SERS signal is highest at the blank sample and lowest at the high cTnI concentration (621 ng/mL), which was the expected response. The addition of BSA and Tween 20 to the sample dilution buffer reduced nonspecific binding and allowed the assay to detect different concentrations. However, more studies need to be conducted to evaluate the assay performance.

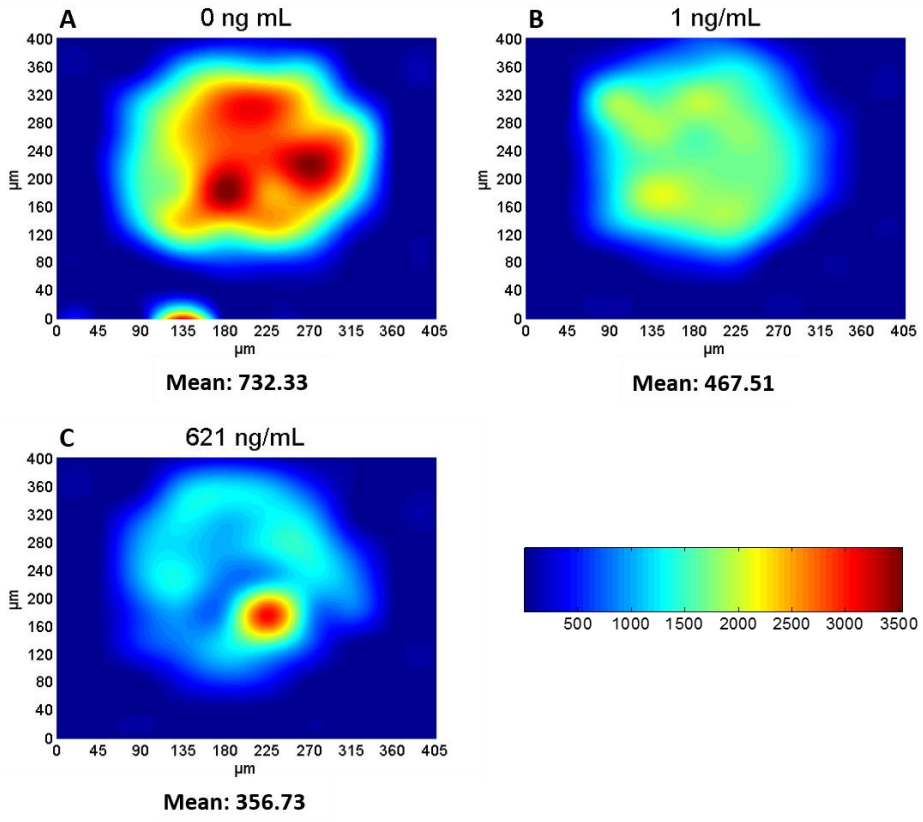


**Figure 69.** SERS intensity maps of collected nanoprobes when 0, 1, and 621 ng/mL of cTnI were tested. A dilution buffer with BSA was used to prepare the samples.

### IV.3.vi Sandwich SERS-Based Assay Concentration Curve Analysis

Several cTnI concentrations (0, 0.01, 0.1, 0.2, 0.5, 0.8, 1, 5, and 10 ng/mL) were measured with the SERS sandwich assay to plot a concentration curve. Each sample was

tested three times to calculate the standard deviation. The assay procedure was the same as previous tests. First, 30 µL of sample was mixed with 5 µL of magnetic particles and incubated for 20 min. Then, 2 µL of nanoprobe was added and incubated for another 20 min. The particles were washed two times, and the 2.5 µL of the supernatant was collected on the collection device to measure the SERS signal. It is important to note that in this case, the background signals were not considered when the different measured points were averaged to obtain a value for each sample measured on its collection area.

It was expected that the SERS signal would decrease with increasing cTnI concentrations. As can be noted in Figure 70, this anticipated trend was observed. The SERS signals of the 1, 5, and 10 ng/mL samples were lower than the signals of the lower concentrations. The largest signal difference occurred between 0.5 and 1 ng/mL. Only one sample (0.8 ng/mL) was measured between these two samples, and its signal was approximately halfway between their signals, which was expected. However, the standard deviation of this measurement was very high. At concentrations above 1 ng/mL the signal did not decrease further, and at concentrations below 0.5 ng/mL the signal appeared to decrease slightly, but the values were still higher than the 1, 5, and 10 ng/mL samples. A four parameter logistic model was used fit a curve to the measured points. As can be observed in Figure 70, the fit was not ideal (it had an R-square of 0.87), but it indicated the trend.

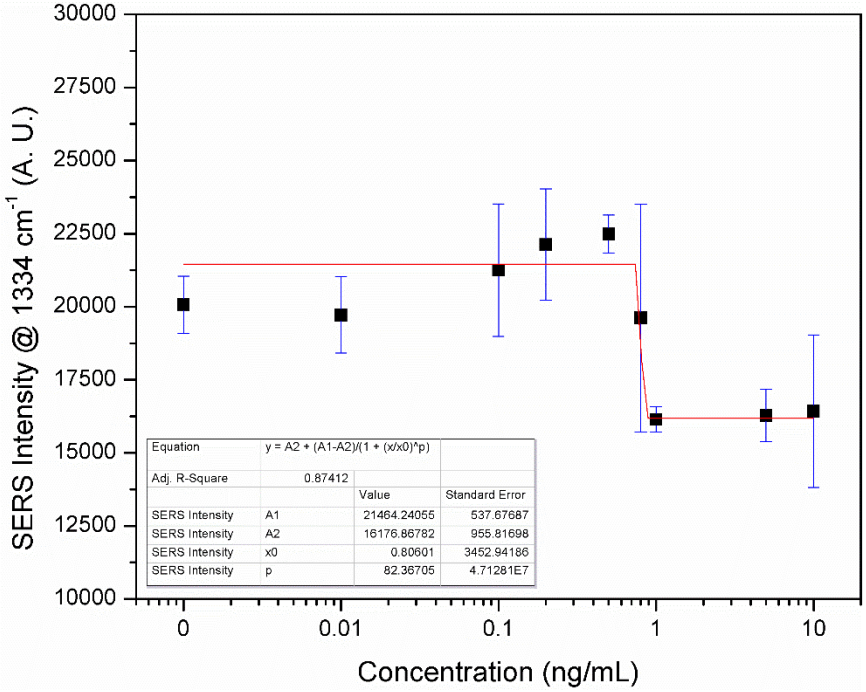


**Figure 70.** SERS-based sandwich assay concentration curve obtained when magnetic particles were conjugated with the 4C2-biotin antibody and the nanoprobes with the 19C7 antibody. A dilution buffer with BSA was used to prepare the cTnI samples.

The results suggest that the dynamic range of the sensor occurs between 0.5 and 1 ng/mL. The goal is to develop a cTnI assay that can measure cTnI from 0.01 ng/mL to 1 ng/mL with less than 10% CV. This means that these two concentrations should be included in the ideal dynamic range. If 0.01 ng/mL and 1 ng/mL are included in the dynamic range, the concentrations between these values can be predicted with the measured signal. Ideally, the SERS signal of the blank concentration should also be different (in this assay higher) than the lowest concentration of interest (0.01 ng/mL). Since the current dynamic range is from 0.5 to 1 ng/mL, the assay needs to be able to detect lower concentrations or it needs to be more sensitive to span across the range of interest. The current limit of detection (LoD) can be estimated to be higher than 0.5 ng/mL

based on the standard deviations of the measurements and the observed dynamic range. Furthermore, the repeatability of the responses should improve to meet the precision requirements. Although a trend is observed with the current assay, it needs further optimization to achieve better sensitivity and precision across the range of interest. Variables such as the amount of components used, amount of antibody conjugated to the particles, blocking agents, and mixing conditions that improve the response need to be controlled and analyzed to find the optimal values.

### *IV.4 Chapter Summary and Conclusions*

In this chapter, the different assay formats were explained. They were analyzed to determine the ones that could be used to implement the cTnI assay. The sandwich assay and the competitive binding assay were identified as the most promising formats for the desired application. Furthermore, it was recognized that the competitive binding assay could be implemented in three different versions: simultaneous mixing, sequential displacement, and sequential saturation. A model was created to predict the response of the sequential displacement version. The model predicted a minimal difference between the minimum and maximum analyte concentrations tested. An additional kinetic rate constants analysis suggested that the sequential saturation competitive binding assay and the sandwich assay were the most promising formats to develop the cTnI assay. The sandwich assay format was ultimately selected to implement the assay with the synthesized nanoprobe, the functionalized magnetic particles, and the collection device.

Initial assay tests indicated the presence of nonspecific binding. To address this, the particles were blocked with an excess of BSA. Also, neutravidin and streptavidin were

conjugated on the nanoprobe and the magnetic particles respectively to attach biotinylated antibodies, control the amount of antibody conjugated, and reduce nonspecific binding. A response that was expected, but with minimal change, was observed after introducing the changes. Additional tests with several antibody pairs were conducted to identify the best pair. In troubleshooting experiments, it was found that adding BSA to the sample dilution buffer was essential to reduce nonspecific binding. A clear improvement in the assay response was observed after using dilution buffer with BSA in the tests. Finally, a concentration curve was measured using the optimized parameters. The expected trend was observed in the test. However, it was concluded that additional assay optimization is needed to detect lower concentrations (0.01 ng/mL) with better repeatability (less than 10% CV).

# CONCLUSIONS

The goal of this work was to develop a SERS-based assay to detect cardiac biomarkers. To do this, the assay components were created first. Different nanoparticles, such as Ag and Au, were synthesized and functionalized with RRM. These SERS active nanoparticles were then conjugated with antibodies and other proteins. Multiple PEG based linkers were used to attach the proteins to the surface of the nanoparticles. In some cases, the nanoparticles were aggregated and encapsulated in silica. This enhanced the SERS signal to create nanoprobes with high SERS intensity that could be used in assays to detect low levels of analyte. The stability of the nanoparticles was achieved by using hydrophilic linkers and stabilizing proteins such as BSA. After comparing the stability and SERS signal of the nanoparticles functionalized in different manners, if was found that the silica encapsulated Ag nanoparticles exhibited stability, the highest SERS signal, and successful bioconjugation of cTnI or cTnI antibodies. Therefore, this nanoprobe was selected to be used in assay experiments moving forward. Magnetic nanoparticles were also synthesized and functionalized with antibodies to be used as the analyte capture components in the assay.

To collect the SERS active nanoparticles for measurement several techniques were explored. A microchannel with magnetic pads was tested to determine if nanoparticles could be captured on them at different flow velocities. The synthesized magnetic nanoparticles used for these tests were not able to be collected. Therefore, magnetic particles of larger size (1 μm) were used instead. The use of larger particles improved the collection on the magnetic areas; however, not all the particles were collected, and the

collection was not localized in a small area, which is ideal for SERS measurements. As a result, other collection techniques were explored. Several devices with a 20 nm pore size membrane were designed to collect the nanoparticles. However, in many cases the nanoparticle collection was not consistent. To address this, a novel collection device was built in which the particles could be aggregated at a defined spot. The sample was placed on the top of the membrane and vacuum was applied form the bottom to aspirate the nanoprobe sample through the specified area. This method allowed for a consistent collection of the nanoprobes to simultaneously obtain very low limits of detection and high repeatability, which is desired in assays. Nanoprobe samples (10 µL) were detected with less than 10 % coefficient of variation (CV) across a range from nearly 27.4 fM to 1.7 pM using the collection method.

Different assay formats were considered to implement the assay. The competitive binding assay and the sandwich assay were the most promising formats. These formats could also be designed in different versions. A model was created to predict the response of a competitive binding sequential displacement assay. Results from the model indicated that the response difference between the minimal and maximum expected cTnI concentrations was minimal. Additional analysis on the dissociation rate constants of the cTnI antibodies suggested that the sequential saturation version of the competitive binding assay format would be the best option for this assay. When comparing the sequential saturation with the sandwich assay, the sandwich assay was selected because it is known to be more sensitive and selective.

After synthesizing the nanoprobe, functionalizing the magnetic particles, creating the collection device, and selecting the assay format, the assay was tested. Blank samples were compared with cTnI samples to determine the assay response. Initial tests indicated the presence of nonspecific binding. To address this, different methods such as adding more BSA and using streptavidin and neutravidin to conjugate the antibodies on the nanoprobe and magnetic particles respectively were implemented. After introducing these changes, the assay response that was expected was observed. However, the performance of the assay was not optimal. Optimization experiments indicated that the composition of the dilution buffer, specifically the addition of BSA or other similar protein to the buffer, was essential to reduce nonspecific binding. After optimizing the dilution buffer, clear improvements in the signal differences between the analyzed concentrations could be distinguished. A concentration curve was measured using the optimized parameters, and the expected trend was observed in the test. The curve implies that the dynamic range of the assay occurs from 0.5 to 1 ng/mL. This means that the assay sensitivity needs to be improved to obtain the ideal dynamic range that spans from 0.01 to 1 ng/mL.

The final assay results suggest that more optimization is need to be able to measure the required low concentrations of cTnI (0.01 ng/mL) with high precision (less than 10% CV). Variables such as amount of antibody labeled, amount of components used, assay conditions, and buffers used can have a significant impact in the results. Therefore, each of them needs to be controlled and optimized.

The results presented in this work demonstrate the proof of concept of a SERS-based assay to detect cardiac biomarkers. This assay can be modified to detect other

analytes. In addition, once it is optimized, it can be implemented on a microfluidic chip to develop a POC device.

REFERENCES

1. World Health Organization Cardiovascular Diseases (CVDs). http://www.who.int/mediacentre/factsheets/fs317/en/ (accessed April 9, 2017).

2. World Health Organization The Top 10 Causes of Death. http://www.who.int/mediacentre/factsheets/fs310/en/ (accessed April 9, 2017).

3. Centers for Disease Control and Prevention Know The Facts About Heart Disease. https://www.cdc.gov/heartdisease/docs/consumered_heartdisease.pdf (accessed March 26, 2017).

4. Centers for Disease Control and Prevention Heart Disease Facts. https://www.cdc.gov/heartdisease/facts.htm (accessed April 3, 2017).

5. American Heart Association About Heart Attacks. http://www.heart.org/HEARTORG/Conditions/HeartAttack/AboutHeartAttacks/About-Heart-Attacks_UCM_002038_Article.jsp#.WLIU1_nyu1s (accessed March 30, 2017).

6. Rui P, Kang K, Albert M National Hospital Ambulatory Medical Care Survey: 2013 Emergency Department Summary Tables. https://www.cdc.gov/nchs/data/ahcd/nhamcs_emergency/2013_ed_web_tables.pdf (accessed April 6, 2017).

7. Antman, E. M.; Anbe, D. T.; Armstrong, P. W.; Bates, E. R.; Green, L. A.; Hand, M.; Hochman, J. S.; Krumholz, H. M.; Kushner, F. G.; Lamas, G. A., ACC/AHA guidelines for the management of patients with ST-elevation myocardial infarction—executive summary: a report of the American College of Cardiology/American Heart Association Task Force on Practice Guidelines (Writing Committee to Revise the 1999 Guidelines for the Management of Patients With Acute Myocardial Infarction). *Journal of the American College of Cardiology* **2004,** *44* (3), 671-719.

8. Amsterdam, E. A.; Wenger, N. K.; Brindis, R. G.; Casey, D. E.; Ganiats, T. G.; Holmes, D. R.; Jaffe, A. S.; Jneid, H.; Kelly, R. F.; Kontos, M. C., 2014 AHA/ACC guideline for the management of patients with non-ST-elevation acute coronary syndromes: Executive summary. *Journal of the American College of Cardiology* **2014,** *64* (24), 2645.

9. Van der Laarse, A.; Cobbaert, C. M.; Gorgels, A. P.; Swenne, C. A., Will future troponin measurement overrule the ECG as the primary diagnostic tool in patients with acute coronary syndrome? *Journal of electrocardiology* **2013,** *46* (4), 312-317.

10. Mion, M. M.; Novello, E.; Altinier, S.; Rocco, S.; Zaninotto, M.; Plebani, M., Analytical and clinical performance of a fully automated cardiac multi-markers strategy

based on protein biochip microarray technology. *Clinical biochemistry* **2007,** *40* (16), 1245-1251.

11. McDonnell, B.; Hearty, S.; Leonard, P.; O'Kennedy, R., Cardiac biomarkers and the case for point-of-care testing. *Clinical biochemistry* **2009,** *42* (7), 549-561.

12. Amsterdam, E. A.; Kirk, J. D.; Bluemke, D. A.; Diercks, D.; Farkouh, M. E.; Garvey, J. L.; Kontos, M. C.; McCord, J.; Miller, T. D.; Morise, A., Testing of low-risk patients presenting to the emergency department with chest pain. *Circulation* **2010,** *122* (17), 1756-1776.

13. Bingisser, R.; Cairns, C.; Christ, M.; Hausfater, P.; Lindahl, B.; Mair, J.; Panteghini, M.; Price, C.; Venge, P., Cardiac troponin: a critical review of the case for point-of-care testing in the ED. *The American journal of emergency medicine* **2012,** *30* (8), 1639-1649.

14. Thygesen, K.; Alpert, J. S.; Jaffe, A. S.; White, H. D.; Simoons, M. L.; Chaitman, B. R.; Katus, H. A.; Apple, F. S.; Lindahl, B.; Morrow, D. A., Third universal definition of myocardial infarction. *Journal of the American College of Cardiology* **2012,** *60* (16), 1581-1598.

15. Diercks, D. B.; Peacock IV, W. F.; Hollander, J. E.; Singer, A. J.; Birkhahn, R.; Shapiro, N.; Glynn, T.; Nowack, R.; Safdar, B.; Miller, C. D., Diagnostic accuracy of a point-of-care troponin I assay for acute myocardial infarction within 3 hours after presentation in early presenters to the emergency department with chest pain. *American heart journal* **2012,** *163* (1), 74-80. e4.

16. Antman, E. M.; Anbe, D. T.; Armstrong, P. W.; Bates, E. R.; Green, L. A.; Hand, M.; Hochman, J. S.; Krumholz, H. M.; Kushner, F. G.; Lamas, G. A., ACC/AHA guidelines for the management of patients with ST-elevation myocardial infarction: a report of the American College of Cardiology/American Heart Association Task Force on Practice Guidelines (Committee to Revise the 1999 Guidelines for the Management of Patients with Acute Myocardial Infarction). *Journal of the American College of Cardiology* **2004,** *44* (3), E1-E211.

17. Hamm, C. W., Cardiac biomarkers for rapid evaluation of chest pain. *Circulation* **2001,** *104* (13), 1454-1456.

18. Blick, K. E., The benefits of a rapid, point-of-care “TnI-Only” zero and 2-hour protocol for the evaluation of chest pain patients in the Emergency Department. *Clinics in laboratory medicine* **2014,** *34* (1), 75-85.

19. Aldous, S. J., Cardiac biomarkers in acute myocardial infarction. *International journal of cardiology* **2013,** *164* (3), 282-294.

20. Gibler, W.; Blomkalns, A., Point of care testing for cardiac biomarkers in the ED: a blueprint for implementation. *Emergency Medicine Cardiac Research Education Group* **2006,** *1*, 1-10.

21. Wright, R. S.; Anderson, J. L.; Adams, C. D.; Bridges, C. R.; Casey, D. E.; Ettinger, S. M.; Fesmire, F. M.; Ganiats, T. G.; Jneid, H.; Lincoff, A. M., 2011 ACCF/AHA focused update incorporated into the ACC/AHA 2007 guidelines for the management of patients with unstable angina/non–ST-elevation myocardial infarction: a report of the American College of Cardiology Foundation/American Heart Association Task Force on Practice Guidelines. *Journal of the American College of Cardiology* **2011,** *57* (19), e215-e367.

22. Ng, S. M.; Krishnaswamy, P.; Morissey, R.; Clopton, P.; Fitzgerald, R.; Maisel, A. S., Ninety-minute accelerated critical pathway for chest pain evaluation. *The American journal of cardiology* **2001,** *88* (6), 611-617.

23. Rathore, S.; Knowles, P.; Mann, A.; Dodds, P., Is it safe to discharge patients from accident and emergency using a rapid point of care Triple Cardiac Marker test to rule out acute coronary syndrome in low to intermediate risk patients presenting with chest pain? *European journal of internal medicine* **2008,** *19* (7), 537-540.

24. Goodacre, S. W.; Bradburn, M.; Cross, E.; Collinson, P.; Gray, A.; Hall, A. S., The Randomised Assessment of Treatment using Panel Assay of Cardiac Markers (RATPAC) trial: a randomised controlled trial of point-of-care cardiac markers in the emergency department. *Heart* **2010**, hrt. 2010.203166.

25. Newby, L. K.; Storrow, A. B.; Gibler, W. B.; Garvey, J. L.; Tucker, J. F.; Kaplan, A. L.; Schreiber, D. H.; Tuttle, R. H.; McNulty, S. E.; Ohman, E. M., Bedside multimarker testing for risk stratification in chest pain units. *Circulation* **2001,** *103* (14), 1832-1837.

26. Scharnhorst, V.; Krasznai, K.; van't Veer, M.; Michels, R., Rapid detection of myocardial infarction with a sensitive troponin test. *American journal of clinical pathology* **2011,** *135* (3), 424-428.

27. Hunkeler, N. M.; Kullman, J.; Murphy, A. M., Troponin I isoform expression in human heart. *Circulation research* **1991,** *69* (5), 1409-1414.

28. Takeda, S.; Yamashita, A.; Maeda, K.; Maeda, Y., Structure of the core domain of human cardiac troponin in the Ca2+-saturated form. *Nature* **2003,** *424* (6944), 35-41.

29. Farah, C.; Reinach, F., The troponin complex and regulation of muscle contraction. *The FASEB Journal* **1995,** *9* (9), 755-767.

30. Sarko, J.; Pollack, C. V., Cardiac troponins. *The Journal of emergency medicine* **2002,** *23* (1), 57-65.

31. Ricchiuti, V.; Zhang, J.; Apple, F. S., Cardiac troponin I and T alterations in hearts with severe left ventricular remodeling. *Clinical chemistry* **1997,** *43* (6), 990-995.

32. Maynard, S.; Menown, I.; Adgey, A., Troponin T or troponin I as cardiac markers in ischaemic heart disease. BMJ Publishing Group Ltd and British Cardiovascular Society: 2000.

33. Wild, D., *The immunoassay handbook: theory and applications of ligand binding, ELISA and related techniques*. Newnes: 2013.

34. Sallach, S. M.; Nowak, R.; Hudson, M. P.; Tokarski, G.; Khoury, N.; Tomlanovich, M. C.; Jacobsen, G.; de Lemos, J. A.; McCord, J., A change in serum myoglobin to detect acute myocardial infarction in patients with normal troponin I levels. *The American journal of cardiology* **2004,** *94* (7), 864-867.

35. Kontos, M. C.; Garg, R.; Anderson, F. P.; Roberts, C. S.; Ornato, J. P.; Tatum, J. L.; Jesse, R. L., Ability of myoglobin to predict mortality in patients admitted for exclusion of myocardial infarction. *The American journal of emergency medicine* **2007,** *25* (8), 873-879.

36. Dolci, A.; Panteghini, M., The exciting story of cardiac biomarkers: from retrospective detection to gold diagnostic standard for acute myocardial infarction and more. *Clinica chimica acta* **2006,** *369* (2), 179-187.

37. Eggers, K. M.; Oldgren, J.; Nordenskjöld, A.; Lindahl, B., Diagnostic value of serial measurement of cardiac markers in patients with chest pain: limited value of adding myoglobin to troponin I for exclusion of myocardial infarction. *American heart journal* **2004,** *148* (4), 574-581.

38. Robinson, D. J.; Christenson, R. H., Creatine kinase and its CK-MB isoenzyme: the conventional marker for the diagnosis of acute myocardial infarction. *The Journal of emergency medicine* **1999,** *17* (1), 95-104.

39. Apple, F. S., Acute myocardial infarction and coronary reperfusion. Serum cardiac markers for the 1990s. *American journal of clinical pathology* **1992,** *97* (2), 217-226.

40. Schneider, C. M.; Dennehy, C. A.; Rodearmel, S. J.; Hayward, J. R., Effects of Physical Activity on Creatine Phosphokinase and the Isoenzyme Creatine Kinase–MB. *Annals of emergency medicine* **1995,** *25* (4), 520-524.

41. Adams, J. r.; Bodor, G. S.; Davila-Roman, V. G.; Delmez, J. A.; Apple, F. S.; Ladenson, J. H.; Jaffe, A. S., Cardiac troponin I. A marker with high specificity for cardiac injury. *circulation* **1993,** *88* (1), 101-106.

42. Antman, E.; Bassand, J.-P.; Klein, W.; Ohman, M.; Sendon, J. L. L.; Rydén, L.; Simoons, M.; Tendera, M., Myocardial infarction redefined—a consensus document of The Joint European Society of Cardiology/American College of Cardiology committee for the redefinition of myocardial infarction: The Joint European Society of Cardiology/American College of Cardiology Committee∗∗ A list of contributors to this ESC/ACC Consensus Document is provided in Appendix B. *Journal of the American College of Cardiology* **2000,** *36* (3), 959-969.

43. Hawkins, R. C., Laboratory turnaround time. *Clinical Biochemist Reviews* **2007,** *28* (4), 179.

44. Giménez, M. R.; Hoeller, R.; Reichlin, T.; Zellweger, C.; Twerenbold, R.; Reiter, M.; Moehring, B.; Wildi, K.; Mosimann, T.; Mueller, M., Rapid rule out of acute myocardial infarction using undetectable levels of high-sensitivity cardiac troponin. *International journal of cardiology* **2013,** *168* (4), 3896-3901.

45. Reimer, K.; Jennings, R., The" wavefront phenomenon" of myocardial ischemic cell death. II. Transmural progression of necrosis within the framework of ischemic bed size (myocardium at risk) and collateral flow. *Laboratory investigation; a journal of technical methods and pathology* **1979,** *40* (6), 633-644.

46. Apple, F. S., A new season for cardiac troponin assays: it's time to keep a scorecard. *Clinical chemistry* **2009,** *55* (7), 1303-1306.

47. Hochholzer, W.; Morrow, D. A.; Giugliano, R. P., Novel biomarkers in cardiovascular disease: update 2010. *American heart journal* **2010,** *160* (4), 583-594.

48. Reichlin, T.; Hochholzer, W.; Bassetti, S.; Steuer, S.; Stelzig, C.; Hartwiger, S.; Biedert, S.; Schaub, N.; Buerge, C.; Potocki, M., Early diagnosis of myocardial infarction with sensitive cardiac troponin assays. *New England Journal of Medicine* **2009,** *361* (9), 858-867.

49. Body, R.; Carley, S.; McDowell, G.; Jaffe, A. S.; France, M.; Cruickshank, K.; Wibberley, C.; Nuttall, M.; Mackway-Jones, K., Rapid exclusion of acute myocardial infarction in patients with undetectable troponin using a high-sensitivity assay. *Journal of the American College of Cardiology* **2011,** *58* (13), 1332-1339.

50. Keller, T.; Zeller, T.; Peetz, D.; Tzikas, S.; Roth, A.; Czyz, E.; Bickel, C.; Baldus, S.; Warnholtz, A.; Fröhlich, M., Sensitive troponin I assay in early diagnosis of acute myocardial infarction. *New England Journal of Medicine* **2009,** *361* (9), 868-877.

51. Storrow, A. B.; Lindsell, C. J.; Han, J. H.; Slovis, C. M.; Miller, K. F.; Gibler, W. B.; Hoekstra, J. W.; Peacock, W. F.; Hollander, J. E.; Pollack, C. V., Discordant cardiac biomarkers: frequency and outcomes in emergency department patients with chest pain. *Annals of emergency medicine* **2006,** *48* (6), 660-665.

52. Jarolim, P., High sensitivity cardiac troponin assays in the clinical laboratories. *Clinical Chemistry and Laboratory Medicine (CCLM)* **2015,** *53* (5), 635-652.

53. Westermann, D.; Neumann, J. T.; Sörensen, N. A.; Blankenberg, S., High-sensitivity assays for troponin in patients with cardiac disease. *Nature Reviews Cardiology* **2017**.

54. Herring, A.; Wilper, A.; Himmelstein, D. U.; Woolhandler, S.; Espinola, J. A.; Brown, D. F.; Camargo Jr, C. A., Increasing length of stay among adult visits to US emergency departments, 2001–2005. *Academic Emergency Medicine* **2009,** *16* (7), 609-616.

55. Azzazy, H. M.; Christenson, R. H., Cardiac markers of acute coronary syndromes: is there a case for point-of-care testing? *Clinical biochemistry* **2002,** *35* (1), 13-27.

56. Takakuwa, K. M.; Ou, F. S.; Peterson, E. D.; Pollack, C. V.; Peacock, W. F.; Hoekstra, J. W.; Ohman, E. M.; Gibler, W. B.; Blomkalns, A. L.; Roe, M. T., The Usage Patterns of Cardiac Bedside Markers Employing Point-of-Care Testing for Troponin in Non-ST-Segment Elevation Acute Coronary Syndrome: Results from CRUSADE. *Clinical cardiology* **2009,** *32* (9), 498-505.

57. Apple, F. S.; Chung, A. Y.; Kogut, M. E.; Bubany, S.; Murakami, M. M., Decreased patient charges following implementation of point-of-care cardiac troponin monitoring in acute coronary syndrome patients in a community hospital cardiology unit. *Clinica Chimica Acta* **2006,** *370* (1), 191-195.

58. Slot, M. H. B.; van der Heijden, G. J.; Stelpstra, S. D.; Hoes, A. W.; Rutten, F. H., Point-of-care tests in suspected acute myocardial infarction: a systematic review. *International journal of cardiology* **2013,** *168* (6), 5355-5362.

59. Kneipp, K.; Kneipp, H.; Itzkan, I.; Dasari, R. R.; Feld, M. S., Ultrasensitive chemical analysis by Raman spectroscopy. *Chemical reviews* **1999,** *99* (10), 2957-2976.

60. Ferraro, J. R., *Introductory raman spectroscopy*. Academic press: 2003.

61. Graves, P.; Gardiner, D.; Graves, P., Practical Raman Spectroscopy. Springer: 1989.

62. Gardiner, D. J., Introduction to Raman scattering. In *Practical Raman Spectroscopy*, Springer: 1989; pp 1-12.

63. Smith, E.; Dent, G., *Modern Raman spectroscopy: a practical approach*. John Wiley & Sons: 2013.

64. Colthup, N., *Introduction to infrared and Raman spectroscopy*. Elsevier: 2012.

65. Lackowicz, J. R., Principles of fluorescence spectroscopy. *Plenum Press,(New York, 1983) Chapter* **1983,** *5*, 111-150.

66. Moskovits, M., Surface-enhanced spectroscopy. *Reviews of modern physics* **1985,** *57* (3), 783.

67. Schatz, G. C.; Van Duyne, R. P., Electromagnetic mechanism of surface-enhanced spectroscopy. *Handbook of vibrational spectroscopy* **2002**.

68. Zhang, Y.; Zhao, S.; He, L.; Zheng, J., Surface-enhanced Raman spectroscopy (SERS) combined techniques for high-performance detection and characterization. *TrAC Trends in Analytical Chemistry* **2017**.

69. Stiles, P. L.; Dieringer, J. A.; Shah, N. C.; Van Duyne, R. P., Surface-enhanced Raman spectroscopy. *Annu. Rev. Anal. Chem.* **2008,** *1*, 601-626.

70. Zeng, S.; Yong, K.-T.; Roy, I.; Dinh, X.-Q.; Yu, X.; Luan, F., A review on functionalized gold nanoparticles for biosensing applications. *Plasmonics* **2011,** *6* (3), 491.

71. Holzinger, M.; Le Goff, A.; Cosnier, S., Nanomaterials for biosensing applications: a review. *Frontiers in chemistry* **2014,** *2*, 63.

72. Li, Y.; Schluesener, H. J.; Xu, S., Gold nanoparticle-based biosensors. *Gold Bulletin* **2010,** *43* (1), 29-41.

73. Knopp, D.; Tang, D.; Niessner, R., Review: bioanalytical applications of biomolecule-functionalized nanometer-sized doped silica particles. *Analytica chimica acta* **2009,** *647* (1), 14-30.

74. Ding, L.; Bond, A. M.; Zhai, J.; Zhang, J., Utilization of nanoparticle labels for signal amplification in ultrasensitive electrochemical affinity biosensors: a review. *Analytica chimica acta* **2013,** *797*, 1-12.

75. Leopold, N.; Lendl, B., A new method for fast preparation of highly surface-enhanced Raman scattering (SERS) active silver colloids at room temperature by

reduction of silver nitrate with hydroxylamine hydrochloride. *The Journal of Physical Chemistry B* **2003,** *107* (24), 5723-5727.

76. Turkevich, J.; Stevenson, P. C.; Hillier, J., A study of the nucleation and growth processes in the synthesis of colloidal gold. *Discussions of the Faraday Society* **1951,** *11*, 55-75.

77. Wu, H.-L.; Tsai, H.-R.; Hung, Y.-T.; Lao, K.-U.; Liao, C.-W.; Chung, P.-J.; Huang, J.-S.; Chen, I.-C.; Huang, M. H., A comparative study of gold nanocubes, octahedra, and rhombic dodecahedra as highly sensitive SERS substrates. *Inorganic chemistry* **2011,** *50* (17), 8106-8111.

78. Fales, A. M.; Yuan, H.; Vo-Dinh, T., Silica-coated gold nanostars for combined surface-enhanced Raman scattering (SERS) detection and singlet-oxygen generation: a potential nanoplatform for theranostics. *Langmuir* **2011,** *27* (19), 12186-12190.

79. von Maltzahn, G.; Centrone, A.; Park, J. H.; Ramanathan, R.; Sailor, M. J.; Hatton, T. A.; Bhatia, S. N., SERS-coded gold nanorods as a multifunctional platform for densely multiplexed near-infrared imaging and photothermal heating. *Advanced Materials* **2009,** *21* (31), 3175-3180.

80. Wang, Y.; Yan, B.; Chen, L., SERS tags: novel optical nanoprobes for bioanalysis. *Chemical reviews* **2012,** *113* (3), 1391-1428.

81. Shiohara, A.; Wang, Y.; Liz-Marzan, L. M., Recent approaches toward creation of hot spots for SERS detection. *Journal of Photochemistry and Photobiology C: Photochemistry Reviews* **2014,** *21*, 2-25.

82. Huang, P. J.; Chau, L. K.; Yang, T. S.; Tay, L. L.; Lin, T. T., Nanoaggregate-Embedded Beads as Novel Raman Labels for Biodetection. *Advanced Functional Materials* **2009,** *19* (2), 242-248.

83. Salehi, M.; Schneider, L.; Ströbel, P.; Marx, A.; Packeisen, J.; Schlücker, S., Two-color SERS microscopy for protein co-localization in prostate tissue with primary antibody–protein A/G–gold nanocluster conjugates. *Nanoscale* **2014,** *6* (4), 2361-2367.

84. Huang, P. J.; Tay, L. L.; Tanha, J.; Ryan, S.; Chau, L. K., Single-Domain Antibody-Conjugated Nanoaggregate-Embedded Beads for Targeted Detection of Pathogenic Bacteria. *Chemistry–A European Journal* **2009,** *15* (37), 9330-9334.

85. Bastús, N. G.; Comenge, J.; Puntes, V., Kinetically controlled seeded growth synthesis of citrate-stabilized gold nanoparticles of up to 200 nm: size focusing versus Ostwald ripening. *Langmuir* **2011,** *27* (17), 11098-11105.

86. You, Y.; Nagaraja, A.; Biswas, A.; Hwang, J.; Cote, G.; McShane, M., SERS-active Smart Hydrogels with Modular Microdomains: from pH to glucose sensing. *IEEE Sensors Journal* **2016**.

87. Wu, A.; Feng, Y., Biochemical differences between cTnT and cTnI and their significance for diagnosis of acute coronary syndromes. *European heart journal* **1998,** *19*, N25-9.

88. Schütz, M.; Salehi, M.; Schlücker, S., Direct Silica Encapsulation of Self-Assembled-Monolayer-Based Surface-Enhanced Raman Scattering Labels with Complete Surface Coverage of Raman Reporters by Noncovalently Bound Silane Precursors. *Chemistry–An Asian Journal* **2014,** *9* (8), 2219-2224.

89. Steinigeweg, D.; Schütz, M.; Salehi, M.; Schlücker, S., Fast and Cost-Effective Purification of Gold Nanoparticles in the 20–250 nm Size Range by Continuous Density Gradient Centrifugation. *Small* **2011,** *7* (17), 2443-2448.

90. Xie, J.; Zheng, Y.; Ying, J. Y., Protein-directed synthesis of highly fluorescent gold nanoclusters. *Journal of the American Chemical Society* **2009,** *131* (3), 888-889.

91. Chon, H.; Lee, S.; Yoon, S.-Y.; Lee, E. K.; Chang, S.-I.; Choo, J., SERS-based competitive immunoassay of troponin I and CK-MB markers for early diagnosis of acute myocardial infarction. *Chemical Communications* **2014,** *50* (9), 1058-1060.

92. Wustholz, K. L.; Henry, A.-I.; McMahon, J. M.; Freeman, R. G.; Valley, N.; Piotti, M. E.; Natan, M. J.; Schatz, G. C.; Duyne, R. P. V., Structure− activity relationships in gold nanoparticle dimers and trimers for surface-enhanced Raman spectroscopy. *Journal of the American Chemical Society* **2010,** *132* (31), 10903-10910.

93. Perry, J. L.; Reuter, K. G.; Kai, M. P.; Herlihy, K. P.; Jones, S. W.; Luft, J. C.; Napier, M.; Bear, J. E.; DeSimone, J. M., PEGylated PRINT nanoparticles: the impact of PEG density on protein binding, macrophage association, biodistribution, and pharmacokinetics. *Nano letters* **2012,** *12* (10), 5304-5310.

94. Chaturvedi, S. K.; Ahmad, E.; Khan, J. M.; Alam, P.; Ishtikhar, M.; Khan, R. H., Elucidating the interaction of limonene with bovine serum albumin: a multi-technique approach. *Molecular BioSystems* **2015,** *11* (1), 307-316.

95. Moore, T. L.; Rodriguez-Lorenzo, L.; Hirsch, V.; Balog, S.; Urban, D.; Jud, C.; Rothen-Rutishauser, B.; Lattuada, M.; Petri-Fink, A., Nanoparticle colloidal stability in cell culture media and impact on cellular interactions. *Chemical Society Reviews* **2015,** *44* (17), 6287-6305.

96. Grubisha, D. S.; Lipert, R. J.; Park, H.-Y.; Driskell, J.; Porter, M. D., Femtomolar detection of prostate-specific antigen: an immunoassay based on surface-enhanced Raman scattering and immunogold labels. *Analytical chemistry* **2003,** *75* (21), 5936-5943.

97. Jehn, C.; Küstner, B.; Adam, P.; Marx, A.; Ströbel, P.; Schmuck, C.; Schlücker, S., Water soluble SERS labels comprising a SAM with dual spacers for controlled bioconjugation. *Physical Chemistry Chemical Physics* **2009,** *11* (34), 7499-7504.

98. Yuan, H.; Khoury, C. G.; Hwang, H.; Wilson, C. M.; Grant, G. A.; Vo-Dinh, T., Gold nanostars: surfactant-free synthesis, 3D modelling, and two-photon photoluminescence imaging. *Nanotechnology* **2012,** *23* (7), 075102.

99. Lee, H.; Yu, M. K.; Park, S.; Moon, S.; Min, J. J.; Jeong, Y. Y.; Kang, H.-W.; Jon, S., Thermally cross-linked superparamagnetic iron oxide nanoparticles: synthesis and application as a dual imaging probe for cancer in vivo. *Journal of the American Chemical Society* **2007,** *129* (42), 12739-12745.

100. Kolhatkar, A. G.; Jamison, A. C.; Litvinov, D.; Willson, R. C.; Lee, T. R., Tuning the magnetic properties of nanoparticles. *International journal of molecular sciences* **2013,** *14* (8), 15977-16009.

101. Wang, Y.; Chen, G.; Yang, M.; Silber, G.; Xing, S.; Tan, L. H.; Wang, F.; Feng, Y.; Liu, X.; Li, S., A systems approach towards the stoichiometry-controlled hetero-assembly of nanoparticles. *Nature communications* **2010,** *1*, 87.

102. Wang, X.; Xu, Y.; Chen, Y.; Li, L.; Liu, F.; Li, N., The gold-nanoparticle-based surface plasmon resonance light scattering and visual DNA aptasensor for lysozyme. *Analytical and bioanalytical chemistry* **2011,** *400* (7), 2085-2091.

103. Guerrini, L.; Graham, D., Molecularly-mediated assemblies of plasmonic nanoparticles for Surface-Enhanced Raman Spectroscopy applications. *Chemical Society Reviews* **2012,** *41* (21), 7085-7107.

104. He, Y.; Wang, Y.; Yang, X.; Xie, S.; Yuan, R.; Chai, Y., Metal organic frameworks combining CoFe2O4 magnetic nanoparticles as highly efficient SERS sensing platform for ultrasensitive detection of N-terminal pro-brain natriuretic peptide. *ACS applied materials & interfaces* **2016,** *8* (12), 7683-7690.

105. Wang, M.; Jing, N.; Chou, I.-H.; Cote, G. L.; Kameoka, J., An optofluidic device for surface enhanced Raman spectroscopy. *Lab on a Chip* **2007,** *7* (5), 630-632.

106. Yazdi, S. H.; White, I. M., A nanoporous optofluidic microsystem for highly sensitive and repeatable surface enhanced Raman spectroscopy detection. *Biomicrofluidics* **2012,** *6* (1), 014105.

107. Wei, W. Y.; White, I. M., A simple filter-based approach to surface enhanced Raman spectroscopy for trace chemical detection. *Analyst* **2012,** *137* (5), 1168-1173.

108. Yang, S.; Dai, X.; Stogin, B. B.; Wong, T.-S., Ultrasensitive surface-enhanced Raman scattering detection in common fluids. *Proceedings of the National Academy of Sciences* **2016,** *113* (2), 268-273.

109. U.S. Department of Health and Human Services, Food and Drug Administration, Center for Drug Evaluation and Research (CDER), Center for Veterinary Medicine (CVM) *Guidance for Industry, Bioanalytical Method Validation, DRAFT GUIDANCE*; September, 2013.

110. Marks, H.; Huang, P.-J.; Mabbott, S.; Graham, D.; Kameoka, J.; Coté, G., Ferric plasmonic nanoparticles, aptamers, and magnetofluidic chips: toward the development of diagnostic surface-enhanced Raman spectroscopy assays. *Journal of Biomedical Optics* **2016,** *21* (12), 127005-127005.

111. Ning, X.; Selesnick, I. W.; Duval, L., Chromatogram baseline estimation and denoising using sparsity (BEADS). *Chemometrics and Intelligent Laboratory Systems* **2014,** *139*, 156-167.

112. McUmber, A. C.; Randolph, T. W.; Schwartz, D. K., Electrostatic interactions influence protein adsorption (but not desorption) at the silica–aqueous interface. *The journal of physical chemistry letters* **2015,** *6* (13), 2583-2587.

113. Gutfreund, H., *Kinetics for the life sciences: receptors, transmitters and catalysts*. Cambridge University Press: 1995.

114. Sanders, C. R., Biomolecular Ligand-Receptor Binding Studies: Theory, Practice, and Analysis. *Vanderbilt University* **2010**, 1-42.

115. Corzo, J., Time, the forgotten dimension of ligand binding teaching. *Biochemistry and Molecular Biology Education* **2006,** *34* (6), 413-416.

116. Wei, J.; Mu, Y.; Song, D.; Fang, X.; Liu, X.; Bu, L.; Zhang, H.; Zhang, G.; Ding, J.; Wang, W., A novel sandwich immunosensing method for measuring cardiac troponin I in sera. *Analytical biochemistry* **2003,** *321* (2), 209-216.